Simulating the Dynamics of Quantum Dots Using Hierarchy of Pure States

Pro Gradu
Turun yliopisto
Teoreettinen fysiikka
2023
LuK Sebastian Toivonen
Tarkastajat:
FT Kimmo Luoma
Prof. Jyrki Piilo

TURUN YLIOPISTO
Fysiikan ja tähtitieteen laitos

Toivonen, Sebastian Kvanttipisteiden dynamiikan simulointi käyttäen puhtaiden tilojen hierarkiamenetelmää

Pro Gradu, 77 s., 12 liites.
Teoreettinen fysiikka
Joulukuu 2023

Kvanttipisteet ovat pieniä, muutamien nanometrien kokoisia puolijohdesysteemejä, joilla on ainutlaatuisia ominaisuuksia niiden koon ja rakenteen ansiosta. Kvanttipisteet ovat saaneet paljon huomiota viimeisten vuosikymmenien aikana, ja niillä on useita mahdollisia sovelluskohteita. Esimerkiksi niitä voidaan käyttää yksifotonilähteinä ja laserlähteinä, sekä mahdollisesti fyysisinä kubitteina kvanttilaskennassa, hyödyntäen niiden kykyä kontrolloida yksittäisiä elektroneja. Tyypillisesti kvanttipisteitä muodostetaan kasvattamalla niitä puolijohteiden pinnoilla. Tämän kasvatustavan seurauksena kvanttipisteet vangitsevat elektroneja paikka-avaruudessa, joka tekee niistä efektiivisesti nollaulotteisia, jolloin niiden energiatasot ovat kvantittuneet. Näin ollen kvanttipisteitä voidaan ajatella keinotekoisina atomeina, ja monet atomeille tyypilliset ilmiöt, kuten resonanssifluoresenssi ja yksittäisten fotonien emissio, ovat kokeellisesti havaittavissa.

Teoreettisesti kvanttipiste edustaa perustavanlaatuista avointa kvanttisysteemiä. Tämän vuoksi kvanttipisteiden tutkiminen tarjoaa mahdollisuuden tutkia avointen kvanttisysteemien keskeisiä ilmiöitä ja prosesseja, kuten dekoherenssia ja termalisaatiota. Avointen kvanttisysteemien dynamiikan tarkasteluun on kehitetty useita lähestymistapoja ja menetelmiä. Tässä työssä syvennytään ei-Markoviseen kvanttitiladiffuusioformalismiin (engl. non-Markovian quantum state diffusion, NMQSD) ja erityisesti puhtaiden tilojen hierarkiamenetelmään (engl. hierarchy of pure states, HOPS). NMQSD-formalismin avulla voidaan ratkaista avointen kvanttisysteemien dynamiikkaa, kun ne ovat kytkeytyneet ei-Markoviseen ympäristöön. NMQSD-yhtälön ratkaiseminen onnistuu joissain erikoistapauksissa tarkasti, mutta usein vaaditaan approksimaatioiden käyttöä. HOPS on numeerisesti tarkka menetelmä, joka on kehitetty ratkaisemaan NMQSD-yhtälö ilman approksimaatioita.

Tässä tutkielmassa tarkastellaan kvanttipistettä kaviteetissa, joka on kytköksissä ympäristön hilavärähtelyihin. Käyttäen HOPS-menetelmää simuloidaan kvanttipisteen ominaisuuksia, kuten absorptiota ja resonanssifluoresenssia, sekä lasketaan vastefunktioita. Tavoitteena on osoittaa HOPS-menetelmän tehokkuus kvanttipisteiden dynamiikan tutkimisessa myös vaikeissa parametrialueissa.

Asiasanat: kvanttipiste, kaviteetti, puhtaiden tilojen hierarkia, HOPS, absorptiospektri, emissiospektri, vastefunktio, ei-Markovinen dynamiikka

Contents

Introduction

Quantum dots (QDs) are tiny semiconductor systems, typically ranging from nanometers to tens of nanometers, showcasing unique quantum mechanical properties due to their structure and size. Over the past 30 years, extensive research has focused on studying these particles [1]. One method of forming the QDs involve depositing a thin layer of indium arsenide (InAs) onto a gallium arsenide (GaAs) base which induces strain due to the difference in lattice constants. Upon reaching a critical thickness, the InAs layer spontaneously starts nucleating, giving rise to the QDs [2–6]. As these particles form within the semiconductor materials, they confine electrons in all spatial dimensions because of the band-gap difference between the two alloys, resulting in energy level quantization similar to those of atoms [7]. These energy levels depend on the size of the QD, and the confinement makes the QDs be effectively zero-dimensional systems, from which the name 'quantum dot' originates. Much like atoms, QDs have transition dipole moments, enabling optical excitation and photon emission, thus being sometimes described as "artificial atoms." In fact, QDs have demonstrated several phenomena observed in atomic quantum optics, such as driven Rabi oscillations [8–11], resonance fluorescence [12–15], single photon emission [16, 17] and entangled photon emission [18].

From a theoretical point of view, a single QD represents a fundamental open quantum system, characterized by a limited set of controllable electronic states interacting with uncontrollable surrounding environment, the solid-state lattice. Therefore QDs offer an avenue for exploring fundamental processes of open quantum systems, such as quantum decoherence and thermalization [19]. Beyond theoretical considerations, QDs are also studied for their potential technological applications, such as single photon sources and few-emitter lasers, and furthermore, their potential in quantum computing emerges from their ability to control single electrons, possibly serving as physical realisations of quantum bits [20–22].

In this thesis, we consider a quantum dot system confined in a cavity and coupled to the surrounding environment lattice, modeled as a phonon bath. The aim is to demonstrate the efficacy of the hierarchy of pure states (HOPS) method [23] in simulating the dynamics of quantum dots across various parameter regimes, including weak and strong phonon coupling as well as finite temperature. HOPS is a numerically exact method for solving the dynamics of open quantum systems that are coupled to non-Markovian environments. It is based on the non-Markovian quantum state diffusion (NMQSD) formalism [24]. Essentially, a problematic functional derivative that appears in the NMQSD equation is transformed into a hierarchy of coupled stochastic differential equations which allows it to be solved numerically. HOPS is considered to be numerically exact since the error can, in principle, be made arbitrarily small by increasing the size of the hierarchy.

Using HOPS, we simulate the absorption spectrum of the quantum dot and demonstrate a general method for computing linear response functions using HOPS. Additionally, we calculate the spectrum of resonance fluorescence for the quantum dot and illustrate how, particularly in the case of two-level systems, HOPS enables the propagation of arbitrary operators. The aim of these results is to highlight the applicability of HOPS in studying the optical properties of QDs and to suggest that it potentially provides a reliable framework for accurately simulating QD dynamics in more challenging parameter regimes.

We start in the first section by presenting the necessary theory for studying the dynamics and optical properties of the QD system. We present the total Hamiltonian and discuss the environment coupling Hamiltonian and other necessary quantities for describing this coupling. Then we study the independent boson model, a model of pure-dephasing, where only the environment coupling is present and solve it exactly. Then we discuss how the driving of the QD can be modeled and how the surrounding cavity mode interactions can be incorporated. Subsequently, we study

linear response theory in general and derive the Kubo's formula, from which we move to study the linear absorption of the QD by applying linear response theory. Finally we derive the formula for the spectrum of resonance fluorescence. In section 2, we discuss the non-Markovian quantum state diffusion. We derive it at zero temperature and present methods for incorporating finite temperature into the model. Subsequently, in section 3, we derive the HOPS method for solving the NMQSD equation and briefly qualitatively discuss its implementation in this work. In section 4, we apply HOPS to study the dynamics of the QD and the optical properties presented in section 1. We simulate the independent boson model to establish the validity of HOPS. Subsequently, we compute the absorption spectra of the QD under various circumstances and demonstrate a general method for computing response functions using HOPS. Then we calculate the spectrum of resonance fluorescence in two different scenarios. First by directly driving the QD without coupling to the cavity, and second, by coupling the QD to the cavity and driving the cavity instead. In the latter case, we eliminate the cavity operators through adiabatic elimination. Finally, we compare the results provided by Redfield theory and HOPS. In this thesis we use units where $k_B = \hbar = 1$.

1 Theoretical Background

In this section, we will present the necessary theoretical tools for studying the dynamics and optical properties of the quantum dot system of interest. First, we will introduce the QD system itself, including the total Hamiltonian, and present the exact form of the phonon coupling Hamiltonian and the spectral density specific to the QD. Next, we will consider a simple model that is exactly solvable. Following that, we will present the exact forms of the Hamiltonians for cavity coupling and external drive and provide a general overview of linear response theory. Finally, we will derive the necessary formulas for computing the absorption and emission spectra of the system.

1.1 Quantum Dot System and Phonon Coupling

In this thesis, we are primarily interested in a coherently driven quantum dot that is placed in a cavity. In particular we consider semiconductor quantum dots where the exciton, i.e. the electron-hole pair, is coupled to the lattice vibrations or phonons which are mathematically modeled as quantum harmonic oscillators. The QD is represented as a two-level system with basis states $|g\rangle$ and $|X\rangle$, which correspond to the ground and excited states, respectively. In addition to the lattice phonons, the QD is also coupled to the cavity modes which are treated in a quantized manner. The coherent drive field is treated as a classical field. The total Hamiltonian is given by

$$H = H_{\mathrm{QD}} + H_{\mathrm{Ph}} + H_{\mathrm{Pt}} + H_{I,\mathrm{Ph}} + H_{I,\mathrm{Pt}} + H_D, \tag{1.1}$$

where H_{QD} is the system Hamiltonian

$$H_{\mathrm{QD}} = \omega_X \left|X\right\rangle \left\langle X\right| \tag{1.2}$$

with the transition energy ω_X, H_{Ph} the free field Hamiltonian for the environment phonons, H_{Pt} the free field Hamiltonian for the cavity modes, $H_{I,\mathrm{Ph}}$ the interaction

Hamiltonian for the exciton-phonon coupling, $H_{I,\mathrm{Pt}}$ the interaction Hamiltonian for the exciton-photon coupling and H_D the Hamiltonian for the coherent external drive. The exact forms of H_{Pt}, $H_{I,\mathrm{Pt}}$ and H_D will be discussed in the following sections.

Let us briefly consider the Hamiltonians relevant to the exciton-phonon coupling. The free field Hamiltonian is given in the harmonic approximation by

$$H_{\mathrm{Ph}} = \sum_{\lambda} \omega_\lambda a_\lambda^\dagger a_\lambda, \tag{1.3}$$

where $a_\lambda^\dagger$ and a_λ are the creation and annihilation operators for modes of frequency ω_λ, respectively. By considering linear coupling to the phonons, the interaction Hamiltonian is given by [25]

$$H_{I,\mathrm{Ph}} = |X\rangle\langle X| \sum_{\lambda} g_\lambda (a_\lambda^\dagger + a_\lambda), \tag{1.4}$$

where $g_\lambda \in \mathbb{R}$ measure the coupling strength of each phonon mode. To move to the continuum limit, it is convenient to define the exciton-phonon spectral density which measures the exciton-phonon coupling strength and is defined as

$$J_{\mathrm{ph}}(\omega) = \sum_{\lambda} |g_\lambda|^2 \delta(\omega - \omega_\lambda). \tag{1.5}$$

We assume throughout this thesis that in the continuum limit the spectral density takes the form

$$J_{\mathrm{ph}}(\omega) = \alpha \omega^3 e^{-\frac{\omega^2}{\xi^2}}, \tag{1.6}$$

where α denotes the coupling strength and ξ is the cut-off frequency. This form is typical for semiconductor QDs where the deformation potential is the dominant exciton-phonon coupling mechanism [25].

1.2 Independent Boson Model

Let us now consider the Hamiltonian (1.1) with only the QD and phonon coupling Hamiltonians; in other words, the total Hamiltonian is

$$H_{\mathrm{IBM}} = H_{\mathrm{QD}} + H_{\mathrm{Ph}} + H_{I,\mathrm{Ph}}, \tag{1.7}$$

where H_{QD}, H_{Ph} and $H_{\mathrm{I,\,Ph}}$ are given in (1.2), (1.3) and (1.4), respectively. The environment phonons are assumed to be independent, and consequently, this form of the Hamiltonian is known as the independent boson model [26–29]. It serves as an example of a model demonstrating pure-dephasing and is a special case of the spin-boson model [30, 31]. Dephasing refers to a process in which the coherences or off-diagonal entries of the density operator decay. Pure dephasing specifically indicates that the population or diagonal elements remain constant. The effect of pure-dephasing is evident directly from the Hamiltonian since $[\sigma_z, H_{\mathrm{IBM}}] = 0$. Studying the independent boson model is valuable, as it represents one of the few models in the theory of open quantum systems that can be solved exactly. It can thus serve as a benchmark model for measuring the accuracy of other methods used to solve the dynamics of open quantum systems. Furthermore, some optical properties of the system can be computed analytically, such as linear absorption.

1.2.1 Evolution of Pure States

In the literature, the most common approach to solving this model involves applying a suitable unitary transformation to the Hamiltonian [27, 32]. However, here we take a different approach by considering pure state evolution. Since the environment phonons are modeled as independent harmonic oscillators, we can describe them using coherent states

$$|\mathbf{z}(t)\rangle = \prod_{\lambda} e^{-\frac{1}{2}|z_\lambda(t)|^2} e^{z_\lambda(t)a^\dagger} |\mathbf{0}\rangle = \prod_{\lambda} D_\lambda(z_\lambda(t)) |\mathbf{0}\rangle ,$$

where $D_\lambda(z_\lambda(t)) = \exp\left(z_\lambda(t)a_\lambda^\dagger - z_\lambda^*(t)a_\lambda\right)$ are displacement operators and $|\mathbf{z}(t)\rangle = |z_1(t), z_2(t), ...\rangle$. We'll first consider the state

$$|\psi_t\rangle = f(t)\,|g\rangle\,|\mathbf{z}_g(t)\rangle$$

with initial conditions $f(0) = 1$ and $|\mathbf{z}_g(0)\rangle = |z_1(0), z_2(0), ...\rangle$. Taking the time derivative gives us

$$\frac{\partial |\psi_t\rangle}{\partial t} = \left(\dot{f}(t) - \frac{1}{2} f(t) \sum_\lambda \frac{\partial |z_{g,\lambda}(t)|^2}{\partial t} \right) |g\rangle |\mathbf{z}_g(t)\rangle + f(t) \sum_\lambda \dot{z}_{g,\lambda}(t) a_\lambda^\dagger |g\rangle |\mathbf{z}_g(t)\rangle$$

and from the Schrödinger equation we obtain

$$\frac{\partial |\psi_t\rangle}{\partial t} = -iH |\psi_t\rangle = -if(t) \sum_\lambda \omega_\lambda z_{g,\lambda}(t) a_\lambda^\dagger |g\rangle |\mathbf{z}_g(t)\rangle .$$

By comparing the terms of these two equations we get the following system of equations

$$\begin{cases} \dot{f}(t) & = \frac{1}{2} f(t) \sum_\lambda \frac{\partial |z_{g,\lambda}(t)|^2}{\partial t} \\ \dot{z}_{g,\lambda}(t) & = -i\omega_\lambda z_{g,\lambda}(t) \text{ for each } \lambda \end{cases} .$$

The second equation, for a fixed λ, can be solved directly and has the solution

$$z_{g,\lambda}(t) = z_\lambda(0) e^{-i\omega_\lambda t}. \tag{1.8}$$

Inserting this into the first equation gives $\dot{f}(t) = 0$ which implies that $f(t) = f(0)$.

Next we apply the same approach to the state

$$|\psi_t\rangle = h(t) |X\rangle |\mathbf{z}_X(t)\rangle ,$$

with initial conditions $h(0) = 1$ and $|\mathbf{z}_X(0)\rangle = |z_1(0), z_2(0), ...\rangle$. Taking the time derivative gives us

$$\frac{\partial |\psi_t\rangle}{\partial t} = \left(\dot{h}(t) - \frac{1}{2} h(t) \sum_\lambda \frac{\partial |z_{X,\lambda}(t)|^2}{\partial t} \right) |X\rangle |\mathbf{z}_X(t)\rangle + h(t) \sum_\lambda \dot{z}_{X,\lambda}(t) a_\lambda^\dagger |X\rangle |\mathbf{z}_X(t)\rangle .$$

Comparing with the Schrödinger equation

$$\begin{aligned} \frac{\partial |\psi_t\rangle}{\partial t} = & - ih(t) \left(\omega_X + \sum_\lambda g_\lambda z_{X,\lambda}(t) \right) |X\rangle |\mathbf{z}_X(t)\rangle \\ & - ih(t) \sum_\lambda (\omega_\lambda z_{X,\lambda}(t) + g_\lambda) a_\lambda^\dagger |X\rangle |\mathbf{z}_X(t)\rangle \end{aligned}$$

we get the system of equations

$$\begin{cases} \dot{h}(t) & = h(t)\left(\frac{1}{2}\sum_{\lambda}\frac{\partial|z_{X,\lambda}(t)|^2}{\partial t} - i\omega_X - i\sum_{\lambda} g_\lambda z_{X,\lambda}(t)\right) \\ \dot{z}_{X,\lambda}(t) & = -i(\omega_\lambda z_{X,\lambda}(t) + g_\lambda) \text{ for each } \lambda \end{cases}.$$

The first equation has the formal solution

$$h(t) = h(0)\exp\left(-i\omega_X t - i\sum_{\lambda} g_\lambda \int_0^t \mathrm{d}s z_{X,\lambda}(s) + \frac{1}{2}\sum_{\lambda}(|z_{X,\lambda}(t)|^2 - |z_\lambda(0)|^2)\right), \tag{1.9}$$

and from the second equation for each $z_{X,\lambda}(t)$ we obtain

$$z_{X,\lambda}(t) = z_\lambda(0)e^{-i\omega_\lambda t} - \frac{g_\lambda}{\omega_\lambda}\left(1 - e^{-i\omega_\lambda t}\right). \tag{1.10}$$

By inserting (1.10) into (1.9) we can write $h(t) = h(0)e^{-i\phi(t)}$ where $\phi(t)$ is a real function

$$\phi(t) = \left(\omega_X - \sum_{\lambda}\frac{g_\lambda^2}{\omega_\lambda}\right)t - \sum_{\lambda}\frac{g_\lambda}{\omega_\lambda}\mathrm{Im}\left[z_\lambda(0)(e^{-i\omega_\lambda t} - 1)\right] - \sum_{\lambda}\frac{g_\lambda^2}{\omega_\lambda^2}\sin\omega_\lambda t.$$

This conveniently implies that $h(t)h^*(t) = 1$. Thus far we have shown that for the propagator $\mathcal{U}_t = e^{-iHt}$, with the Hamiltonian given in (1.7), the states evolve as

$$\mathcal{U}_t\,|g\rangle\,|\mathbf{z}_0\rangle = |g\rangle\,|\mathbf{z}_g(t)\rangle = |g\rangle \otimes \prod_{\lambda} D_\lambda(z_{g,\lambda}(t))\,|\mathbf{0}\rangle \tag{1.11}$$

$$\mathcal{U}_t\,|X\rangle\,|\mathbf{z}_0\rangle = h(t)\,|X\rangle\,|\mathbf{z}_X(t)\rangle = h(t)\,|X\rangle \otimes \prod_{\lambda} D_\lambda(z_{X,\lambda}(t))\,|\mathbf{0}\rangle \tag{1.12}$$

with $\mathbf{z}_g(t)$, $h(t)$ and $\mathbf{z}_X(t)$ given in (1.8), (1.9) and (1.10), respectively.

1.2.2 Decoherence Function

We want to consider the case where the phonon bath is in the thermal state

$$\rho_E = \frac{e^{-\beta H_{\mathrm{Ph}}}}{\mathrm{tr}[e^{-\beta H_{\mathrm{Ph}}}]}.$$

It is useful, and in our case essential, that we represent it in terms of coherent states by using the Sudarshan-Glauber P representation [33, 34]

$$\rho_E = \int \mathrm{d}^2\boldsymbol{\xi} P(\boldsymbol{\xi}) \left|\boldsymbol{\xi}\right\rangle \left\langle\boldsymbol{\xi}\right|, \tag{1.13}$$

where $\mathrm{d}^2\boldsymbol{\xi} \equiv \prod_\lambda \mathrm{dRe}(\xi_\lambda)\mathrm{dIm}(\xi_\lambda)$. The Glauber-Sudarhan P function for the thermal state is derived in detail in appendix A. For the independent boson environment we have

$$P(\mathbf{z}) = \prod_\lambda P_\lambda(z_\lambda) = \prod_\lambda \frac{e^{-\frac{|z_\lambda|^2}{\bar{n}_\lambda}}}{\pi\bar{n}_\lambda}, \tag{1.14}$$

where $\bar{n}_\lambda = (e^{\beta\omega_\lambda} - 1)^{-1}$ is the Bose-Einstein distribution for the mode λ.

Now we can consider the general initial state

$$\varrho_0 = \left|\psi\right\rangle \left\langle\psi\right| \otimes \rho_E = \rho_0 \otimes \rho_E,$$

where $\left|\psi\right\rangle = C_g \left|g\right\rangle + C_X \left|X\right\rangle$, $C_g, C_X \in \mathbb{C}$ and ρ_E is prepared in the thermal state. By representing ρ_E using the P-representation (1.13) and taking the trace over the environmental degrees of freedom [32], we obtain the reduced density matrix

$$\begin{aligned}
\rho_t &= \mathrm{tr}_E \left\{ \mathcal{U}_t \rho_0 \otimes \rho_E \mathcal{U}_t^\dagger \right\} \\
&= \int \mathrm{d}^2\mathbf{z}_0 P(\mathbf{z}_0) \mathrm{tr}_E \Big\{ \left|C_g\right|^2 \mathcal{U}_t \left|g\right\rangle \left|\mathbf{z}_0\right\rangle \left\langle g\right| \left\langle \mathbf{z}_0\right| \mathcal{U}_t^\dagger + C_g C_X^* \mathcal{U}_t \left|g\right\rangle \left|\mathbf{z}_0\right\rangle \left\langle X\right| \left\langle \mathbf{z}_0\right| \mathcal{U}_t^\dagger \\
&\quad + C_g^* C_X \mathcal{U}_t \left|X\right\rangle \left|\mathbf{z}_0\right\rangle \left\langle g\right| \left\langle \mathbf{z}_0\right| \mathcal{U}_t^\dagger + \left|C_X\right|^2 \mathcal{U}_t \left|X\right\rangle \left|\mathbf{z}_0\right\rangle \left\langle X\right| \left\langle \mathbf{z}_0\right| \mathcal{U}_t^\dagger \Big\} \\
&= \left|C_g\right|^2 \left|g\right\rangle \left\langle g\right| + C_g C_X^* \left|g\right\rangle \left\langle X\right| \int \mathrm{d}^2\mathbf{z}_0 P(\mathbf{z}_0) h^*(t) \mathrm{tr}_E \{ \left|\mathbf{z}_g(t)\right\rangle \left\langle \mathbf{z}_X(t)\right| \} \\
&\quad + C_g^* C_X \left|X\right\rangle \left\langle g\right| \int \mathrm{d}^2\mathbf{z}_0 P(\mathbf{z}_0) h(t) \mathrm{tr}_E \{ \left|\mathbf{z}_X(t)\right\rangle \left\langle \mathbf{z}_g(t)\right| \} + \left|C_X\right|^2 \left|X\right\rangle \left\langle X\right| \\
&= \left|C_g\right|^2 \left|g\right\rangle \left\langle g\right| + C_g C_X^* \Lambda(t) \left|g\right\rangle \left\langle X\right| + C_g^* C_X \Lambda^*(t) \left|X\right\rangle \left\langle g\right| + \left|C_X\right|^2 \left|X\right\rangle \left\langle X\right|.
\end{aligned}$$

Here we have used (1.11) and (1.12), and utilized the fact that $h(t)h^*(t) = 1$. We can clearly see that the populations are kept constant and only the coherences evolve, which is expected for a process of pure-dephasing. The function $\Lambda(t)$ is given by

$$\Lambda(t) = \int \mathrm{d}^2\mathbf{z}_0 P(\mathbf{z}_0) h^*(t) \left\langle \mathbf{z}_X(t) | \mathbf{z}_g(t)\right\rangle. \tag{1.15}$$

By inserting (1.8), (1.9), (1.10) and (1.14) into (1.15) we get

$$\Lambda(t) = \frac{e^{i\omega_X t}}{\pi} \prod_\lambda \frac{\exp(-i\frac{g_\lambda^2}{\omega_\lambda}t - \frac{g_\lambda^2}{\omega_\lambda^2}(1-e^{i\omega_\lambda t}))}{\bar{n}_\lambda} \times \int \mathrm{d}^2 z_\lambda \exp\left(-\frac{|z_\lambda|^2}{\bar{n}_\lambda} + \frac{g_\lambda}{\omega_\lambda}(1-e^{-i\omega_\lambda t})z_\lambda + \frac{g_\lambda}{\omega_\lambda}(1-e^{+i\omega_\lambda t})z_\lambda^*\right).$$

Using the change of variables $y_\lambda = z_\lambda - \frac{\bar{n}_\lambda g_\lambda}{\omega_\lambda}(1-e^{i\omega_\lambda t})$ and defining the phonon-shifted transition energy $\omega'_X = \omega_X - \sum_\lambda \frac{g_\lambda^2}{\omega_\lambda}$ [19], we get

$$\Lambda(t) = e^{i\omega'_X t} \exp\left[-\sum_\lambda \frac{g_\lambda^2}{\omega_\lambda^2}\left((1+2\bar{n}_\lambda)(1-\cos\omega_\lambda t) - i\sin\omega_\lambda t\right)\right].$$

To consider the continuum limit we use the exciton-phonon spectral density defined in equation (1.5). Then in the continuum limit we have

$$\omega'_X = \omega_X - \int \mathrm{d}\omega \frac{J_{\mathrm{Ph}}(\omega)}{\omega} \tag{1.16}$$

$$\Lambda(t) = e^{i\omega'_X t} e^{\Gamma(t)} \tag{1.17}$$

where the function $\Gamma(t)$ is the *decoherence function* [32]

$$\Gamma(t) = -\int \mathrm{d}\omega \frac{J_{\mathrm{Ph}}(\omega)}{\omega^2}\left(\coth\left(\frac{\beta\omega}{2}\right)(1-\cos\omega t) - i\sin\omega t\right). \tag{1.18}$$

Figure 1 shows the evolution of the coherence of the QD, which is initially prepared in the equal superposition state $|\psi\rangle = |+\rangle = \frac{1}{\sqrt{2}}(|g\rangle + |X\rangle)$. We have moved to a reference frame that rotates at the phonon-shifted transition frequency (1.16). For each temperature, we observe an initial decrease in coherence, which then reaches a constant value that decreases as the temperature increases.

1.3 Monochromatic Drive

It is desirable to be able to excite the QD in a controlled way, as it enables us to study optical phenomena such as spontaneous emission and resonance fluorescence. This can be done by externally driving the QD with a monochromatic light source.

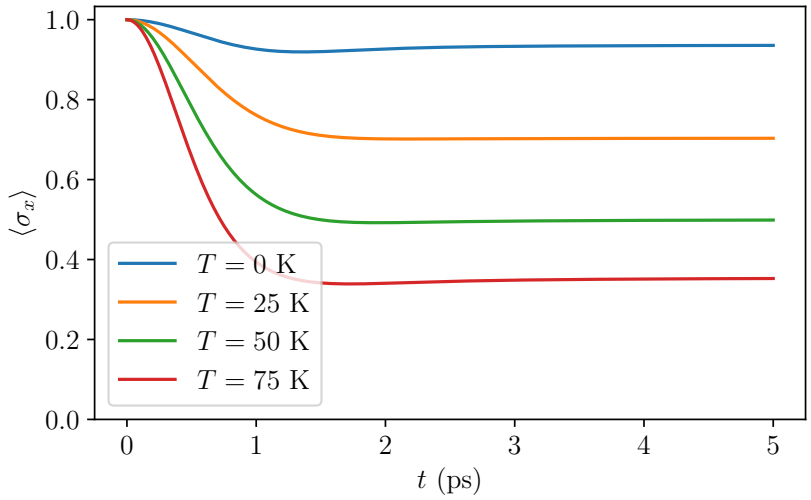

Figure 1. The evolution of the QD coherence in various temperatures with coupling strength $\alpha = 0.027$ ps^2 and cut-off frequency $\xi = 1.447$ meV.

For this we simply consider the Hamiltonian (1.1) with only the QD and drive Hamiltonians and treat the driving field as a classical field. Now in the dipole approximation the Hamiltonian is [35]

$$H = H_S + H_D = \omega_X \left|X\right\rangle \left\langle X\right| - \mathbf{d} \cdot \mathbf{E}(t), \tag{1.19}$$

where $\mathbf{E}(t) = \boldsymbol{\epsilon} E_0 \cos \omega_D t$ is the monochromatic field with the polarization vector $\boldsymbol{\epsilon}$, amplitude E_0 and driving frequency ω_D, and $\mathbf{d}$ is the dipole operator. We define the two-level transition dipole moment as

$$\tilde{\boldsymbol{\mu}} = \langle g|\mathbf{d}|X\rangle \,. \tag{1.20}$$

Now since the dipole operator has odd parity, i.e., $\langle g|\mathbf{d}|g\rangle = \langle X|\mathbf{d}|X\rangle = 0$ and assuming no permanent dipole moment, we can write [26]

$$\mathbf{d} = \tilde{\boldsymbol{\mu}} \left|g\right\rangle \left\langle X\right| + \tilde{\boldsymbol{\mu}}^* \left|X\right\rangle \left\langle g\right| . \tag{1.21}$$

From this form we can see that the drive field causes transitions between the basis states $|g\rangle$ and $|X\rangle$. Without loss of generality we can assume that the dipole matrix

elements $\langle g|\mathbf{d}|X\rangle$ are real [35] and thus we can write the Hamiltonian (1.19) in the form

$$H = \omega_X \left|X\right\rangle \left\langle X\right| + \Omega \cos(\omega_D t)(\left|g\right\rangle \left\langle X\right| + \left|X\right\rangle \left\langle g\right|). \tag{1.22}$$

Here $\Omega = -E_0 \langle g|\mathbf{d}|X\rangle \cdot \boldsymbol{\epsilon}$ is called the Rabi frequency. It quantifies the coupling strength between the system and the field. By defining a time-dependent field amplitude $E_0(t)$ it would be possible to consider pulsed excitations. In that case the Rabi frequency would also become time-dependent. For our case continuous-wave driving suffices so the Rabi frequency is time-independent.

Later we are interested in the situation where the driving frequency is close to the excitation energy ω_X, i.e., close to resonance. Thus we can simplify the Hamiltonian (1.22) by making a rotating-wave approximation, which removes fast oscillations [35]. The Hamiltonian in the rotating frame, frequency ω_D, is given by the transformation

$$H' = U(t)HU^\dagger(t) - iU(t)\frac{\partial}{\partial t}U^\dagger(t),$$

where $U(t) = e^{i\omega_D|X\rangle\langle X|t}$. This gives

$$H' = (\omega_X - \omega_D)\left|X\right\rangle \left\langle X\right| + \Omega\frac{e^{i\omega_D t} + e^{-i\omega_D t}}{2}(e^{-i\omega_D t}\left|g\right\rangle \left\langle X\right| + e^{i\omega_D t}\left|X\right\rangle \left\langle g\right|).$$

Now the rotating-wave approximation is performed by neglecting the fast oscillations at frequencies $\pm 2\omega_D$. With this we obtain the Hamiltonian

$$\begin{aligned} H_{\mathrm{RWA}} &= \Delta \left|X\right\rangle \left\langle X\right| + \frac{\Omega}{2}(\left|g\right\rangle \left\langle X\right| + \left|X\right\rangle \left\langle g\right|) \\ &= \Delta\sigma_+\sigma_- + \frac{\Omega}{2}(\sigma_- + \sigma_+), \end{aligned} \tag{1.23}$$

where $\Delta = \omega_X - \omega_D$ denotes the detuning. It is worth noting that the rotating-wave approximation is valid when $\Delta << \omega_D$ and $\Omega << \omega_D$.

1.4 Cavity Coupling

In the independent boson model the QD has only coupling to the environment phonons. We are interested in having the two-level system to also have coupling to a cavity, i.e., we want to confine the system inside a cavity. As such it will be coupled to the surrounding field modes. Instead of considering classical fields, as we did for the drive in the previous section, we will consider a fully quantized model.

For simplicity let us consider only a single field mode. Again assuming that the dipole approximation is valid, the system-field interaction Hamiltonian takes the form

$$H_I = -\mathbf{d} \cdot \mathbf{E},$$

where for a uniform cavity we have [35]

$$\mathbf{E} = \boldsymbol{\epsilon} \sqrt{\frac{\omega_c}{2\epsilon_0 V}} (b + b^\dagger),$$

where b and $b^\dagger$ are the annihilation and creation operators of the cavity mode, $\boldsymbol{\epsilon}$ is the polarisation vector, ω_c is the cavity mode frequency, V is the quantization volume. The annihilation and creation operators define the harmonic cavity Hamiltonian

$$H_{\text{cav}} = \omega_c b^\dagger b.$$

Assuming the same form for the dipole operator as (1.21), we have

$$H_I = u(|g\rangle \langle X| + |X\rangle \langle g|)(b + b^\dagger),$$

where u describes the coupling strength

$$u = -\sqrt{\frac{\omega_c}{2\epsilon_0 V}} \langle g|\mathbf{d}|X\rangle \cdot \boldsymbol{\epsilon}.$$

Again for later purposes, we assume that the system and cavity modes are close to resonance $\omega_X \approx \omega_c$. Thus we can perform the rotating wave approximation. It can be shown that $b(t)$ and $b^\dagger(t)$ evolve in the free field case as [35]

$$b(t) = b(0)e^{-i\omega_c t}, \; b^\dagger(t) = b(0)e^{i\omega_c t}.$$

Similarly $|g\rangle\langle X| = \sigma_-$ and $|X\rangle\langle g| = \sigma_+$ can be shown to evolve in the free QD case as

$$\sigma_\pm(t) = \sigma_\pm(0)e^{\pm i\omega_X t}.$$

Thus we discard terms $\sigma_- b$ and $\sigma_+ b^\dagger$ in the rotating-wave approximation, and we obtain

$$H_{I,\mathrm{RWA}} = u(|g\rangle\langle X| b^\dagger + |X\rangle\langle g| b).$$

The total Hamiltonian is now of the Jaynes-Cummings form [36]

$$H = \omega_X |X\rangle\langle X| + \omega_c b^\dagger b + u(|g\rangle\langle X| b^\dagger + |X\rangle\langle g| b).$$

This can be generalized for multimode fields with

$$H_{\mathrm{Pt}} = \sum_\lambda \nu_\lambda b_\lambda^\dagger b_\lambda,$$

with $[b_\lambda, b_\kappa^\dagger] = \delta_{\lambda\kappa}\mathbb{1}$. With the rotating-wave approximation applied again, the interaction Hamiltonian is

$$H_{I,\mathrm{Pt}} = \sum_\lambda u_\lambda(|g\rangle\langle X| b_\lambda^\dagger + |X\rangle\langle g| b_\lambda), \tag{1.24}$$

where the coupling strengths are

$$u_\lambda = \sqrt{\frac{\nu_\lambda}{2\epsilon_0 V}}\,\langle g|\mathbf{d}|X\rangle \cdot \boldsymbol{\epsilon}_\lambda.$$

1.5 Linear Response Theory

Linear response theory [37] provides a framework to describe how a physical system responds to small external perturbations. In particular for quantum systems, it provides a way to examine how atoms or molecules respond to external fluctuations, such as an electric field. In linear response theory it is assumed that this response is linearly proportional to the magnitude of the external perturbation and

all that needs to be calculated is the proportionality constant [38]. Linear response theory introduces the concept of response functions or after-effect functions. These functions quantify how the system responds to the perturbations of the system and can often be measured experimentally [39]. For example electric conductivity, magnetic susceptibility and optical absorption can be examined through linear response theory [38].

Let us consider a system that is in thermal equilibrium. An external force $F(t)$ is then applied to it from the distant past, specifically when $t \to -\infty$, at the time when the system was in thermal equilibrium. The dynamics of the system is described by the total Hamiltonian

$$H = H_0 + V(t),$$

where H_0 is the time-independent or equilibrium Hamiltonian and $V(t) = -AF(t)$ represents the perturbation induced by the external force $F(t)$, where A is an operator that is the dynamical quantity conjugate to the force $F(t)$ [40]. The response function or after-effect function $\phi_{BA}(t)$ of an observable B under the influence of the operator A is defined by [37]

$$\begin{aligned} \delta \langle B(t) \rangle &= \langle B(t) \rangle - \langle B_{\text{eq}} \rangle \\ &= \int_0^\infty \mathrm{d}\tau \phi_{BA}(\tau) F(t-\tau). \end{aligned} \tag{1.25}$$

We can obtain the eigenvectors $|\psi_n(t)\rangle$ of the total Hamiltonian H by using time-dependent perturbation theory [41]. In the first order of the external perturbation we obtain

$$|\psi_n(t)\rangle = e^{-i\epsilon_n t} |n\rangle + \sum_k a_{nk}(t) e^{-i\epsilon_k t} |k\rangle + \mathcal{O}(V^2), \tag{1.26}$$

where $\{|n\rangle\}$ are the eigenvectors of the equilibrium Hamiltonian H_0 and the coefficients $a_{nk}(t)$ are given by [41]

$$a_{nk}(t) = -i \int_{-\infty}^{t} \mathrm{d}s \; e^{i(\epsilon_k - \epsilon_n)s} \langle k|V(s)|n\rangle \,. \tag{1.27}$$

The thermal statistical mean of an observable O is given by

$$\langle O(t)\rangle = \sum_n P_n \langle\psi_n(t)|O|\psi_n(t)\rangle\,, \tag{1.28}$$

where P_n is the probability of the system to be in the perturbed state $|\psi_n(t)\rangle$. The next step is to assign the probabilities $\{P_n\}$. This is done via the *thermal assumption* [40] which states that the perturbation is small enough such that the thermal statistical distribution of the eigenstates is left unchanged. Under this assumption we have

$$P_n \approx P_{\mathrm{eq},n}.$$

Using this we can calculate the mean value $\langle B(t)\rangle$ by insterting (1.26) into (1.28)

$$\begin{aligned}\langle B(t)\rangle &= \sum_n P_{\mathrm{eq},n} \langle\psi_n(t)|B|\psi_n(t)\rangle \\ &= \sum_n P_{\mathrm{eq},n} \langle n|B|n\rangle + \sum_{n,k} P_{\mathrm{eq},n} \big[\langle k|B|n\rangle\, a^*_{nk}(t) e^{i(\epsilon_k-\epsilon_n)t} \\ &\quad + \langle n|B|k\rangle\, a_{nk}(t) e^{i(\epsilon_n-\epsilon_k)t}\big] + \mathcal{O}(V^2).\end{aligned}$$

The first term on the second line is the mean value in the equilibrium state $\langle B_{\mathrm{eq}}\rangle$. Since we are considering linear response, we get

$$\begin{aligned}\delta\langle B(t)\rangle &= \langle B(t)\rangle - \langle B_{\mathrm{eq}}\rangle \\ &= \sum_{n,k} iP_{\mathrm{eq},n} \int_{-\infty}^{t} \mathrm{d}s \left[e^{i\epsilon_k(t-s)} \langle n|V(s)|k\rangle \langle k|B|n\rangle e^{-i\epsilon_n(t-s)}\right. \\ &\quad \left. - e^{-i\epsilon_k(t-s)} \langle n|B|k\rangle \langle k|V(s)|n\rangle e^{i\epsilon_n(t-s)}\right].\end{aligned}$$

Using the fact that the eigenvectors $\{|k\rangle\}$ form a basis, and denoting $\varrho_{eq} = \sum_n P_{\mathrm{eq},n} |n\rangle\langle n|$, we obtain

$$\begin{aligned}\delta\langle B(t)\rangle &= \int_{-\infty}^{t} \mathrm{d}s\; i \sum_n P_{\mathrm{eq},n} \langle n|V(s)e^{iH_0(t-s)}Be^{-iH_0(t-s)} - e^{iH_0(t-s)}Be^{-iH_0(t-s)}V(s)|n\rangle \\ &= \int_{-\infty}^{t} \mathrm{d}s\; i \sum_n P_{\mathrm{eq},n} \langle n|V(s)B(t-s) - B(t-s)V(s)|n\rangle \\ &= \int_{-\infty}^{t} \mathrm{d}s\; i\mathrm{tr}\{\varrho_{\mathrm{eq}}[V(s), B(t-s)]\}.\end{aligned}$$

Now performing the change of variables $\tau = t - s$ and writing explicitly the perturbation $V(s) = -AF(s)$ we finally get

$$\delta \langle B(t) \rangle = \int_0^\infty \mathrm{d}\tau i \mathrm{tr}\{\varrho_{\mathrm{eq}}[B(\tau), A]\} F(t-\tau).$$

By comparing this with equation (1.25) we get the response function

$$\phi_{BA}(\tau) = i\mathrm{tr}\{\varrho_{\mathrm{eq}}[B(\tau), A]\} = i\mathrm{tr}\{B(\tau)[A, \varrho_{\mathrm{eq}}]\}. \tag{1.29}$$

This is known as Kubo's theorem [37, 40]. To ensure causality it is assumed that $\tau > 0$ so the Heaviside stepfunction is often included [42]

$$\phi_{BA}(\tau) = i\Theta(\tau)\mathrm{tr}\{\varrho_{\mathrm{eq}}[B(\tau), A]\}.$$

If the external force is periodic, i.e., $F(t) = F_0 \cos \omega t$ and using the convolution theorem, the complex susceptibility or admittance $\chi_{BA}(\omega)$ is then given by the half-sided Fourier transform of the response function [37]

$$\chi_{BA}(\omega) = \int_0^\infty \mathrm{d}\tau \phi_{BA}(\tau) e^{i\omega t}.$$

1.6 Linear Absorption

Absorption is one of the three fundamental interactions between light and matter. Linear absorption is considered when the material absorbs light at a rate that is linearly proportional to the intensity of the incident light. Nonlinear absorption involves more complex interactions, such as multi-photon interactions where the absorptions depends on higher powers of the intensity of the incident light [42]. We will consider only linear absorption.

1.6.1 Polarization

When an electric field is applied to a medium, the charges of each atom or molecule comprising the medium will react to the external field, leading to a distortion in the

molecular charge density. Furthermore, the multipole moments of each constituent will deviate from their values in the absence of the external field. Assuming that the medium consists of a single type of atom or molecule and that the dominant molecular multipole moment is the dipole moment, the macroscopic electric polarization vector $\mathbf{P}(\mathbf{x})$ is given by [43]

$$\mathbf{P}(\mathbf{x}) = \frac{N_{\text{mol}}}{\Delta V}\mathbf{d}(\mathbf{x}, t) = n_{\text{mol}}\mathbf{d}(\mathbf{x}, t), \tag{1.30}$$

where n_{mol} is the volume density of molecules in the sample volume ΔV and $\mathbf{d}(\mathbf{x}, t)$ is the molecular dipole moment.

Considering a medium that is isotropic, the polarization vector is parallel to the external field $\mathbf{E}$ [43]

$$\mathbf{P} = \chi\mathbf{E}, \tag{1.31}$$

where χ is the *electric susceptibility* of the medium which is in general a second rank tensor. In general $\mathbf{P}$ would be a nonlinear functional of the electric field $\mathbf{E}$ [39]. Since we are considering only linear absorption, the first order approximation is sufficient. In reality a material doesn't polarize instantly in response to the external field and as such we have generally [42]

$$\mathbf{P}(t) = \int_{-\infty}^{t} \mathrm{d}s\chi(t - s)\mathbf{E}(s). \tag{1.32}$$

For an isotropic and linear system, it is convenient to take the Fourier transform of (1.32) and using the convolution theorem we obtain the frequency dependence

$$\mathbf{P}(\omega) = \chi(\omega)\mathbf{E}(\omega).$$

We see that in the first order approximation the response of the system is determined completely by the susceptibility χ. The linear absorption coefficient $\mathcal{A}(\omega)$ is then given by [44]

$$\mathcal{A}(\omega) = \frac{4\pi\omega}{n}\mathrm{Im}\chi(\omega), \tag{1.33}$$

where n is the reflection coefficient of the medium. The frequency dependence of $\chi(\omega)$ is determined by the properties of the medium through linear response theory discussed in the previous section.

1.6.2 Dipole-dipole Correlation Function

Let us consider the Hamiltonian

$$H = H_0 + H_{\text{field}}(t), \tag{1.34}$$

where H_0 describes the system, possibly with an environment and its associated coupling, and $H_{\text{field}}(t)$ is the electric field Hamiltonian

$$H_{\text{field}}(t) = -\boldsymbol{\mu} \cdot \mathbf{E}(t) = -(\boldsymbol{\mu} \cdot \boldsymbol{\epsilon})E(t) = -\mu_{\text{eff}}E(t)$$

where we have defined the effective dipole moment operator $\mu_{\text{eff}} = \boldsymbol{\mu} \cdot \boldsymbol{\epsilon}$ with the dipole moment operator $\boldsymbol{\mu}$ and polarization $\boldsymbol{\epsilon}$. We can now employ linear response theory. Using Kubo's theorem (1.29), we can write the linear dielectric susceptibility $\chi(\tau)$ as the response function [42]

$$\chi(\tau) = \phi_{\mu_{\text{eff}}\mu_{\text{eff}}}(\tau) = i\Theta(\tau)M(\tau),$$

where $M(\tau)$ is the *dipole-dipole correlation function* [39]

$$M(\tau) = \text{tr}\{\varrho_{\text{eq}}[\mu_{\text{eff}}(\tau), \mu_{\text{eff}}]\},$$

where $\varrho_{\text{eq}} = \exp(-\beta H_0)/\text{tr}\{\exp(-\beta H_0)\}$ is the equilibrium density matrix with no electric field present and $\mu_{\text{eff}}(\tau) = \mathcal{U}_\tau'^{\dagger}\mu_{\text{eff}}\mathcal{U}_\tau'$ with the propagator $\mathcal{U}_\tau' = \exp(-iH_0\tau)$. This can also be expressed in a form that is sometimes more convenient

$$\begin{aligned} M(\tau) &= \sum_j \text{tr}\left\{\varrho_{\text{eq}}[\mu_{\text{eff}}(\tau), \mu_{\text{eff}}]\right\} \\ &= \text{tr}\left\{\mu_{\text{eff}}\mathcal{U}_t'[\mu_{\text{eff}}, \varrho_{\text{eq}}]\mathcal{U}_t'^{\dagger}\right\} \\ &= \text{tr}\{\mu_{\text{eff}}\kappa(\tau)\}. \end{aligned} \tag{1.35}$$

With this form, one can calculate the dipole-dipole correlation function by propagating the commutator $\kappa(\tau)$. If we consider pure states instead of mixed states, equation (1.35) can be put into an explicit form. We assume that $\varrho_{\text{eq}} = |\Psi_g\rangle\langle\Psi_g|$ where $|\Psi_g\rangle$ is the ground state, an eigenstate of H_0, i.e., $\mathcal{U}_t' |\Psi_g\rangle = e^{-iE_g t} |\Psi_g\rangle$ where E_g is the ground state energy. Now $M(t)$ gets the form

$$\begin{aligned} M(t) &= \operatorname{tr}\left\{\mu_{\text{eff}}(\mathcal{U}_t'\mu_{\text{eff}} |\Psi_g\rangle\langle\Psi_g| e^{iE_g t} - e^{-iE_g t} |\Psi_g\rangle\langle\Psi_g| \mu_{\text{eff}}\mathcal{U}_t')\right\} \\ &= e^{iE_g t}\langle\Psi_g|\mu_{\text{eff}}\mathcal{U}_t'\mu_{\text{eff}}|\Psi_g\rangle - e^{-iE_g t}\langle\Psi_g|\mu_{\text{eff}}\mathcal{U}_t'^{\dagger}\mu_{\text{eff}}|\Psi_g\rangle . \end{aligned}$$

If we assume no permanent dipole moment, we can consider the dipole operator of the form

$$\boldsymbol{\mu} = \sum_n \boldsymbol{\mu}_n(|\Psi_n\rangle\langle\Psi_g| + |\Psi_g\rangle\langle\Psi_n|),$$

where $\boldsymbol{\mu}_n$ are the transition dipole moments. With this form the dipole-dipole correlation function can be written as

$$M(t) = e^{iE_g t}\sum_n |\boldsymbol{\mu}_n\cdot\boldsymbol{\epsilon}|^2\langle\Psi_n|\mathcal{U}_t'|\Psi_n\rangle - e^{-iE_g t}\sum_n |\boldsymbol{\mu}_n\cdot\boldsymbol{\epsilon}|^2\langle\Psi_n|\mathcal{U}_t'^{\dagger}|\Psi_n\rangle . \tag{1.36}$$

1.6.3 Linear Absorption Coefficient

The linear absorption spectrum can now be obtained from (1.33)

$$\mathcal{A}(\omega) = \frac{4\pi\omega}{n}\text{Im}\chi(\omega).$$

Here $\chi(\omega)$ is the Fourier transform of $\chi(\tau)$

$$\chi(\omega) = \int_{-\infty}^{\infty} \mathrm{d}\tau\chi(\tau)e^{i\omega\tau}$$

We can express the absorption spectrum directly in terms of the dipole-dipole correlation function

$$\begin{aligned} \mathcal{A}(\omega) &= \frac{4\pi\omega}{n}\text{Im}\left[\int_{-\infty}^{\infty}\mathrm{d}\tau i\Theta(\tau)M(\tau)e^{i\omega\tau}\right] \\ &= \frac{4\pi\omega}{n}\text{Re}\int_0^{\infty}\mathrm{d}\tau M(\tau)e^{i\omega\tau}. \end{aligned} \tag{1.37}$$

We are considering only positive frequencies $\omega > 0$, so using (1.36) and discarding the antiresonant contribution we get

$$\mathcal{A}(\omega) = \frac{4\pi\omega}{n} \sum_k |\boldsymbol{\mu}_k \cdot \boldsymbol{\epsilon}|^2 \mathrm{Re} \int_0^\infty \mathrm{d}\tau e^{i(\omega+E_g)\tau} \langle \Psi_k | \mathcal{U}_t' | \Psi_k \rangle .$$

If we further consider a two-level system, we have

$$\mathcal{A}(\omega) = \frac{4\pi\omega}{n} |\tilde{\boldsymbol{\mu}} \cdot \boldsymbol{\epsilon}|^2 \mathrm{Re} \int_0^\infty \mathrm{d}\tau e^{i(\omega+E_g)\tau} \langle \Psi(0) | \Psi(t) \rangle , \tag{1.38}$$

where $\tilde{\boldsymbol{\mu}}$ is the two-level transition dipole moment (1.20) and $|\Psi(t)\rangle = \mathcal{U}_t' |\Psi(0)\rangle$ with $|\Psi(0)\rangle = |\Psi_X\rangle = |X\rangle \langle g|\Psi_g\rangle$.

As an example, it is straightforward to calculate the absorption spectrum for the independent boson model discussed in section 1.2. Here we set the ground state energy $E_g = 0$, so for the absorption spectrum we have from (1.38)

$$\mathcal{A}(\omega) \propto \mathrm{Re} \int_0^\infty \mathrm{d}\tau e^{i\omega\tau} \langle \Psi(0) | \Psi(t) \rangle .$$

In this case it is easy to verify, by using (1.11) and (1.8), that the ground state $|\Psi_g\rangle = |g\rangle |\mathbf{0}\rangle$ is an eigenstate. Then $|\Psi(0)\rangle = |\Psi_X\rangle = |X\rangle |\mathbf{0}\rangle$ and inserting equation (1.10) into (1.9) we obtain

$$h(t) = \exp\left(-i\omega_X t + i \sum_\lambda \frac{g_\lambda^2}{\omega_\lambda} t - \sum_\lambda \frac{g_\lambda^2}{\omega_\lambda^2} (1 - e^{-i\omega_\lambda}) + \frac{1}{2} \sum_\lambda |z_{X,\lambda}(t)|^2 \right) .$$

For the overlap $\langle \Psi(0)|\Psi(t)\rangle$ we now get

$$\begin{aligned} \langle \Psi(0)|\Psi(t)\rangle &= \langle X| \langle \mathbf{0}| h(t) |X\rangle |\mathbf{z}_X(t)\rangle \\ &= \exp\left(-i(\omega_X - \sum_\lambda \frac{g_\lambda^2}{\omega_\lambda}) t - \sum_\lambda \frac{g_\lambda^2}{\omega_\lambda^2} (1 - e^{-i\omega_\lambda}) \right) . \end{aligned}$$

In the continuum limit, with the spectral density (1.5), we have

$$\langle \Psi(0)|\Psi(t)\rangle = \exp\left(-i\omega_X' t - \int d\omega \frac{J(\omega)}{\omega^2} (1 - e^{-i\omega t}) \right) ,$$

with the phonon-shifted transition energy ω_X' defined in (1.16). To ease the subsequent calculations, we add a damping term of $-\gamma t$ to the exponent. For all calculations, we set $\gamma = 0.015$ ps^{-1}.

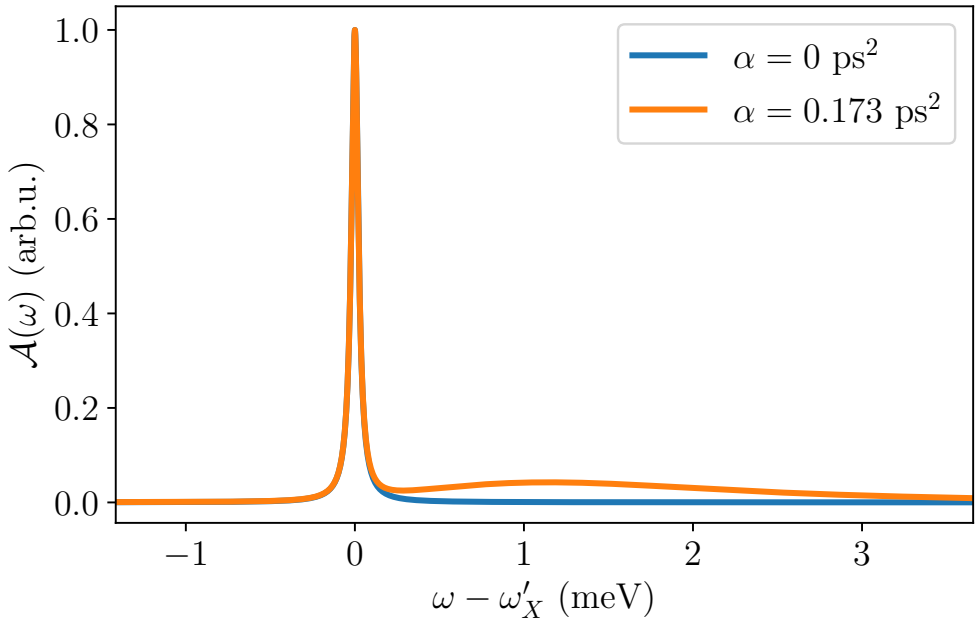

Figure 2. Linear absorption spectra for the independent boson model both with and without coupling to the environment with the cut-off frequency $\xi = 1.447$ meV.

Figure 2 shows the absorption spectrum for the independent boson model with and without coupling to the reservoir phonons. In the case of no coupling, a singular peak is observed at the transition energy which in this case is the same as the phonon-shifted transition energy ω'_X due to the lack of coupling. The finite width of the singular peak is due to the added damping term. When the coupling is present, a clear asymmetry appears to the right of the peak which is due to the phonon reservoir. We used the spectral density specific to our QD system defined in equation (1.6).

Figure 3 shows the linear absorption spectrum with different spectral density parameters. In figure 3(a) the cut off frequency is varied and in figure 3(b) the coupling strength is varied. In both cases, as expected, the peak is clearly shifted since the phonon-shifted transition energy decreases as the coupling strength increases. As already seen in figure 2 the phonon reservoir induced asymmetry in the spectrum

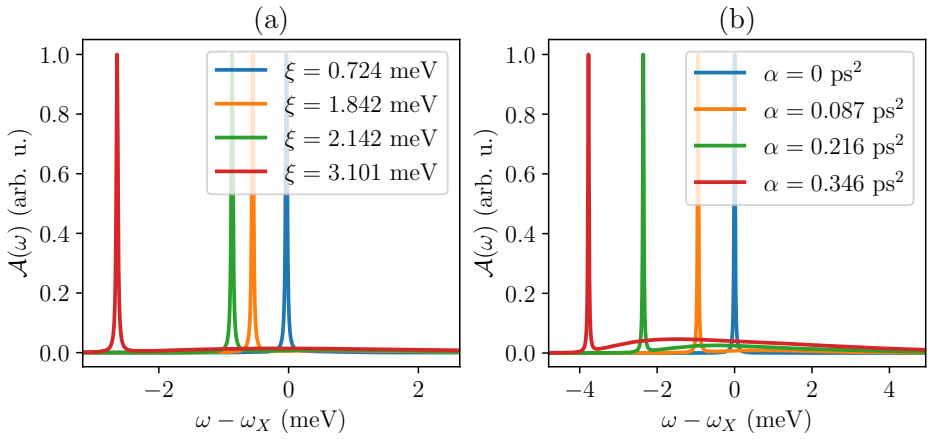

Figure 3. Linear absorption spectra for the independent boson model with different (a) environment coupling strengths α and (b) spectral density cut-off frequencies ξ. For (a) the coupling strength is $\alpha = 0.087$ ps^2 and for (b) the cut-off frequency is $\xi = 1.447$ meV.

appears and gets spread out as α and ξ increase.

1.7 Spectrum of Resonance Fluorescence

The spectrum of resonance fluorescence is another important experimentally accessible quantity of quantum optics and was first theoretically studied by Mollow in [45]. In this section we will derive the equation for the spectrum of resonance fluorescence. We start with relating the radiated output field to the system operators. Finally we express the emission intensity spectrum in terms of a correlation function involving only system operators.

1.7.1 Output Field

Let us consider the total Hamiltonian (1.1) in frame rotating at frequency ω_D. Performing the rotating-wave approximation, we have for the QD Hamiltonian

$$H_S = \Delta \left|X\right\rangle \left\langle X\right|$$

with the detuning $\Delta = \omega_X - \omega_D$ and the drive Hamiltonian

$$H_D = \frac{\Omega}{2}(|g\rangle\langle X| + |X\rangle\langle g|)$$

and the exciton-cavity interaction Hamiltonian (1.24) has the form

$$H_{I,\mathrm{Pt}} = \sum_\lambda u_\lambda (e^{-i\omega_D t}|g\rangle\langle X| b_\lambda^\dagger + e^{i\omega_D t}|X\rangle\langle g| b_\lambda),$$

with the other Hamiltonians staying unchanged. Now we consider the electric field operator

$$\mathbf{E}(t) = \mathbf{E}_+(t) + \mathbf{E}_-(t),$$

where

$$\mathbf{E}_+(t) = \sum_\lambda E_\lambda^0 \boldsymbol{\epsilon}_\lambda b_\lambda(t),$$

with the field amplitude $E_\lambda^0 = \sqrt{\frac{\omega_\lambda}{2\epsilon_0 V}}$, polarization $\boldsymbol{\epsilon}_\lambda$ and $\mathbf{E}_-(t) = \mathbf{E}_+^\dagger(t)$. Our goal is to find a relation between the field operators and the system operators. By considering the Heisenberg equation of motion for the ladder operators with the total Hamiltonian we get

$$\frac{d}{dt}b_\lambda(t) = -i[b_\lambda(t), H] = -i\omega_\lambda b_\lambda(t) - iu_\lambda e^{-i\omega_D t}\sigma_-(t),$$

where $\sigma_- = |g\rangle\langle X|$. This has the formal solution

$$b_\lambda(t) = e^{-i\omega_\lambda t}b_\lambda(0) - i\int_0^t \mathrm{d}s u_\lambda e^{-i\omega_D s}\sigma_-(s)e^{-i\omega_\lambda(t-s)}.$$

Inserting this into $\mathbf{E}_+(t)$ gives us the positive frequency component

$$\mathbf{E}_+(t) = \sum_\lambda E_\lambda^0 \boldsymbol{\epsilon}_\lambda e^{-i\omega_\lambda t}b_\lambda(0) - i\sum_\lambda E_\lambda^0\boldsymbol{\epsilon}_\lambda \int_0^t \mathrm{d}s u_\lambda e^{-i\omega_D s}\sigma_-(s)e^{-i\omega_\lambda(t-s)}.$$

The free field evolution that would be obtained when the QD is absent is described by the first term. It remains in the vacuum state so it can be ignored since it

doesn't contribute to the field correlation functions. Now we assume that the light-matter coupling is approximately constant $u_\lambda \approx \sqrt{\kappa}$ and $E^0_\lambda \approx E^0$ [46] and take the continuum limit

$$\begin{aligned} E(t) &\approx -iE^0\sqrt{\kappa}\int_0^t \mathrm{d}s \int_{-\infty}^{\infty} \mathrm{d}\omega e^{-i\omega_D s}\sigma_-(s)e^{-i\omega(t-s)} \\ &= -2i\pi E^0\sqrt{\kappa}\int_0^t \mathrm{d}s e^{-i\omega_D s}\sigma_-(s)\delta(t-s) \\ &= -i\pi E^0\sqrt{\kappa}e^{-i\omega_D t}\sigma_-(t). \end{aligned} \tag{1.39}$$

Note that we have dropped the polarization vectors since they induce geometric factors for the field correlation functions but do not affect their qualitative behaviour [47].

1.7.2 Emission Spectrum

Thus far, we have derived a relationship between the system's internal dynamics and the output field. We can now determine the emission spectrum under resonant driving conditions, i.e., when we consider resonance fluorescence. The Wiener-Khinchin theorem states that for a stationary random process, the spectral decomposition of the autocorrelation function can be obtained from the power spectral density of the process [48]. More precisely, the power spectral density is the Fourier transform of the autocorrelation function. Utilizing the optical Wiener-Kinchin theorem and equation (1.39), we can express the emission intensity spectrum as [19]

$$\begin{aligned} I(\omega) &= \frac{1}{2\pi}\int_{-\infty}^{\infty} \mathrm{d}\tau \left\langle E_-(t)E_+(t+\tau)\right\rangle \\ &= (E^0)^2\pi^2\kappa \int_{-\infty}^{\infty} \mathrm{d}\tau \left\langle \sigma_+(t)\sigma_-(t+\tau)\right\rangle e^{i(\omega-\omega_D)\tau}. \end{aligned}$$

The spectral component can then be defined as the Fourier transform [19]

$$S(\omega) = \lim_{t\to\infty} I(\omega) = \frac{1}{2\pi}\int_{-\infty}^{\infty} \mathrm{d}\tau g^{(1)}(\tau)e^{i(\omega-\omega_D)\tau},$$

where $g^{(1)}(\tau)$ is the system first order correlation function in the long time limit

$$\begin{aligned} g^{(1)}(\tau) &= \lim_{t\to\infty} \langle \sigma_+(t)\sigma_-(t+\tau)\rangle \\ &= \lim_{t\to\infty} \mathrm{tr}\{\sigma_+(t)\sigma_-(t+\tau)\rho(0)\} \\ &= \lim_{t\to\infty} \mathrm{tr}\{\sigma_+\sigma_-(\tau)\rho(t)\} \\ &= \langle \sigma_+\sigma_-(\tau)\rangle_{ss}\,, \end{aligned}$$

where the subscript denotes the steady state expectation value.

The spectrum decomposes into two components

$$S(\omega) = S_{\mathrm{coh}}(\omega) + S_{\mathrm{inc}}(\omega),$$

where $S_{\mathrm{coh}}(\omega)$ corresponds to coherent scattering and $S_{\mathrm{inc}}(\omega)$ corresponds to incoherent scattering which arises from quantum fluctuations [47]. These can be expressed as

$$\begin{aligned} S_{\mathrm{coh}}(\omega) &= \frac{1}{2\pi}\int_{-\infty}^{\infty} \mathrm{d}\tau\, \langle \sigma_+\rangle_{ss} \langle \sigma_-\rangle_{ss} e^{i(\omega-\omega_D)\tau} = \langle \sigma_+\rangle_{ss} \langle \sigma_-\rangle_{ss}\, \delta(\omega-\omega_D) \\ S_{\mathrm{inc}}(\omega) &= \frac{1}{2\pi}\int_{-\infty}^{\infty} \mathrm{d}\tau\, \langle \tilde{\sigma}_+\tilde{\sigma}_-(\tau)\rangle_{ss} e^{i(\omega-\omega_D)\tau}, \end{aligned} \tag{1.40}$$

where we have defined

$$\tilde{\sigma}_\pm(t) = \sigma_\pm(t) - \langle \sigma_\pm\rangle_{ss}\,,$$

with the steady state expectation values $\langle \sigma_\pm\rangle_{ss} = \mathrm{tr}\{\sigma_\pm\rho(\infty)\}$. Evidently the operators $\tilde{\sigma}_\pm(t)$ characterise the fluctuations of $\sigma_+(t)$ and $\sigma_-(t)$ from their steady state values. As expected, the coherent scattering produces a singular peak at the driving frequency. The incoherent scattering has to be calculated by other means, e.g. via the quantum regression theorem.

2 Non-Markovian Quantum State Diffusion

In the theory of open quantum systems, the evolution of the reduced density matrix is given by the linear map

$$\rho_{\mathrm{S}}(t) = \mathcal{L}(\rho_{\mathrm{S}}).$$

This form does not take into consideration whether the quantum process is Markovian or non-Markovian. For a Markovian process, the evolution is described by the Gorini-Kossakowski-Sudarshan-Lindblad (GKSL) master equation [49, 50]

$$\partial_t \rho_{\mathrm{S}}(t) = -i[H, \rho_{\mathrm{S}}(t)] + \sum_m \gamma_m \left(L_m \rho_{\mathrm{S}}(t) L_m^\dagger - \frac{1}{2}\{L_m^\dagger L_m, \rho_{\mathrm{S}}(t)\} \right),$$

where $\gamma_m \geq 0$ are the decay rates and L_m are the jump operators describing the decoherence and dissipation, i.e., how the environment acts on the system. The GKSL master equation applies to many physically relevant scenarios and allows for both analytical and numerical solutions.

This can be unraveled into stochastic quantum trajectories or stochastic unravelings [47]. Such unravelings are stochastic Schrödinger equations (SSE) for the state $|\psi_t(z^*)\rangle$ where z_t^* is a stochastic noise process, such that the mean of the solutions of the SSE is equal to the density operator

$$\rho_{\mathrm{S}}(t) = \mathcal{M}[|\psi_t(z^*)\rangle \langle\psi_t(z^*)|].$$

However, these unravelings are not unique; in fact there exist infinitely many for any master equation. Some notable examples of these unravelings include the Monte Carlo wave-function method, also known as quantum jump trajectories [47, 51, 52], and the quantum state diffusion (QSD) unraveling [53].

The stochastic unraveling of the master equation can also be studied for non-Markovian processes. One notable such unraveling is the non-Markovian quantum state diffusion (NMQSD) [24, 54], which, in the Markovian limit, reduces to the QSD unraveling. In this section we will present NMQSD. First, we will present

the unnormalized coherent states and their properties required for the subsequent derivations. Following that, we will perform the derivation of the linear NMQSD equation considering zero temperature, and subsequently derive a non-linear version of the NMQSD equation. For these derivations, we follow refs. [24, 54, 55]. Finally, we will incorporate finite temperature into the model in various ways.

2.1 Bargmann Coherent States

The Bargmann coherent states [56] are defined as

$$||z\rangle = e^{za^\dagger} |0\rangle = \sum_n \frac{z^n}{\sqrt{n!}} |n\rangle ,$$

where $z \in \mathbb{C}$. Comparing them to the Glauber coherent states

$$|z\rangle = D(z) |0\rangle = e^{-\frac{1}{2}|z|^2} e^{za^\dagger} |0\rangle ,$$

it is evident that the Bargmann states lack the normalization factor and are thus also called unnormalized coherent states. Notably, Bargmann states depend solely on the complex number z and not its conjugate.

Bargmann coherent states have some important properties. Firstly the resolution of identity

$$\int \mathrm{d}^2 z \frac{e^{-|z|^2}}{\pi} ||z\rangle \langle z|| = \mathbb{1}, \tag{2.1}$$

where $\mathrm{d}^2 z = \mathrm{dRe}(z)\mathrm{dIm}(z)$. Any state $|\psi\rangle$ can be mapped to an analytic function

$$f(z^*) = \langle z||\psi\rangle . \tag{2.2}$$

The argument z^* is justified since Bargmann states depend solely on z. The creation and annihilation operators act on the analytic function as

$$\langle z||a|\psi\rangle = \frac{\partial}{\partial z^*} f(z^*), \ \langle z||a^\dagger|\psi\rangle = z^* f(z^*). \tag{2.3}$$

Another key property is a type of orthogonality

$$f(\tilde{z}^*) = \int \mathrm{d}^2 z \frac{e^{-|z|^2}}{\pi} f(z^*) \langle \tilde{z} || z \rangle \,. \tag{2.4}$$

Note that Bargmann coherent states are not orthogonal. In the multimode case we have

$$||\mathbf{z}\rangle = \prod_\lambda e^{z_\lambda a_\lambda^\dagger} |\mathbf{0}\rangle \,,$$

and the aforementioned properties generalize accordingly.

2.2 Linear NMQSD

Let us consider a system that is linearly coupled to an environment which is modeled as a bath of quantum harmonic oscillators. The total Hamiltonian is given by

$$H = H_\mathrm{S} + H_\mathrm{E} + H_\mathrm{I},$$

where H_S is the system Hamiltonian, arbitrary for now, $H_\mathrm{E} = \sum_\lambda \omega_\lambda a_\lambda^\dagger a_\lambda$ the environment Hamiltonian and system-environment interaction Hamiltonian is given by

$$H_\mathrm{I} = \sum_\lambda (g_\lambda^* L a_\lambda^\dagger + g_\lambda L^\dagger a_\lambda).$$

Here the operator L is an operator in the system's Hilbert space and $g_\lambda \in \mathbb{C}$ quantifies the coupling strength of the system and the mode ω_λ. By moving to the interaction picture with respect to H_E we get the following Schrödinger equation for the total state $|\Psi_t\rangle$

$$\partial_t |\Psi_t\rangle = -iH_\mathrm{S} |\Psi_t\rangle - i \left(L B^\dagger(t) + L^\dagger B(t) \right) |\Psi_t\rangle \,, \tag{2.5}$$

where the operator $B(t)$ is given by

$$B(t) = \sum g_\lambda e^{-i\omega_\lambda t} a_\lambda.$$

The dynamics of the system is clearly influenced by the environment operator $B(t)$ whose statistical properties are characterized by the bath correlation function (BCF) $\alpha(t,s)$. The BCF provides information about how the system and environment are correlated in time and characterizes the memory of the environmental fluctuations. In this case it is given by [39]

$$\alpha(t,s) = \mathrm{tr_E}\{(B(t)+B^\dagger(t))(B(s)+B^\dagger(s))\rho_\mathrm{E}\}.$$

If we assume that the environment is in the thermal state and $\mathrm{tr}\{a_\lambda^\dagger \rho_\mathrm{E}\} = \mathrm{tr}\{a_\lambda \rho_\mathrm{E}\} = 0$, we find the bath correlation kernel of the quantum Brownian motion model [57]

$$\alpha(t-s) = \sum_\lambda |g_\lambda|^2 \left(\coth\left(\frac{\beta\omega_\lambda}{2}\right)\cos(\omega_\lambda(t-s)) - i\sin(\omega_\lambda(t-s))\right). \tag{2.6}$$

Recalling the definition for the spectral density (1.5), we can write in the continuum limit

$$\alpha(\tau) = \int_0^\infty \mathrm{d}\omega J(\omega)\left(\coth\left(\frac{\beta\omega}{2}\right)\cos(\omega\tau) - i\sin(\omega\tau)\right),$$

where $\tau = t-s$.

Now we eliminate the bath operators. To do this we consider zero temperature case. The BCF then obtains the form

$$\alpha(\tau) = \sum_\lambda |g_\lambda|^2 e^{-i\omega_\lambda\tau}.$$

The state vector can be expressed in terms of the Bargmann coherent states

$$|\Psi_t\rangle = \int \prod_\lambda \mathrm{d}^2 z_\lambda \frac{e^{-|z_\lambda|^2}}{\pi} |\psi_t(\mathbf{z}^*)\rangle \, ||\mathbf{z}\rangle,$$

where $|\psi_t(\mathbf{z}^*)\rangle = \langle \mathbf{z}||\Psi_t\rangle$. The reduced density matrix can now be obtained by tracing over the environment

$$\begin{aligned}
\rho_\mathrm{S}(t) &= \mathrm{tr_E}\{|\Psi_t\rangle\langle\Psi_t|\} \\
&= \int \prod_\lambda \mathrm{d}^2 z_\lambda \frac{e^{-|z_\lambda|^2}}{\pi} \langle \mathbf{z}||\Psi_t\rangle\langle\Psi_t||\mathbf{z}\rangle \\
&= \int \prod_\lambda \mathrm{d}^2 z_\lambda \frac{e^{-|z_\lambda|^2}}{\pi} |\psi_t(\mathbf{z}^*)\rangle\langle\psi_t(\mathbf{z})|.
\end{aligned}$$

The crucial step is to interpret this in a Monte-Carlo sense. The coherent state amplitudes z_λ are turned into complex valued Gaussian distributed random variables with zero mean

$$\mathcal{M}[z_\lambda] = \mathcal{M}[z_\lambda^*] = 0 \tag{2.7}$$

and covariance

$$\mathcal{M}[z_\lambda z_\mu] = \mathcal{M}[z_\lambda^* z_\mu^*] = 0,\ \mathcal{M}[z_\lambda z_\mu^*] = \delta_{\lambda\mu}. \tag{2.8}$$

Thus the reduced density matrix can be regarded as an ensemble average

$$\rho_{\mathrm{S}}(t) = \mathcal{M}[|\psi_t(\mathbf{z}^*)\rangle \langle\psi_t(\mathbf{z})|].$$

Next we find the equation of motion for $|\psi_t(\mathbf{z}^*)\rangle$. Since we are considering zero temperature, we assume the initial condition $|\Psi_0\rangle = |\psi_0\rangle |\mathbf{0}\rangle$. Applying $\langle\mathbf{z}||$ on both sides of equation (2.5) and using the properties (2.3) we get

$$\partial_t |\psi_t(\mathbf{z}^*)\rangle = -iH_{\mathrm{S}} |\psi_t(\mathbf{z}^*)\rangle + z_t^* L |\psi_t(\mathbf{z}^*)\rangle - iL^\dagger \sum_\lambda g_\lambda e^{-i\omega_\lambda t} \langle\mathbf{z}||a_\lambda \mathcal{U}_t|\Psi_0\rangle , \tag{2.9}$$

where $\mathcal{U}_t$ is the propagator in the interaction picture and we have defined

$$z_t^* = -i \sum_\lambda g_\lambda^* z_\lambda^* e^{i\omega_\lambda t}. \tag{2.10}$$

The last term in (2.9) can be written as

$$\langle\mathbf{z}||a_\lambda \mathcal{U}_t|\Psi_0\rangle = \langle\mathbf{z}||\mathcal{U}_t a_\lambda(t)|\Psi_0\rangle .$$

Here the Heisenberg equation of motion for $a_\lambda(t)$, with initial condition $a_\lambda(0) = a_\lambda$, can be formally solved to yield

$$a_\lambda(t) = a_\lambda - i \int_0^t \mathrm{d}s g_\lambda e^{i\omega_\lambda s} L(s), \tag{2.11}$$

where $L(s) = \mathcal{U}_s^\dagger L \mathcal{U}_s$. Inserting this back into (2.9) we have in the continuum limit

$$\partial_t |\psi_t(\mathbf{z}^*)\rangle = -iH_{\mathrm{S}} |\psi_t(\mathbf{z}^*)\rangle + z_t^* L |\psi_t(\mathbf{z}^*)\rangle - iL^\dagger \int_0^t \mathrm{d}s \alpha(t-s) \langle\mathbf{z}||\mathcal{U}_t L(s)|\Psi_0\rangle . \tag{2.12}$$

As discussed above, by the Monte-Carlo interpretation, the function z_t^* turns into a stochastic process. By using (2.7) and (2.8) we obtain the statistics

$$\mathcal{M}[z_t] = \mathcal{M}[z_t^*] = \mathcal{M}[z_t^* z_s^*] = \mathcal{M}[z_t z_s] = 0,$$
$$\mathcal{M}[z_t z_s^*] = \alpha(t-s),$$

i.e., the process z_t^* is determined by the BFC.

To obtain the standard form the NMQSD equation, we can study the mean $\mathcal{M}[z_t \left|\psi_t(\mathbf{z}^*)\right\rangle \left\langle\psi_t(\mathbf{z})\right|]$. Using the properties of the Bargmann states and the evolution of $a_\lambda(t)$ we have

$$\begin{aligned}\mathcal{M}[z_t \left|\psi_t(\mathbf{z}^*\right\rangle \left\langle\psi_t(\mathbf{z})\right|] &= i\sum_\lambda g_\lambda e^{-i\omega_\lambda t}\mathcal{M}[z_\lambda \left|\psi_t(\mathbf{z}^*\right\rangle \left\langle\psi_t(\mathbf{z})\right|] \\ &= i\sum_\lambda g_\lambda e^{-i\omega_\lambda t}\mathcal{M}[\left\langle\mathbf{z}\right|\left|a_\lambda\right|\Psi_t\rangle \left\langle\psi_t(\mathbf{z})\right|] \\ &= \int_0^t \mathrm{d}s\alpha(t-s)\mathcal{M}[\left\langle\mathbf{z}\right|\left|\mathcal{U}_t L(s)\right|\Psi_0\rangle \left\langle\psi_t(\mathbf{z})\right|].\end{aligned}$$

On the other hand the Furutsu-Novikov theorem [58–60] states that

$$\begin{aligned}\mathcal{M}[z_t \left|\psi_t(\mathbf{z}^*)\right\rangle \left\langle\psi_t(\mathbf{z})\right|] &= \int_0^t \mathrm{d}s\mathcal{M}[z_t z_s^*]\mathcal{M}\left[\frac{\delta}{\delta z_s^*}\left|\psi_t(\mathbf{z}^*)\right\rangle \left\langle\psi_t(\mathbf{z})\right|\right] \\ &= \int_0^t \mathrm{d}s\alpha(t-s)\mathcal{M}\left[\frac{\delta}{\delta z_s^*}\left|\psi_t(\mathbf{z}^*)\right\rangle \left\langle\psi_t(\mathbf{z})\right|\right].\end{aligned}$$

Thus we have

$$\left\langle\mathbf{z}\right|\left|\mathcal{U}_t L(s)\right|\Psi_0\rangle = \frac{\delta}{\delta z_s^*}\left|\psi_t(\mathbf{z}^*)\right\rangle.$$

Inserting this into (2.12) we obtain the linear NMQSD equation

$$\partial_t \left|\psi_t(z^*)\right\rangle = -iH_\mathrm{S}\left|\psi_t(z^*)\right\rangle - z_t^* L\left|\psi_t(z^*)\right\rangle - L^\dagger\int_0^t \mathrm{d}s\alpha(t-s)\frac{\delta}{\delta z_s^*}\left|\psi_t(z^*)\right\rangle. \quad (2.13)$$

Here we have denoted the dependence on $\mathbf{z}^*$ by z^* due to the fact that z_t^* is linearly dependent on $\mathbf{z}^*$.

The NMQSD equation is a stochastic differential equation. The reduced density matrix is obtained by solving it with many independent realisations of the noise z_t^*

and then taking the ensemble average $\mathcal{M}[|\psi_t(z^*)\rangle\langle\psi_t(z)|]$. The difficulty arises from the functional derivative because it is generally difficult to determine how it acts on the state $|\psi_t(z^*)\rangle$. One way to determine it is through the Ansatz [24]

$$\frac{\delta|\psi_t(z_t^*)\rangle}{\delta z_s^*} = \mathcal{O}(t,s,\mathbf{z}^*)|\psi_t(z_t^*)\rangle, \tag{2.14}$$

and requiring the consistency condition

$$\frac{\partial}{\partial t}\frac{\delta}{\delta z_s^*}|\psi_t(z_t^*)\rangle = \frac{\delta}{\delta z_s^*}\frac{\partial}{\partial t}|\psi_t(z_t^*)\rangle.$$

Inserting the Ansatz (2.14) into the linear NMQSD gives

$$\partial_t|\psi_t(z_t^*)\rangle = (-iH_\mathrm{S} + z_t^*L - L^\dagger\bar{\mathcal{O}}(t,\mathbf{z}^*))|\psi_t(z_t^*)\rangle,$$

where $\bar{\mathcal{O}}(t,\mathbf{z}^*) = \int_0^t \mathrm{d}s\alpha(t-s)\mathcal{O}(t,s,\mathbf{z}^*)$. Now using the consistency condition we find the formal equation of motion for the operator $\mathcal{O}(t,s,\mathbf{z}^*)$

$$\partial_t\mathcal{O}(t,s,\mathbf{z}^*) = [-iH_\mathrm{S} + z_t^*L - L^\dagger\bar{\mathcal{O}}(t,\mathbf{z}^*),\mathcal{O}(t,s,\mathbf{z}^*)] - L^\dagger\frac{\delta\bar{\mathcal{O}}(t,\mathbf{z}^*)}{\delta z_s^*}, \tag{2.15}$$

which has to be then solved for all s with the initial condition $\mathcal{O}(t,s,\mathbf{z}^*) = L$.

2.3 Non-linear NMQSD

The linear NMQSD doesn't preserve the norm $||\psi_t(z^*)||$ and consequently each trajectory contribute with different weight to the ensemble

$$\rho_\mathrm{S}(t) = \mathcal{M}[|\psi_t(z^*)\rangle\langle\psi_t(z)|] = \int\prod_\lambda \mathrm{d}^2z_\lambda\frac{e^{-|z_\lambda|^2}}{\pi}\langle\psi_t(z)|\psi_t(z^*)\rangle\frac{|\psi_t(z^*)\rangle\langle\psi_t(z)|}{\langle\psi_t(z)|\psi_t(z^*)\rangle}.$$

For strong system-environment coupling, this becomes especially problematic since the norm of the trajectories may vary significantly [55]. In theory this isn't a problem since we would consider infinite number of trajectories. In practice, we have to limit to finite number of trajectories to approximate the ensemble mean. Consequently, a few trajectories may dominate the ensemble, rendering other realizations obsolete. This problem can be remedied by using importance sampling [61, 62]. In this case, it

is done through the Girsanov transform [63]. Ultimately, this leads to the non-linear NMQSD equation.

We begin by writing the reduced density matrix

$$\begin{aligned}\rho_{\mathrm{S}}(t) &= \mathcal{M}[|\psi_t(z^*)\rangle \langle\psi_t(z)|] \\ &= \int \prod_\lambda \mathrm{d}^2 z_\lambda \frac{e^{-|z_\lambda|^2}}{\pi} |\psi_t(z^*)\rangle \langle\psi_t(z)| \\ &= \int \prod_\lambda \mathrm{d}^2 z_\lambda \frac{e^{-|z_\lambda|^2}}{\pi} ||\psi_t(z^*)||^2 \frac{|\psi_t(z^*)\rangle \langle\psi_t(z)|}{||\psi_t(z^*)||^2} \\ &= \int \mathrm{d}^2\mathbf{z} Q_t(\mathbf{z},\mathbf{z}^*) \frac{|\psi_t(z^*)\rangle \langle\psi_t(z)|}{||\psi_t(z^*)||^2}\end{aligned}$$

and identifying the Husimi Q-function [35]

$$Q_t(\mathbf{z},\mathbf{z}^*) = \prod_\lambda \frac{e^{-|z_\lambda|^2}}{\pi} \langle\Psi_t||\mathbf{z}\rangle \langle\mathbf{z}||\Psi_t\rangle .$$

Utilizing (2.5), we can consider the time evolution of the Husimi function

$$\begin{aligned}\partial_t Q_t(\mathbf{z},\mathbf{z}^*) &= \prod_\lambda \frac{e^{-|z_\lambda|^2}}{\pi} (\langle\dot{\Psi}_t||\mathbf{z}\rangle \langle\mathbf{z}||\Psi_t\rangle + \langle\Psi_t||\mathbf{z}\rangle \langle\mathbf{z}||\dot{\Psi}_t\rangle) \\ &= -\sum_\lambda \frac{\partial}{\partial z_\lambda^*} [i g_\lambda e^{-i\omega_\lambda t} \langle L^\dagger\rangle_t Q_t(\mathbf{z},\mathbf{z}^*)] + h.c.\end{aligned}$$

where $\langle L^\dagger\rangle_t = \frac{\langle\psi_t(\mathbf{z})|L^\dagger|\psi_t(\mathbf{z})\rangle}{||\psi_t(\mathbf{z}^*)||^2}$. Since the Husimi Q-function can be regarded as a pseudo probability distribution, namely it is normalized, we can interpret the time evolution above as the Liouville equation [64]. The Liouville equation describes deterministic drift with

$$\dot{z}_\lambda^*(t) = i g_\lambda e^{-i\omega_\lambda t} \langle L^\dagger\rangle_t \tag{2.16}$$

for which we have

$$Q_t(\mathbf{z},\mathbf{z}^*) = \int \prod_\lambda \mathrm{d}^2 z_{\lambda,0} Q_0(\mathbf{z}_0,\mathbf{z}_0^*) \delta^2(\mathbf{z} - \mathbf{z}_t(\mathbf{z}_0)).$$

The ordinary differential equation (2.16) has the formal solution

$$\tilde{z}_\lambda^*(t) = z_\lambda^* + i g_\lambda \int_0^t \mathrm{d}s e^{-i\omega_\lambda s} \langle L^\dagger\rangle_s .$$

This leads to a shifted noise process

$$\begin{aligned}\tilde{z}_t^* &= -i\sum_\lambda g_\lambda^* \tilde{z}_\lambda^* e^{i\omega_\lambda t} \\ &= -i\sum_\lambda g_\lambda^* z_\lambda^* e^{i\omega_\lambda t} + \int_0^t \mathrm{d}s \sum_\lambda |g_\lambda|^2 e^{i\omega_\lambda (t-s)} \left\langle L^\dagger \right\rangle_s \\ &= z_t^* + \int_0^t \mathrm{d}s \alpha^*(t-s) \left\langle L^\dagger \right\rangle_s . \end{aligned} \tag{2.17}$$

The reduced density matrix is now given by the modified ensemble average

$$\begin{aligned}\rho_{\mathrm{S}}(t) &= \int \mathrm{d}^2\mathbf{z} Q_t(\mathbf{z},\mathbf{z}^*) \frac{|\psi_t(\mathbf{z}^*)\rangle \langle\psi_t(\mathbf{z})|}{||\psi_t(\mathbf{z}^*)||^2} \\ &= \int d^2\mathbf{z} \int \mathrm{d}^2\mathbf{z}_0 Q_0(\mathbf{z}_0,\mathbf{z}_0^*)\delta^2(\mathbf{z}-\tilde{\mathbf{z}}_t(\mathbf{z}_0)) \frac{|\psi_t(\mathbf{z}^*)\rangle \langle\psi_t(\mathbf{z})|}{||\psi_t(\mathbf{z}^*)||^2} \\ &= \int \prod_\lambda \mathrm{d}^2 z_{\lambda,0} \frac{e^{-|z_{\lambda,0}|^2}}{\pi} \frac{|\psi_t(\tilde{\mathbf{z}}^*)\rangle \langle\psi_t(\tilde{\mathbf{z}})|}{||\psi_t(\tilde{\mathbf{z}}^*)||^2} \\ &= \mathcal{M}\left[\frac{|\psi_t(\tilde{\mathbf{z}}^*)\rangle \langle\psi_t(\tilde{\mathbf{z}})|}{||\psi_t(\tilde{\mathbf{z}}^*)||^2}\right]. \end{aligned}$$

Clearly now each realisation is taken into account with equal weight which will prove to be important for numerical performance. By utilizing the linear NMQSD equation (2.13) with the new shifted noise process, we obtain

$$\begin{aligned}\frac{d}{dt}|\psi_t(\tilde{z}^*)\rangle =& \frac{\partial |\psi_t(\tilde{z}^*)\rangle}{\partial t} + \sum_\lambda \frac{\partial z_\lambda^*(t)}{\partial t} \frac{\partial |\psi_t(\tilde{z}^*)\rangle}{\partial z_\lambda^*} \\ =& \left[-iH_{\mathrm{S}} + \tilde{z}_t^* L - L^\dagger \int_0^t \mathrm{d}s \alpha(t-s) \frac{\delta}{\delta \tilde{z}_s^*}\right] |\psi_t(\tilde{z}^*)\rangle \\ &+ \sum_\lambda i g_\lambda e^{-i\omega_\lambda t} \left\langle L^\dagger \right\rangle_t \langle \tilde{\mathbf{z}}||a_\lambda \mathcal{U}_t|\Psi_0\rangle . \end{aligned}$$

Treating the last term the same way as for the linear NMQSD equation, we obtain finally the sought after non-linear NMQSD equation

$$\partial_t |\psi_t(\tilde{z}^*)\rangle = -iH_{\mathrm{S}}|\psi_t(\tilde{z}^*)\rangle + \tilde{z}_t^* L|\psi_t(\tilde{z}^*)\rangle - (L^\dagger - \langle L^\dagger\rangle_t)\int_0^t \mathrm{d}s \alpha(t-s)\frac{\delta}{\delta \tilde{z}_s^*}|\psi_t(\tilde{z}^*)\rangle . \tag{2.18}$$

2.4 Finite Temperature

2.4.1 Encoding the Temperature in the BCF

The derived NMQSD equations in the previous section assumed zero temperature. As outlined in ref. [24], assuming $L \neq L^\dagger$, non-zero temperature can be incorporated by using two independent noise processes leading the the linear NMQSD equation

$$\begin{aligned}\partial_t |\psi_t(z^{-*}, z^{+*})\rangle = &\left[-iH_{\mathrm{S}} + z_t^{-*}L - L^\dagger \int_0^t \mathrm{d}s\alpha^-(t-s)\frac{\delta}{\delta z_s^{-*}}\right]|\psi_t(z^{-*}, z^{+*})\rangle \\ &+ \left[z_t^{+*}L^\dagger - L\int_0^t \mathrm{d}s\alpha^+(t-s)\frac{\delta}{\delta z_s^{+*}}\right]|\psi_t(z^{-*}, z^{+*})\rangle\,,\end{aligned}$$

where the processes z_t^{-*} and z_t^{+*} follow the statistics

$$\begin{aligned}\mathcal{M}[z_t^{-*}] = \mathcal{M}[z_t^-] = \mathcal{M}[z_t^{-*}z_s^{-*}] = \mathcal{M}[z_t^- z_s^-] = 0,\\ \mathcal{M}[z_t^- z_s^{-*}] = \sum_\lambda (\bar{n}_\lambda + 1)|g_\lambda|^2 e^{-i\omega_\lambda(t-s)} \equiv \alpha^-(t-s),\\ \mathcal{M}[z_t^{+*}] = \mathcal{M}[z_t^+] = \mathcal{M}[z_t^{+*}z_s^{+*}] = \mathcal{M}[z_t^+ z_s^+] = 0,\\ \mathcal{M}[z_t^+ z_s^{+*}] = \sum_\lambda \bar{n}_\lambda |g_\lambda|^2 e^{i\omega_\lambda(t-s)} \equiv \alpha^+(t-s),\end{aligned}$$

where $\bar{n}_\lambda$ is the Bose-Einstein distribution for the environmental mode ω_λ. This way of treating the temperature is called the thermo field method [65]. As expected, as temperature approaches zero, the NMQSD equation above reduces to the zero temperature case (2.13). This can be simplified for the special case $L = L^\dagger$. Here the noise processes are combined into a sum process $z_t = z_t^- + z_t^+$ with

$$\begin{aligned}\mathcal{M}[z_t] = \mathcal{M}[z_t^*] = \mathcal{M}[z_t z_s] = \mathcal{M}[z_t^* z_s^*] = 0,\\ \mathcal{M}[z_t z_s^*] = \alpha^-(t-s) + \alpha^+(t-s) \equiv \alpha(t-s),\end{aligned}$$

where $\alpha(t-s)$ is the BCF given in (2.6). Now the linear NMQSD is the same form as in the zero temperature case, only now the BCF is the finite temperature version given in (2.6).

2.4.2 Thermal Stochastic Process

Encoding the temperature dependence in the BCF is convenient but numerically brings complications since the noise process and BCF increases in magnitude as temperature increases. Another way to incorporate temperature into the model is by introducing a new noise process to model the temperature fluctuations [55]. We assume that the environment is in the thermal state

$$\rho_{\mathrm{E}} = \int \prod_{\lambda} \mathrm{d}^2\eta_\lambda \frac{e^{-\frac{|\eta_\lambda|^2}{\bar{n}_\lambda}}}{\pi\bar{n}_\lambda} |\boldsymbol{\eta}\rangle \langle\boldsymbol{\eta}| \tag{2.19}$$

and define a new state $|\Phi(t)\rangle = D^\dagger(\boldsymbol{\eta}) |\Psi_t\rangle$ where $|\Psi_t\rangle$ is a solution to the equation (2.5) with the initial condition $|\Psi_0\rangle = |\psi_0\rangle |\boldsymbol{\eta}\rangle$. This state in turn satisfies the Schrödinger equation

$$\begin{aligned}
\partial_t |\Phi(t)\rangle =& D^\dagger(\boldsymbol{\eta})\mathcal{U}_t D(\boldsymbol{\eta}) |\psi_0\rangle |\mathbf{0}\rangle \\
=& -iH_{\mathrm{S}} |\Phi(t)\rangle - i\sum_\lambda (g_\lambda L^\dagger(a_\lambda + \eta_\lambda)e^{-i\omega_\lambda t} + g_\lambda^* L(a_\lambda^\dagger + \eta_\lambda^*)e^{i\omega_\lambda t}) |\Phi(t)\rangle \\
=& -iH_{\mathrm{S}} |\Phi(t)\rangle + (LB^\dagger(t) + L^\dagger B(t)) |\phi(t)\rangle - i(\eta_t^* L + \eta_t L^\dagger) |\Phi(t)\rangle
\end{aligned}$$

where we have defined the function

$$\eta_t = \sum_\lambda g_\lambda e^{-i\omega_\lambda t}\eta_\lambda.$$

By comparing to equation (2.5), we see that there are additional terms present. Proceeding with a Monte-Carlo interpretation, the initial thermal state is obtained by sampling the initial condition $\boldsymbol{\eta}$ from the distribution (2.19). By direct calculation we get the following statistics

$$\mathcal{M}[\eta_\lambda] = \mathcal{M}[\eta_\lambda^*] = \mathcal{M}[\eta_\lambda\eta_\mu] = \mathcal{M}[\eta_\lambda^*\eta_\mu^*] = 0,\ \mathcal{M}[\eta_\lambda\eta_\mu^*] = \delta_{\lambda\mu}\bar{n}_\lambda.$$

With these the function η_t becomes a Gaussian stochastic process with the statistics

$$\begin{aligned}
\mathcal{M}[\eta_t] = \mathcal{M}[\eta_t^*] = \mathcal{M}[\eta_t\eta_s] = \mathcal{M}[\eta_t^*\eta_s^*] = 0, \\
\mathcal{M}[\eta_t\eta_s^*] = \sum_\lambda \bar{n}_\lambda |g_\lambda|^2 e^{-i\omega_\lambda(t-s)}.
\end{aligned}$$

In the continuum limit we obtain for the correlation

$$\mathcal{M}[\eta_t \eta_s^*] = \int d\omega \bar{n}(\omega) J(\omega) e^{-i\omega(t-s)},$$

with $\bar{n}(\omega) = (e^{\beta\omega} - 1)^{-1}$. The reduced density matrix now becomes

$$\begin{aligned}
\rho_{\mathrm{S}}(t) &= \int \prod_\lambda \mathrm{d}^2\eta_\lambda \frac{e^{-\frac{|\eta_\lambda|^2}{\bar{n}_\lambda}}}{\pi \bar{n}_\lambda} \mathrm{tr}_{\mathrm{E}}\{D^\dagger(\boldsymbol{\eta}) \mathcal{U}_t \rho_{\mathrm{S}}(0) \otimes D(\boldsymbol{\eta}) \left|\mathbf{0}\right\rangle \left\langle \mathbf{0}\right| D^\dagger(\boldsymbol{\eta}) \mathcal{U}_t^\dagger D(\boldsymbol{\eta})\} \\
&= \int \prod_\lambda \mathrm{d}^2\eta_\lambda \frac{e^{-\frac{|\eta_\lambda|^2}{\bar{n}_\lambda}}}{\pi \bar{n}_\lambda} \mathrm{tr}_{\mathrm{E}}\{\tilde{\mathcal{U}}_t \left|\Psi_0\right\rangle \left\langle \Psi_0\right| \tilde{\mathcal{U}}_t\} \\
&= \int \prod_\lambda \mathrm{d}^2\eta_\lambda \frac{e^{-\frac{|\eta_\lambda|^2}{\bar{n}_\lambda}}}{\pi \bar{n}_\lambda} \rho_t(\boldsymbol{\eta}),
\end{aligned}$$

where $\tilde{\mathcal{U}}_t = D^\dagger(\boldsymbol{\eta}) \mathcal{U}_t D(\boldsymbol{\eta})$. By the Monte-Carlo interpretation we can write

$$\rho_{\mathrm{S}}(t) = \underset{\boldsymbol{\eta}}{\mathcal{M}}[\rho_t(\boldsymbol{\eta})],$$

i.e., we can compute the reduced density matrix as an average over the density matrices $\rho_t(\boldsymbol{\eta})$ where $\boldsymbol{\eta}$ is sampled from the thermal distribution. Each density matrix $\rho_t(\boldsymbol{\eta})$ can in turn be computed using the NMQSD equations with the added noise term $\eta_t^* L + \eta_t L^\dagger$ with the initial condition $\rho_{\mathrm{S}} \otimes \left|\mathbf{0}\right\rangle \left\langle \mathbf{0}\right|$. Thus we average over two independent noise processes z_t^* and η_t and therefore we can write

$$\rho_{\mathrm{S}}(t) = \underset{z^*,\eta}{\mathcal{M}}[\left|\psi_t(z^*, \eta)\right\rangle \left\langle \psi_t(z, \eta)\right|].$$

3 Hierarchy of Pure States

NMQSD determines the dynamics of open quantum systems that are linearly coupled to a bath of quantum harmonic oscillators. While numerical errors and sampling errors may arise during numerical calculations, the derivation does not rely on any approximations, and thus it is considered exact. The most challenging aspect of solving NMQSD lies in handling the functional derivative. In section (2.2) the formal evolution equation (2.15) was derived for the ansatz (2.14). However, this

evolution equation also involves a functional derivative and generally approximations are necessary for this to be solved. One such approximation is the so-called zeroth-order functional expansion (ZOFE) [66, 67], where the functional derivative is essentially approximated as $\mathcal{O}(t,s,\mathbf{z}^*) \approx \mathcal{O}_0(t,s)$, with $\mathcal{O}_0(t,s)$ representing the zeroth-order term in the functional expansion of $\mathcal{O}(t,s,\mathbf{z}^*)$ in terms of z_t^*. This makes the evolution of $\mathcal{O}_0(t,s)$ simpler to solve but at the cost of being an approximation. Fortunately, an exact method for solving the NMQSD has been developed, known as the hierarchy of pure states method (HOPS) [23].

In this section, we will present the HOPS formalism and derive the hierarchy of stochastic pure states, a system of coupled stochastic differential equations. Following this, we will qualitatively describe its numerical implementation in this thesis. Subsequently, the non-linear HOPS will be introduced with a discussion on its implementation. Finally, we will explore a method to express the BCF as a sum of exponential functions and demonstrate how the stochastic processes z_t^* and η_t appearing in NMQSD and HOPS can be generated for numerical computation. For the derivation of HOPS we follow ref. [23].

3.1 Linear HOPS

We will first consider zero temperature. The HOPS method relies on the BCF being expressed as a sum of exponential functions

$$\alpha(t-s) = \sum_{\mu=1}^{K} \mathcal{G}_\mu e^{-W_\mu (t-s)}. \tag{3.1}$$

In fact this form is suitable for a wide variety of spectral densities and BCF [68]. Now we write the linear NMQSD (2.13) as

$$\partial_t \left|\psi_t(z^*)\right\rangle = -iH_{\mathrm{S}} \left|\psi_t(z^*)\right\rangle + z_t^* L \left|\psi_t(z^*)\right\rangle - L^\dagger \left|\psi_t^{(1)}(z^*)\right\rangle, \tag{3.2}$$

where we have defined the auxiliary state

$$\left|\psi_t^{(1)}(z^*)\right\rangle = \int_0^t \mathrm{d}s \alpha(t-s) \frac{\delta}{\delta z_s^*} \left|\psi_t(z^*)\right\rangle.$$

The initial condition $|\Psi_0\rangle = |\psi_0\rangle|\mathbf{0}\rangle$ used in the derivation of the linear NMQSD equation implies that $\frac{\delta|\psi_0(z^*)\rangle}{\delta z_s^*} = 0$ for $s \in \mathbb{R}$. Furthermore $|\psi_t(z^*)\rangle$ must be independent of the noise process z_s^* for $s < 0$ and $s > t$. This allows us to write the auxiliary state as $|\psi_t^{(1)}(z^*)\rangle = \mathcal{D}_t|\psi_t(z^*)\rangle$ with

$$\mathcal{D}_t = \int_{-\infty}^{\infty} \mathrm{d}s\alpha(t-s)\frac{\delta}{\delta z_s^*}. \tag{3.3}$$

Using the reasoning which lead to the above in reverse allows us to write [23]

$$\dot{\mathcal{D}}_t|\psi_t(z^*)\rangle = \int_0^t \mathrm{d}s\dot{\alpha}(t-s)\frac{\delta}{\delta z_s^*}|\psi_t(z^*)\rangle.$$

By expressing the BCF as the sum of exponential functions (3.1), we can decompose $\mathcal{D}_t$ into

$$\mathcal{D}_t = \sum_{\mu=1}^{K}\mathcal{D}_{\mu,t} = \sum_{\mu=1}^{K}\int_0^t \mathrm{d}s\mathcal{G}_\mu e^{-W_\mu(t-s)}\frac{\delta}{\delta z_s^*},$$

from which we have

$$\dot{\mathcal{D}}_{\mu,t} = -W_\mu\mathcal{D}_{\mu,t}.$$

With the decomposed form, we get for (3.2)

$$\partial_t|\psi_t(z^*)\rangle = -iH_\mathrm{S}|\psi_t(z^*)\rangle + z_t^*L|\psi_t(z^*)\rangle - L^\dagger\sum_{\mu=1}^{K}\mathcal{D}_{\mu,t}|\psi_t(z^*)\rangle. \tag{3.4}$$

Next we consider the commutator $[\mathcal{D}_{\mu,t}, z_s^*]F[z^*]$, where $F[z^*]$ is some operator depending on the noise z_t^*. We obtain

$$\begin{aligned}
[\mathcal{D}_{\mu,t}, z_s^*]F[z^*] &= \mathcal{D}_{\mu,t}\left(z_s^*F[z^*]\right) - z_s^*\mathcal{D}_{\mu,t}F[z^*] \\
&= \mathcal{D}_{\mu,t}(z_s^*)F[z^*] + z_s^*\mathcal{D}_{\mu,t}F[z^*] - z_s^*\mathcal{D}_{\mu,t}F[z^*] \\
&= \int_0^t \mathrm{d}s'\mathcal{G}_\mu e^{-W\mu(t-s')}\frac{\delta z_s^*}{\delta z_{s'}^*}F[z^*] \\
&= \int_0^t \mathrm{d}s'\mathcal{G}_\mu e^{-W_\mu(t-s')}\delta(s'-s)F[z^*] \\
&= \mathcal{G}_\mu e^{-W_\mu(t-s)}F[z^*],
\end{aligned}$$

and thus we have

$$\mathcal{D}_{\mu,t}\left(z_t^* F[z^*]\right) = \mathcal{G}_\mu F[z^*] + z_t^* \mathcal{D}_{\mu,t} F[z^*]. \tag{3.5}$$

This can be generalized further by induction. Furthermore we consider the tuple $\mathbf{k} = (k_1, k_2, ..., k_K)$, with $k_\mu \geq 0,\ k_\mu \in \mathbb{N}$ and for this we define

$$\mathcal{D}_t^{\mathbf{k}} = \prod_{\mu=1}^{K} (D_{\mu,t})^{k_\mu}. \tag{3.6}$$

With this notation we can also write

$$\mathcal{D}_{\mu,t} = \mathcal{D}_t^{\mathbf{e}_\mu},$$

where $\mathbf{e}_\mu$ is the μ:th unit tuple. We claim that (3.5) is generalized for $\mathcal{D}_t^{\mathbf{k}}$ as

$$\mathcal{D}_t^{\mathbf{k}}(z_t^* F[z^*]) = \left(\sum_\mu k_\mu \mathcal{G}_\mu \mathcal{D}^{\mathbf{k}-\mathbf{e}_\mu} + z_t^* D_t^{\mathbf{k}} \right) F[z^*]. \tag{3.7}$$

To prove this we consider $\mathcal{D}_t^{\mathbf{k}+\mathbf{e}_\nu}(z_t^* F[z^*])$

$$\begin{aligned}
\mathcal{D}_t^{\mathbf{k}+\mathbf{e}_\nu}(z_t^* F[z^*]) &= \mathcal{D}_t^{\mathbf{e}_\nu} \mathcal{D}_t^{\mathbf{k}}(z_t^* F[z^*]) \\
&= \mathcal{D}_t^{\mathbf{e}_\nu} \left(\sum_\mu k_\mu \mathcal{G}_\mu \mathcal{D}_t^{\mathbf{k}-\mathbf{e}_\mu} F[z^*] + z_t^* \mathcal{D}_t^{\mathbf{k}} F[z^*] \right) \\
&= \left(\sum_\mu k_\mu \mathcal{G}_\mu \mathcal{D}_t^{\mathbf{k}-\mathbf{e}_\mu+\mathbf{e}_\nu} + \mathcal{G}_\nu \mathcal{D}_t^{\mathbf{k}} + z_t^* \mathcal{D}_t^{\mathbf{k}+\mathbf{e}_\nu} \right) F[z^*].
\end{aligned}$$

On the second line we used the induction hypothesis (3.7) and on the third the base case (3.5). Since we can write $\mathcal{G}_\nu \mathcal{D}_t^{\mathbf{k}} F[z^*] = \mathcal{G}_\nu \mathcal{D}_t^{\mathbf{k}+\mathbf{e}_\nu-\mathbf{e}_\nu} F[z^*]$, we can include it in the sum and obtain the final form

$$\mathcal{D}_t^{\mathbf{k}+\mathbf{e}_\nu}(z_t^* F[z^*]) = \left(\sum_\mu k_\mu \mathcal{G}_\mu \mathcal{D}_t^{\mathbf{k}+\mathbf{e}_\nu-\mathbf{e}_\mu} + z_t^* \mathcal{D}_t^{\mathbf{k}+\mathbf{e}_\nu} \right) F[z^*].$$

Hence by mathematical induction (3.7) is correct for $\mathbf{k} \neq \mathbf{0}$ with $k_\mu \geq 0$ for all $\mu \in \{1, ..., K\}$. For the case $\mathbf{k} = \mathbf{0}$ we have $\mathcal{D}_t^{\mathbf{0}} = \mathbb{1}$. For the derivative $\dot{\mathcal{D}}_t^{\mathbf{k}}$ we have

$$\dot{\mathcal{D}}_t^{\mathbf{k}} = \frac{d}{dt}\left[\prod_{\mu=1}^{K} (\mathcal{D}_{\mu,t})^{k_\mu} \right] = -\sum_{\mu=1}^{K} k_\mu W_\mu \prod_{\nu=1}^{K} (\mathcal{D}_{\nu,t})^{k_\nu} = -\sum_{\mu=1}^{K} k_\mu W_\mu \mathcal{D}_t^{\mathbf{k}}. \tag{3.8}$$

Let us now consider the time-evolution of the state $|\psi_t^{\mathbf{k}}(z^*)\rangle = \mathcal{D}_t^{\mathbf{k}} |\psi_t(z^*)\rangle$

$$\partial_t |\psi_t^{\mathbf{k}}(z^*)\rangle = \dot{\mathcal{D}}_t^{\mathbf{k}} |\psi_t(z^*)\rangle + \mathcal{D}_t^{\mathbf{k}} |\dot{\psi}_t(z^*)\rangle .$$

By using (3.4), (3.7) and (3.8) we finally get an infinite system of coupled stochastic differential equations, i.e., hierarchy of pure states (HOPS)

$$\begin{aligned}\partial_t |\psi_t^{\mathbf{k}}(z^*)\rangle = &\left(-iH_{\mathrm{S}} - \sum_{\mu=1}^{K} k_\mu W_\mu + z_t^* L\right) |\psi_t^{\mathbf{k}}(z^*)\rangle + L \sum_{\mu=1}^{K} k_\mu \mathcal{G}_\mu |\psi_t^{\mathbf{k}-\mathbf{e}_\mu}(z^*)\rangle \\ &- L^\dagger \sum_{\mu=1}^{K} |\psi_t^{\mathbf{k}+\mathbf{e}_\mu}(z^*)\rangle . \end{aligned} \tag{3.9}$$

Solving this hierarchy of equations is equivalent to solving the linear NMQSD for $|\psi_t(z^*)\rangle = |\psi_t^{\mathbf{0}}(z^*)\rangle$. Note that the initial conditions are $|\psi_t^{\mathbf{0}}(z^*)\rangle = |\psi_0\rangle$ and $|\psi_0^{\mathbf{k}}(z^*)\rangle = 0$ for all $\mathbf{k} \neq \mathbf{0}$ [23].

For the finite temperature case, if $L = L^\dagger$ and the temperature is encoded in the BCF, HOPS has the same form as above, with the sum process $z_t^* = z_t^{-*} + z_t^{+*}$ defined in section 2.4.1. If the temperature is modeled by using the thermal stochastic process, the stochastic potential $\eta_t^* L + \eta_t L^\dagger$ is simply added to the HOPS

$$\begin{aligned}\partial_t |\psi_t^{\mathbf{k}}(z^*)\rangle = &\left(-iH_{\mathrm{S}} - \sum_{\mu=1}^{K} k_\mu W_\mu + z_t^* L - i\left(\eta_t^* L + \eta_t L^\dagger\right)\right) |\psi_t^{\mathbf{k}}(z^*)\rangle \\ &+ L \sum_{\mu=1}^{K} k_\mu \mathcal{G}_\mu |\psi_t^{\mathbf{k}-\mathbf{e}_\mu}(z^*)\rangle - L^\dagger \sum_{\mu=1}^{K} |\psi_t^{\mathbf{k}+\mathbf{e}_\mu}(z^*)\rangle .\end{aligned}$$

In principle HOPS gives exact solutions to the NMQSD. However, in practice the hierarchy needs to be truncated at some finite level for it to be a practical method. This is done by setting a terminator state for the last level of the hierarchy. An example of such terminator would be [23]

$$|\psi_t^{\mathbf{k}+\mathbf{e}_\mu}(z^*)\rangle = \sum_{\nu=1}^{K} \frac{(\mathbf{k}+\mathbf{e}_\mu)_\nu \mathcal{G}_\nu}{(\mathbf{k}+\mathbf{e}_\mu)\cdot\mathbf{W}} L |\psi_t^{\mathbf{k}+\mathbf{e}_\mu-\mathbf{e}_\nu}(z^*)\rangle ,$$

where $\mathbf{W} = (W_1, W_2, ..., W_K)$ and $\mathbf{k}$ is chosen such that the components are large. The value of $\mathbf{k}$ can be determined in several ways. One of the simplest ways is

by using the triangular truncation condition where $\mathbf{k}$ is chosen such that $|\mathbf{k}| = \sum_\mu k_\mu \leq \mathcal{K}$, for some predetermined $\mathcal{K}$. More sophisticated truncation conditions and terminators have also been considered, e.g. see ref. [69]. In this thesis, we will use the triangular truncation condition with the simple terminator

$$|\psi_t^{\mathbf{k}+\mathbf{e}_\mu}(z^*)\rangle = 0.$$

The final size of the hierarchy, i.e., the number of auxiliary states, depends on two factors. Firstly, it clearly depends on the depth of the hierarchy, meaning that the truncation condition dictates how deep the hierarchy will be. Secondly, the width of the hierarchy depends on how many terms we include in the exponential sum representing the BCF. Depending on the truncation condition, varying the depth of the hierarchy might have a more significant impact on its size. However, for the triangular truncation condition, increasing the number of terms in the BCF sum increases the size of the hierarchy significantly more compared to varying the depth.

The linear HOPS, where the hierarchy has been truncated with some condition, can be written formally as

$$\partial_t \boldsymbol{\Psi} = \mathcal{B}\boldsymbol{\Psi} + z_t^* \mathcal{L}\boldsymbol{\Psi}, \tag{3.10}$$

where $\boldsymbol{\Psi} = (|\psi_t^{\mathbf{0}}(z^*)\rangle, |\psi_t^{\mathbf{e}_1}(z^*)\rangle, ...)^T$ contains the pure states of the hierarchy. The block matrices $\mathcal{B}$ and $\mathcal{L}$ can be expressed illustratively

$$\mathcal{B} = \begin{pmatrix} -iH_{\mathrm{S}} & -L^\dagger & -L^\dagger & 0 & \cdots \\ k_1\mathcal{G}_1 L & -iH_{\mathrm{S}} - \sum_\mu k_\mu W_\mu & 0 & 0 & \cdots \\ \vdots & \vdots & \vdots & \vdots & \ddots \end{pmatrix},$$

$$\mathcal{L} = \mathrm{diag}(L, L, \cdots)$$

where the blocks in $\mathcal{B}$ are placed such that (3.10) produces the HOPS. If the Hamiltonian H_{S} is time-independent, then the matrix $\mathcal{B}$ is truly constant and can be calculated once in the beginning of the simulation. This is desirable, since most

of the entries in $\mathcal{B}$ are zero and for this reason the matrix can be represented as a sparse matrix. Sparse matrices are both memory efficient and allow for efficient matrix vector multiplication. However, sparse matrices aren't efficiently modifiable and thus they should be constructed once. This is also the reason why the noise process in (3.10) is separated from $\mathcal{B}$. To incorporate the noise in an efficient manner, we can sample the noise first, multiply $\mathcal{L}$ with $\mathbf{\Psi}$ and then scale the resulting vector with the noise z_t^*. One could also first scale the vector with the noise and then perform the matrix vector multiplication.

For a time dependent Hamiltonian we have the following form

$$\partial_t \mathbf{\Psi} = \sum_{i,j} H_{\mathrm{S},ij}(t)\mathcal{H}^{(ij)}\mathbf{\Psi} + \mathcal{B}'\mathbf{\Psi} + z_t^*\mathcal{L}\mathbf{\Psi}.$$

Here $H_{\mathrm{S},ij}(t)$ are the entries of the Hamiltonian and $\mathcal{H}^{(ij)}$ the block matrix corresponding to those entries. For example for a two-level system we would have

$$\mathcal{H}^{(ij)} = \mathrm{diag}\left(\begin{pmatrix} \delta_{0i}\delta_{0j} & \delta_{0i}\delta_{1j} \\ \delta_{1i}\delta_{0j} & \delta_{1i}\delta_{1j} \end{pmatrix}, \begin{pmatrix} \delta_{0i}\delta_{0j} & \delta_{0i}\delta_{1j} \\ \delta_{1i}\delta_{0j} & \delta_{1i}\delta_{1j} \end{pmatrix}, \cdots\right).$$

The block matrix $\mathcal{B}'$ is otherwise the same as $\mathcal{B}$ but the Hamiltonians have been removed from the diagonal. For finite temperature, when $L = L^\dagger$ and the temperature is encoded in the BCF, i.e., in $\{\mathcal{G}_\mu\}$, $\{W_\mu\}$ and z_t^* , the forms presented above apply. For the thermal noise process a slight modification needs to be made

$$\partial_t \mathbf{\Psi} = \sum_{i,j} H_{\mathrm{S},ij}(t)\mathcal{H}^{(ij)}\mathbf{\Psi} + \mathcal{B}'\mathbf{\Psi} + (z_t^* - i\eta_t^*)\mathcal{L}\mathbf{\Psi} - i\eta_t\mathcal{L}^\dagger\mathbf{\Psi}$$

with $\mathcal{L}^\dagger = \mathrm{diag}(L^\dagger, L^\dagger, \cdots)$. The integration of each of the presented situations can be done with an ordinary differential equation integrator since the noise processes z_t^* and η_t are coloured noise. In this thesis we use the explicit Runge-Kutta method of order 4(5), which uses the Dormand-Prince pair of formulas [70], which is provided in scipy [71].

3.2 Non-linear HOPS

The convergence of NMQSD was improved by the use of importance sampling, where the trajectories get equally weighted in the ensemble average, resulting in the non-linear NMQSD equation (2.18). HOPS can also be derived for this case. The only difference in the derivation is that the starting point is the non-linear NMQSD equation instead of the linear one. One then arrives at the non-linear HOPS

$$\partial_t \left|\psi_t^{\mathbf{k}}(\tilde{z}^*)\right\rangle = \left(-iH_{\mathrm{S}} - \sum_{\mu=1}^{K} k_\mu W_\mu + \tilde{z}_t^* L\right)\left|\psi_t^{\mathbf{k}}(\tilde{z}^*)\right\rangle + L\sum_{\mu=1}^{K} k_\mu \mathcal{G}_\mu \left|\psi_t^{\mathbf{k}-\mathbf{e}_\mu}(\tilde{z}^*)\right\rangle - \left(L^\dagger - \langle L^\dagger\rangle_t\right)\sum_{\mu=1}^{K}\left|\psi_t^{\mathbf{k}+\mathbf{e}_\mu}(\tilde{z}^*)\right\rangle, \tag{3.11}$$

where $\tilde{z}_t^*$ is the shifted noise process (2.17) and the expectation value is now given by the zeroth level state

$$\langle L^\dagger\rangle_t = \frac{\langle\psi_t^{\mathbf{0}}(\tilde{z})|L^\dagger|\psi_t^{\mathbf{0}}(\tilde{z}^*)\rangle}{\langle\psi_t^{\mathbf{0}}(\tilde{z})|\psi_t^{\mathbf{0}}(\tilde{z}^*)\rangle}.$$

When considering finite temperature, the temperature is represented using the thermal stochastic process η_t and the thermal noise terms are just added as in the case of linear HOPS

$$\partial_t \left|\psi_t^{\mathbf{k}}(\tilde{z}^*)\right\rangle = \left(-iH_{\mathrm{S}} - \sum_{\mu=1}^{K} k_\mu W_\mu + \tilde{z}_t^* L - i\left(\eta_t^* L + \eta_t L^\dagger\right)\right)\left|\psi_t^{\mathbf{k}}(\tilde{z}^*)\right\rangle + L\sum_{\mu=1}^{K} k_\mu \mathcal{G}_\mu \left|\psi_t^{\mathbf{k}-\mathbf{e}_\mu}(\tilde{z}^*)\right\rangle - \left(L^\dagger - \langle L^\dagger\rangle_t\right)\sum_{\mu=1}^{K}\left|\psi_t^{\mathbf{k}+\mathbf{e}_\mu}(\tilde{z}^*)\right\rangle.$$

Similarly to the linear HOPS, the truncated non-linear HOPS can be formally written as

$$\partial_t \mathbf{\Psi} = \mathcal{B}\mathbf{\Psi} + \tilde{z}_t^* \mathcal{L}\mathbf{\Psi} + \langle L^\dagger\rangle_t \mathcal{P}\mathbf{\Psi},$$

where $\mathcal{B}$ and $\mathcal{L}$ are the same block matrices as for the linear HOPS but a new term is added where the block matrix

$$\mathcal{P} = \begin{pmatrix} 0 & \mathbb{1} & \mathbb{1} & \cdots & 0 & \cdots \\ 0 & 0 & \cdots & \mathbb{1} & 0 & \cdots \\ \vdots & \vdots & \ddots & \vdots & \vdots & \ddots \end{pmatrix}$$

contains identity matrices on the indices of the positive neighbour states, i.e., for a fixed $\mathbf{k}$ the indices of the auxiliary states $|\psi_t^{\mathbf{k}+\mathbf{e}_\mu}(\tilde{z}^*)\rangle$. This separation is again done due to the use of sparse matrices. In the time-dependent case matrix $\mathcal{B}$ is split into the time-dependent and time-independent parts resulting in

$$\partial_t \mathbf{\Psi} = \sum_{i,j} H_{\mathrm{S},ij}(t)\mathcal{H}^{(ij)}\mathbf{\Psi} + \mathcal{B}'\mathbf{\Psi} + \tilde{z}_t^*\mathcal{L}\mathbf{\Psi} + \langle L^\dagger \rangle_t \mathcal{P}\mathbf{\Psi},$$

where $H_{\mathrm{S},ij}$, $\mathcal{H}^{(ij)}$ and $\mathcal{B}'$ are the same as for the linear case.

One non-trivial challenge is the computation of the shifted noise process $\tilde{z}_t^*$. A naive way of implementing this is by storing the expectation values $\langle L^\dagger \rangle_t$ at each time step and then computing the convolution like integral $\int_0^t \mathrm{d}s\alpha^*(t-s)\langle L^\dagger \rangle_s$. This integral has to be recomputed at each time step which will become inefficient if the time step is very small and if one wishes to simulate for a long time period. In other words the the time complexity of each time step would be $\mathcal{O}(N)$ where N is the number of time steps taken. This will become very inefficient compared to the linear HOPS which has constant or $\mathcal{O}(1)$ time complexity each time step.

Due to the construction of HOPS, this can be solved quite simply [55]. Since it is already assumed that the BCF is expressed as a sum of exponential functions, we can rewrite the shifted noise as

$$\begin{aligned}
\tilde{z}_t^* &= z_t^* + \int_0^t \mathrm{d}s\alpha^*(t-s)\langle L^\dagger \rangle_s \\
&= z_t^* + \sum_{\mu=1}^{K} \int_0^t \mathrm{d}s\mathcal{G}_\mu^* e^{-W_\mu^*(t-s)}\langle L^\dagger \rangle_s \\
&= z_t^* + \sum_{\mu=1}^{K} \xi_\mu(t),
\end{aligned}$$

where we have defined $\xi_\mu(t) = \int_0^t \mathrm{d}s\mathcal{G}_\mu^* e^{-W_\mu^*(t-s)}$. By taking the time derivative of $\xi_\mu(t)$ we find

$$\begin{aligned}
\dot{\xi}_\mu(t) &= \mathcal{G}_\mu^* \langle L^\dagger \rangle_t - \int_0^t \mathrm{d}s\mathcal{G}_\mu^* W_\mu^* e^{-W_\mu^*(t-s)} \\
&= \mathcal{G}_\mu^* \langle L^\dagger \rangle_t - W_\mu^* \xi_\mu(t).
\end{aligned}$$

Using this we can compute the shifted noise by propagating each $\xi_\mu(t)$ along with the HOPS and then summing them together. This has two obvious benefits. Firstly, each time step is now $\mathcal{O}(1)$ as in the case of linear HOPS. Secondly, the expectation values $\langle L^\dagger \rangle_t$ no longer need to be stored, reducing memory usage.

For completeness, when considering finite temperature, the noise terms are added for the thermal stochastic process resulting in

$$\partial_t \mathbf{\Psi} = \sum_{i,j} H_{\mathrm{S},ij}(t)\mathcal{H}^{(ij)}\mathbf{\Psi} + \mathcal{B}'\mathbf{\Psi} + (\tilde{z}_t^* - i\eta_t^*)\mathcal{L}\mathbf{\Psi} - i\eta_t\mathcal{L}^\dagger\mathbf{\Psi} + \langle L^\dagger \rangle_t \mathcal{P}\mathbf{\Psi}.$$

3.3 Approximating the BCF Exponential Sum

HOPS formalism requires the BCF to be expressed as a series of exponential functions. Some bath correlation functions may already be in an exponential form but for the general case this sum has to be approximated. There are two major requirements for this approximation. Firstly, it ought to be accurate. Secondly, we want to achieve this high accuracy with the least amount of terms in the sum as possible. This is because the numerical effort required to solve the HOPS is directly proportional to the size of the hierarchy. The accuracy of HOPS also increases with the depth of the hierarchy [55]. To be able to increase the depth of the hierarchy, we don't want the size of the hierarchy to increase unnecessarily much due to its width. A popular method of constructing this approximation is by using the Padé spectrum decomposition method [72]. In this thesis we use the time-domain Prony fitting decomposition (t-PFD) method [73] which we will walk through next.

Let us write the BCF as

$$\alpha(\tau) = \alpha^{(r)}(\tau) + i\alpha^{(i)}(\tau),$$

where $\alpha^{(r)}(\tau) = \mathrm{Re}\ \alpha(\tau)$ and $\alpha^{(i)}(\tau) = \mathrm{Im}\ \alpha(\tau)$. The t-PFD method will be applied separately to the real- and imaginary part, i.e., we will have

$$\alpha(\tau) \approx \sum_{\mu=1}^{K} \mathcal{G}_\mu e^{-W_\mu \tau} = \sum_{\mu=1}^{K_r} \mathcal{G}_\mu^{(r)} e^{-W_\mu^{(r)}\tau} + i\sum_{\mu=1}^{K_i} \mathcal{G}_\mu^{(i)} e^{-W_\mu^{(i)}\tau},$$

where $K = K_r + K_i$. Let us consider the real part. First $\alpha^{(r)}(\tau)$ is sampled to obtain

$$\phi_i = \alpha^{(r)}(k\Delta\tau), k = 0, ..., 2N,$$

where $\Delta\tau = \frac{\tau_c}{2N}$ with τ_c being the cut-off time of $\alpha^{(r)}(\tau)$. Next from these samples the corresponding Hankel matrix is constructed

$$S = \begin{pmatrix} \phi_0 & \phi_1 & \cdots & \phi_N \\ \phi_1 & \phi_2 & \cdots & \phi_{N+1} \\ \vdots & \vdots & \ddots & \vdots \\ \phi_N & \phi_{N+1} & \cdots & \phi_{2N} \end{pmatrix}.$$

This can be decomposed with Takagi's factorization [74]

$$S\mathbf{u}_m = \sigma_m \mathbf{u}_m^*, \ m = 0, ..., N,$$

where σ_m are the c-eigenvalues and $\mathbf{u}_m$ the corresponding c-eigenvectors. The values $\{|\sigma_m|\}$ are sorted in descending order with vectors $\{\mathbf{u}_m\}$ sorted accordingly. The K_r:th vector $\mathbf{u}_{K_r}$ is then chosen with which the following polynomial is constructed

$$f(z) = \sum_{n=0}^{N} (\mathbf{u}_{K_r})_n z^n,$$

whose roots we denote $\{z_i\}_{i=1}^N$. K_r of these roots are inside the unit circle [75], i.e., $|z_k| < 1$. Now the exponents $\{W_\mu^{(r)}\}$ are obtained by

$$W_\mu^{(r)} = -\frac{2N}{\tau_c} \left(\ln |z_\mu| + i \arg(z_\mu) \right),$$

where $\arg(z_\mu) \in (-\pi, \pi]$. The coefficients $\{\mathcal{G}_\mu^{(r)}\}$ are obtained by least-square fitting the system of $2N + 1$ equations

$$\phi_k = \sum_{\mu=1}^{K_r} \mathcal{G}_\mu^{(r)} z_\mu^k, k = 0, ..., 2N,$$

where the roots z_μ are those for which $|z_\mu| < 1$. Now we have obtained the exponential series expansion for $\alpha^{(r)}(\tau)$. Using the same steps for $\alpha^{(i)}(\tau)$, we obtain the final series expansion for $\alpha(\tau)$.

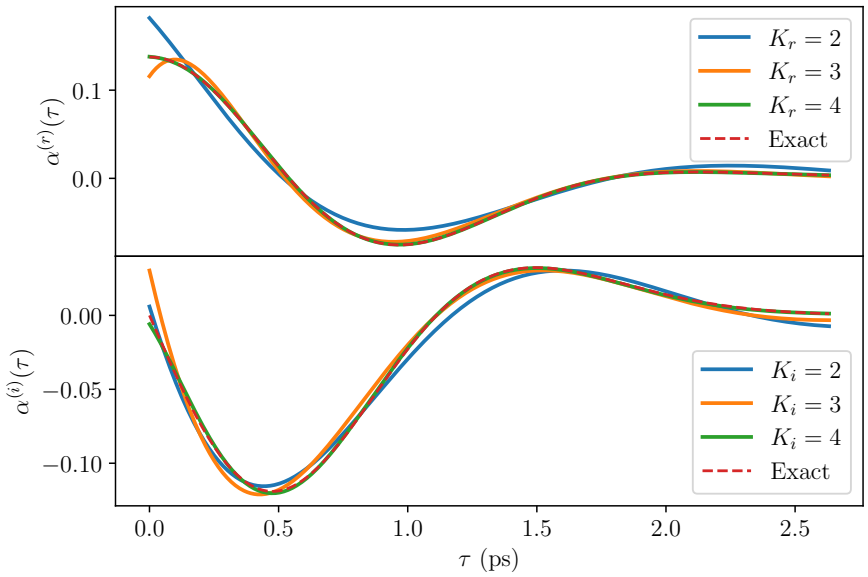

Figure 4. t-PFD fittings of the BCF were performed with varying numbers of terms included, with $N = 3000$. The spectral density parameters used were $\alpha = 0.027$ ps^2 and $\xi = 1.45$ meV.

Figure 4 illustrates the t-PFD fittings obtained using various values for K_r and K_i to represent the real and imaginary parts of the BCF, as given in (2.6), at zero temperature with the QD spectral density (1.6). At $K_r = K_i = 2$, the shape of the fitted real and imaginary parts closely resemble the exact curves. Already at $K_r = K_i = 4$, an almost precise approximation is achieved which is highly desirable for HOPS. Therefore for practical purposes, including more than four terms for each part would be unnecessary and throughout this thesis we use $K_r = K_i = 4$.

3.4 Noise Generation

NMQSD and consequently HOPS yields the reduced density matrix by taking the ensemble average over different realizations of the noise process z_t^*. In other words, each stochastic process results in a new stochastic pure state $|\psi_t(z^*)\rangle$ and the reduced density matrix is obtained by averaging over the dyads $|\psi_t(z^*)\rangle \langle\psi_t(z)|$. For NMQSD

and HOPS to be effective numerical methods, we need a way to generate these processes. Additionally, when finite temperature is considered using the thermal noise processes, those need to be generated as well. Both of these noise processes can be generated similarly with a simple method.

Let us start by considering zero-temperature. The BCF can be expressed as the Riemann sum

$$\alpha(t-s) = \int \mathrm{d}\omega J(\omega) e^{-i\omega(t-s)} \approx \sum_k \Delta\omega J(k\Delta\omega) e^{-ik\Delta\omega(t-s)}.$$

The noise process z_t^* has the statistics as derived earlier

$$\mathcal{M}[z_t^*] = 0,\ \mathcal{M}[z_t^* z_s^*] = 0,\ \mathcal{M}[z_t z_s^*] = \alpha(t-s).$$

For a fixed $\Delta\omega$ we define the noise process

$$Z_t^* = \sum_k \xi_k^* \sqrt{J(k\Delta\omega)} e^{ik\Delta\omega t}, \tag{3.12}$$

where $\{\xi_k^*\}$ are random variables such that

$$\mathcal{M}[\xi_k^*] = \mathcal{M}[\xi_k] = \mathcal{M}[\xi_k^* \xi_l^*] = \mathcal{M}[\xi_k \xi_l] = 0,\ \mathcal{M}[\xi_k \xi_l^*] = \Delta\omega \delta_{kl}.$$

By using these statistics, we obtain by direct calculation

$$\begin{aligned}
\mathcal{M}[Z_t^*] &= \sum_k \mathcal{M}[\xi_k^*] \sqrt{J(k\Delta\omega)} e^{ik\Delta\omega t} = 0 \\
\mathcal{M}[Z_t^* Z_s^*] &= \sum_k \sum_l \mathcal{M}[\xi_k^* \xi_l^*] \sqrt{J(k\Delta\omega) J(l\Delta\omega)} e^{ik\Delta\omega t - il\Delta\omega s} = 0 \\
\mathcal{M}[Z_t Z_s^*] &= \sum_k \sum_l \mathcal{M}[\xi_k \xi_l^*] \sqrt{J(k\Delta\omega) J(l\Delta\omega)} e^{-ik\Delta\omega t + il\Delta\omega s} \\
&= \sum_k \Delta\omega J(k\Delta\omega) e^{-ik\Delta\omega(t-s)} \\
&\approx \alpha(t-s).
\end{aligned}$$

The process (3.12) satisfies the required statistics and is thus applicable to be used as the noise z_t^*. In practice, the noise is generated by sampling Gaussian distributed

random variables $\{\xi_k\}$ with zero mean and variance $\{\xi_k \xi_k^*\} = \Delta\omega$. Further more since ξ_k^* are complex numbers the real and imaginary parts can be sampled independently from Gaussian distributions with

$$\mathcal{M}[\text{Re } \xi_k^*] = \mathcal{M}[\text{Im } \xi_k^*] = 0,\ \mathcal{M}[(\text{Re } \xi_k^*)^2] = \mathcal{M}[(\text{Im } \xi_k^*)^2] = \frac{\Delta\omega}{2}.$$

Note that the noise generated by this method is periodic with period $\frac{2\pi}{\Delta\omega}$. Thus one needs to make sure that $\Delta\omega$ is chosen such that the maximum simulation time $t_{\max}$ does not exceed the period of the noise, i.e., $t_{\max} < \frac{2\pi}{\Delta\omega}$.

When incorporating the temperature in the BCF, we ended up with two noise processes. These can be generated similarly by

$$z_t^{-*} = \sum_k \xi_k^{-*} \sqrt{J(k\Delta\omega)} e^{ik\Delta\omega t},$$
$$z_t^{+*} = \sum_k \xi_k^{+*} \sqrt{J(k\Delta\omega)} e^{-ik\Delta\omega t},$$

where $\{\xi_k^{-*}\}$ and $\{\xi_k^{+*}\}$ are Gaussian random variables with

$$\mathcal{M}[\xi_k^{-*}] = 0,\ \mathcal{M}[\xi_k^- \xi_l^{-*}] = \Delta\omega(\bar{n}_k + 1)\delta_{kl},$$
$$\mathcal{M}[\xi_k^{+*}] = 0,\ \mathcal{M}[\xi_k^+ \xi_l^{+*}] = \Delta\omega\bar{n}_k\delta_{kl},$$

where $\bar{n}_k = (e^{\beta k\Delta\omega} - 1)^{-1}$. By direct calculation we get

$$\mathcal{M}[z_t^- z_t^{-*}] = \sum_k \Delta\omega(\bar{n}_k + 1) J(k\Delta\omega) e^{-ik\Delta\omega(t-s)} \approx \alpha^-(t-s),$$
$$\mathcal{M}[z_t^+ z_t^{+*}] = \sum_k \Delta\omega\bar{n}_k J(k\Delta\omega) e^{ik\Delta\omega(t-s)} \approx \alpha^+(t-s).$$

For the special case $L = L^\dagger$, the noise $z_t^* = z_t^{-*} + z_t^{+*}$ can be generated by simply generating z_t^{-*} and z_t^{+*} separately and then summing them together.

The thermal stochastic process can also be generated in the same way. By sampling Gaussian distributed random variables $\{\xi_k\}$ with zero mean and for a fixed $\Delta\omega$

$$\mathcal{M}[\xi_k \xi_l] = 0,\ \mathcal{M}[\xi_k \xi_l^*] = \Delta\omega\bar{n}_k\delta_{kl},$$

we can define the process

$$\eta_t = \sum_k \xi_k \sqrt{J(k\Delta\omega)} e^{-ik\Delta\omega t}. \tag{3.13}$$

By direct calculation we find the correct covariance

$$\mathcal{M}[\eta_t \eta_s^*] = \sum_k \Delta\omega \bar{n}_k J(k\Delta\omega) e^{-ik\Delta\omega(t-s)} \approx \int \mathrm{d}\omega \bar{n}(\omega) J(\omega) e^{-i\omega(t-s)}.$$

4 Simulating Quantum Dot Dynamics Using HOPS

NMQSD and HOPS are methods to solve the dynamics of any system that is coupled to a bath of harmonic oscillators and therefore we can apply them to the QD system of interest. The derivation of NMQSD was based on the assumption that the environment coupling is linear, without any specific assumptions made about the strength of the coupling. As such, we can investigate the dynamics of the QD system in both weak and strong coupling, and low and high temperatures. In this section, as a benchmark, we will first compare the exact solution of the independent boson model to the solutions obtained with HOPS. Then, we will compute the absorption spectra for the QD in the absence of the cavity, only needing to consider one trajectory. After that, we will demonstrate how HOPS can be used to calculate response functions in general for the QD. Subsequently, we will compute the spectrum of resonance fluorescence for the QD driven both directly and indirectly. In the direct case, we consider the QD to have no cavity coupling, and the monochromatic drive is applied to the QD directly. In the other case, we couple the QD to the cavity and drive the cavity instead. The cavity operators are eliminated by adiabatic elimination to simplify the analysis. Finally, we will consider the weak coupling limit by comparing the dynamics obtained from Redfield theory to the exact HOPS solution.

4.1 Simulation of the Independent Boson Model

In Section 1.2, we derived the exact dynamics of the independent boson model. Now, we can benchmark HOPS against it to assess its performance. In fact, for the independent boson model, we can derive an exact expression for the functional derivative that appears in the NMQSD equation. As outlined in Section 2.2, we can try the ansatz

$$\mathcal{O}(t, s, \mathbf{z}^*) = \mathcal{O} = L = |X\rangle \langle X| .$$

We immediately see that this satisfies the evolution equation (2.15) since $\partial_t \mathcal{O} = 0$ and $\mathcal{O}$ commutes with H_{S}, L and $\bar{\mathcal{O}}(t)$. Thus for the independent boson model we can set

$$\frac{\delta}{\delta z_s^*} = |X\rangle \langle X| ,$$

and the linear NMQSD obtains the form

$$\partial_t |\psi_t(z^*)\rangle = \left(-i\omega_X + z_t^* - \int_0^t \mathrm{d}s \alpha(t-s) \right) |X\rangle \langle X|\psi_t(z^*)\rangle .$$

This enables us to compare single trajectories of NMQSD and HOPS to see how different hierarchy depths compare to the exact solution given by NMQSD.

Figures 5 and 6 display the coherences of the QD calculated using linear HOPS. For both figures, in panels (a), the temperature was incorporated with the thermal stochastic process, and in panels (b), with the thermo field method. It is evident from both figures that the thermal stochastic process yields more rapidly converging results. Particularly in figure 6, we observe a significant deviation in coherence at $T = 75$ K even with 16384 trajectories using the thermo field method. This deviation is pronounced due to the fact that linear HOPS do not preserve the norm of the state vector. Consequently, certain trajectories may dominate the ensemble average, as illustrated in figure 6. The coherence obtained with non-linear HOPS is presented in figure 7. Here, we clearly observe rapid convergence due to the

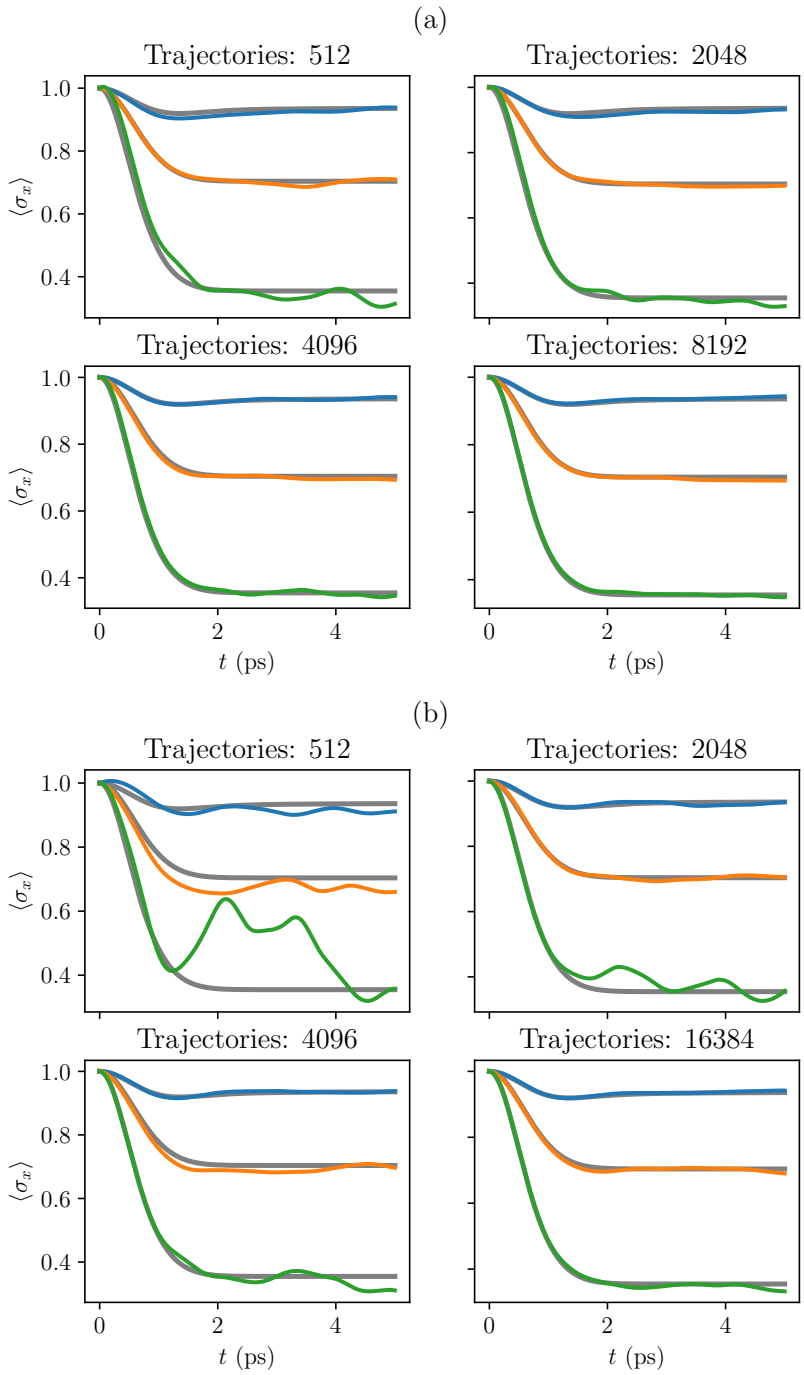

Figure 5. Coherence of the QD for the independent boson model across various trajectory amounts and temperatures. The temperatures are 0 K, 25 K and 75 K from top to bottom on each panel. The gray lines represent the coherences acquired from the exact solution. Panels (a) model the temperature using the thermal stochastic process, while panels (b) employ the thermo field method. Other parameters used: $\alpha = 0.027$ ps^2, $\xi = 1.447$ meV and $\mathcal{K} = 4$.

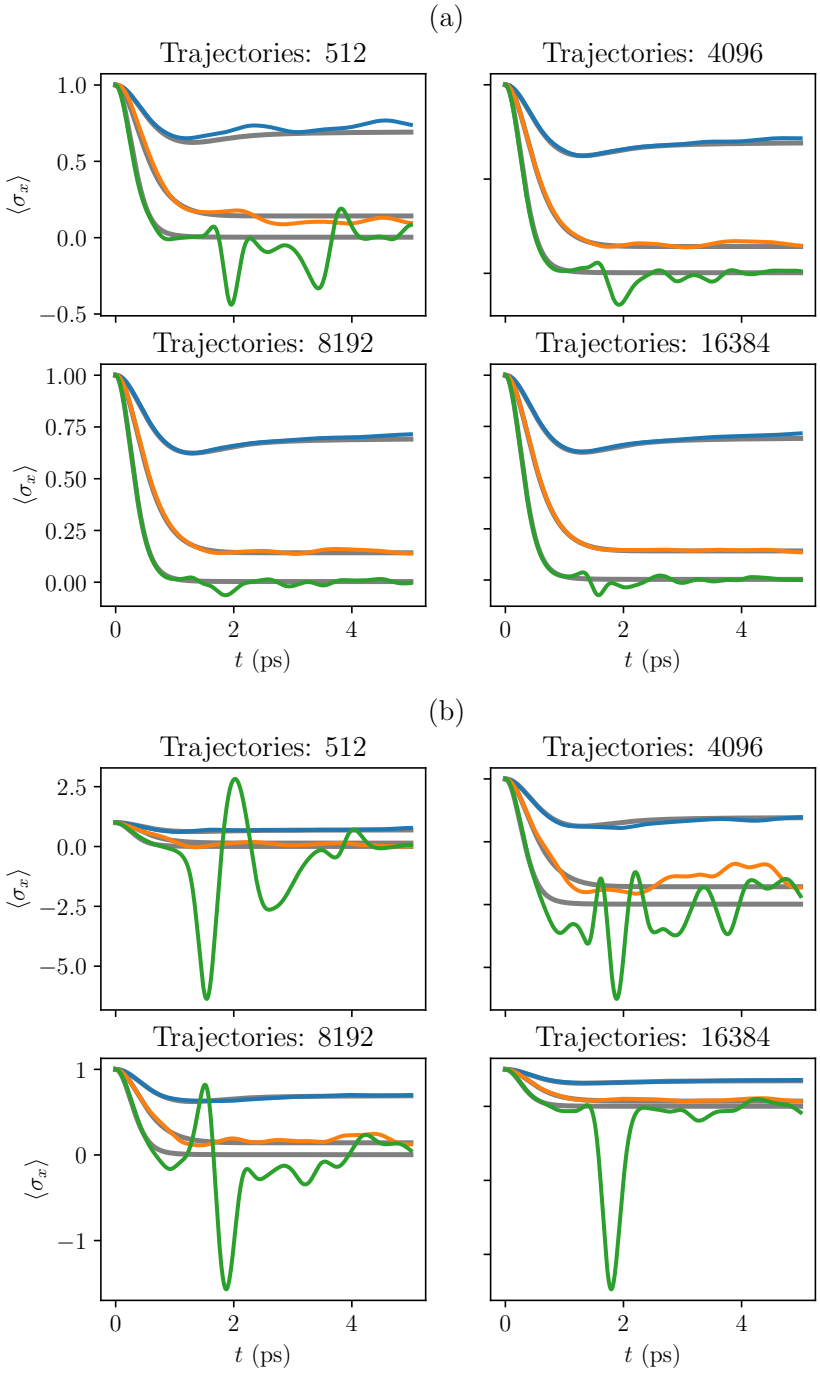

Figure 6. Coherence of the QD for the independent boson model across various trajectory amounts and temperatures. The temperatures are 0 K, 25 K and 75 K from top to bottom on each panel. The gray lines represent the coherences acquired from the exact solution. Panels (a) model the temperature using the thermal stochastic process, while panels (b) employ the thermo field method. Other parameters used: $\alpha = 0.15$ ps^2, $\xi = 1.447$ meV and $\mathcal{K} = 4$.

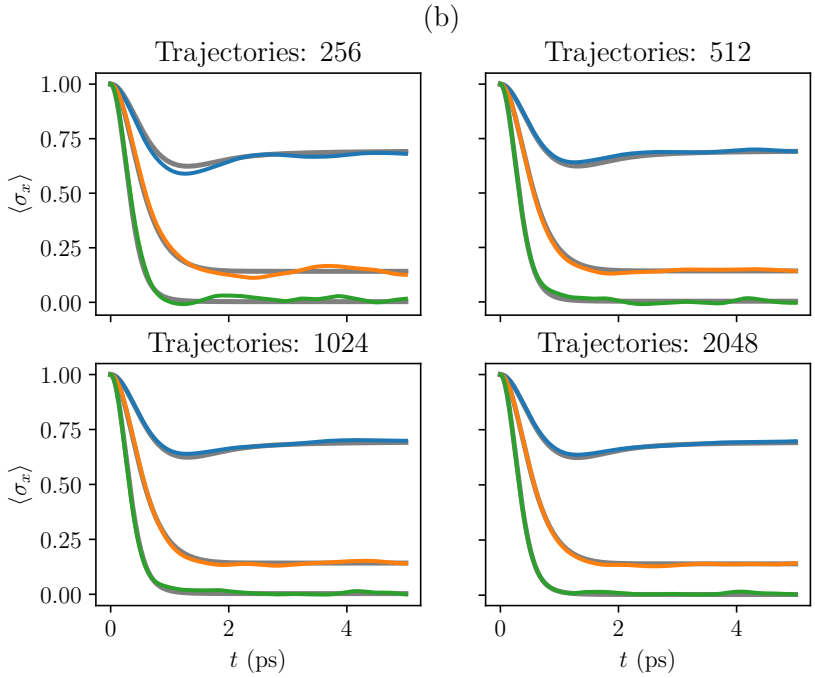

Figure 7. Coherence of the QD for the independent boson model across various trajectory amounts and temperatures obtained using non-linear HOPS. The temperatures are 0 K, 25 K and 75 K from top to bottom on each panel. The gray lines represent the coherences acquired from the exact solution. Other parameters used: $\alpha = 0.15$ ps^2, $\xi = 1.447$ meV and $\mathcal{K} = 4$.

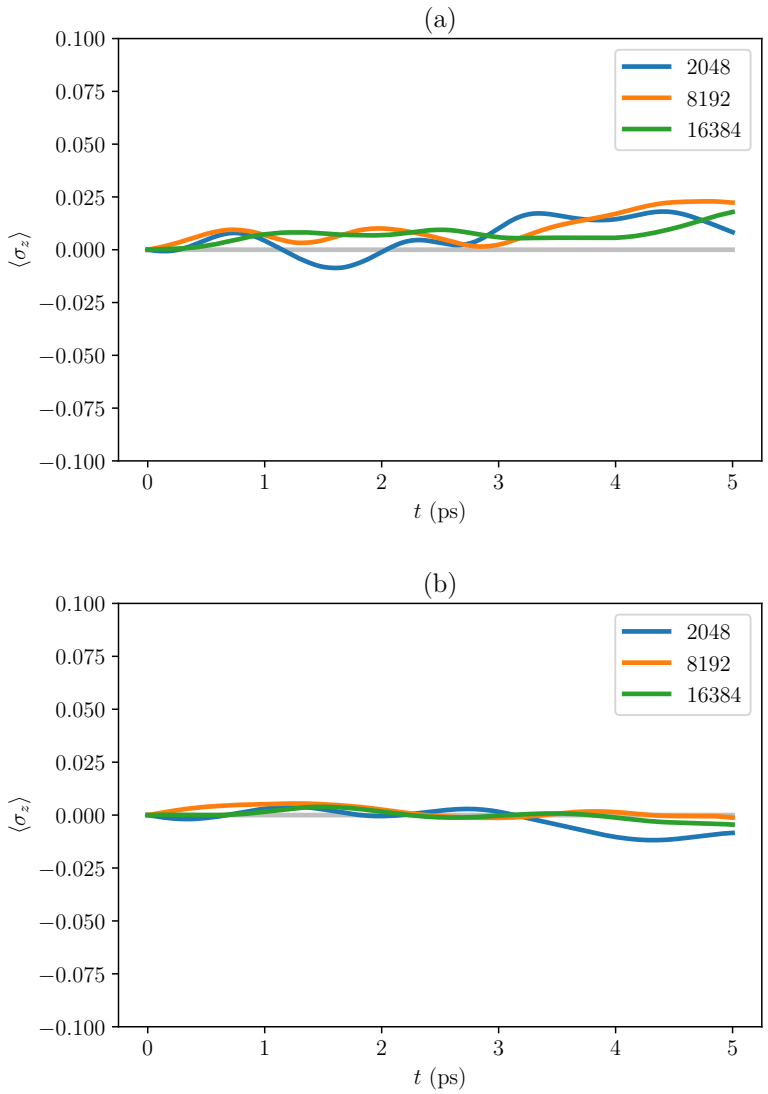

Figure 8. Population of the QD across various trajectory amounts calculated with (a) linear HOPS and (b) non-linear HOPS. The gray lines represent the population acquired from the exact solution for the density matrix. Other parameters used: $\alpha = 0.027$ ps^2, $\xi = 1.447$ meV, $\mathcal{K} = 4$ and $T = 25$ K.

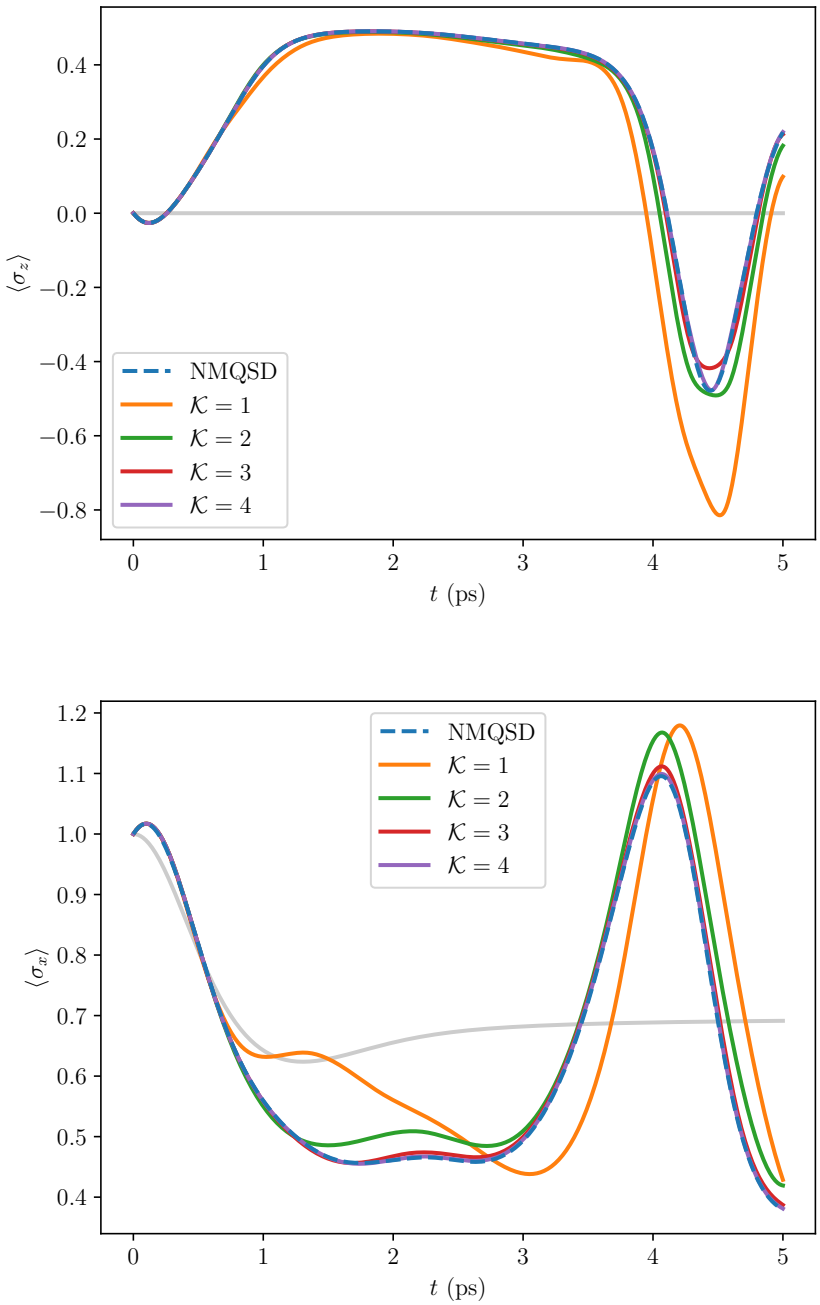

Figure 9. The population and coherence of the QD for a single trajectory with various hierarchy depths compared against the ones obtained from NMQSD exact solution. For reference, the gray lines represent the population and coherence acquired from the exact solution for the density matrix. Other parameters used: $\alpha = 0.15$ ps^2, $\xi = 1.447$ meV and $T = 0$ K.

importance sampling, demonstrating significantly better performance compared to the linear HOPS results. At 512 trajectories, the solutions have already converged to an acceptable accuracy.

The population of the QD is depicted in figure 8. Here, we also observe that non-linear HOPS yield results more consistent with the exact solution. In both cases, the temperature was incorporated using the thermal stochastic process. As previously mentioned, we can compare single trajectories to the NMQSD equation, since the functional derivative obtains an explicit form, namely $\frac{\delta}{\delta z_s^*} = |X\rangle\langle X|$. Figure 9 displays the population and coherence of the QD for single trajectories with varying hierarchy depths. At $\mathcal{K} = 4$, we observe an almost perfect agreement between HOPS and NMQSD.

4.2 Linear Absorption of the Quantum Dot

The linear absorption spectrum for the QD system can be calculated in a straightforward way using NMQSD and HOPS, by propagating only a single trajectory [66]. We neglect cavity coupling. The Hamiltonian is of the form

$$H = H_0 + H_{\text{field}} = \omega_X |X\rangle\langle X| + \sum_\lambda \omega_\lambda a_\lambda^\dagger a_\lambda + |X\rangle\langle X| \sum_\lambda g_\lambda (a_\lambda + a_\lambda^\dagger) + H_{\text{field}}.$$

Here the coupling operator can be identified to be $L = L^\dagger = |X\rangle\langle X|$, which enables us to write the NMQSD equation for the Hamiltonian without the external field

$$\partial_t |\psi_t(z^*)\rangle = \left(-i\omega_X + z_t^* - \int_0^t \mathrm{d}s \alpha(t-s)\right) |X\rangle\langle X|\psi_t(z^*)\rangle\,. \tag{4.1}$$

The QD is a two-level system and therefore we can compute the absorption spectrum by using equation (1.38). Here we have $E_g = 0$ and $|\Psi(0)\rangle = |X\rangle|\mathbf{0}\rangle$ since the ground state of H_0 is $|\Psi_g\rangle = |g\rangle|\mathbf{0}\rangle$. To utilize NMQSD we express the state $|\Psi(t)\rangle$ with Bargmann states

$$|\Psi(t)\rangle = \int \prod_\lambda \mathrm{d}^2 z_\lambda \frac{e^{-|z_\lambda|^2}}{\pi} |\psi_t(z^*)\rangle\,||\mathbf{z}\rangle\,.$$

Now we find for the overlap

$$\langle\Psi(0)|\Psi(t)\rangle = \int \prod_{\lambda} \mathrm{d}^2 z_\lambda \frac{e^{-|z_\lambda|^2}}{\pi} \langle X|\psi_t(z^*)\rangle \langle \mathbf{0}||\mathbf{z}\rangle = \langle X|\psi_t(z^*=0)\rangle \,.$$

Here we see directly that only one trajectory needs to be propagated since $z_t^* = 0$. For the NMQSD equation this means

$$\partial_t \left|\psi_t(z^*=0)\right\rangle = \left(-i\omega_X - \int_0^t \mathrm{d}s \alpha(t-s)\right) |X\rangle \langle X|\psi_t(z^*=0)\rangle \,,$$

which has the solution

$$|\psi_t(z^*=0)\rangle = C_g |g\rangle + C_X \exp\left(-i\omega_X t - \int_0^t \mathrm{d}s \int_0^s \mathrm{d}s' \alpha(s-s')\right) |X\rangle \,.$$

For the absorption spectrum we have by equation (1.38)

$$\mathcal{A}(\omega) \propto \mathrm{Re} \int_0^\infty \mathrm{d}\tau \exp\left(-i(\omega_X - \omega)t - \int_0^t \mathrm{d}s \int_0^s \mathrm{d}s' \alpha(s-s')\right) .$$

This is a case where encoding the temperature in the BCF is especially useful since the noise process is set to be zero. This enables us to still only need to consider a single trajectory while being able to study finite temperature. One could of course use the thermal noise process to model the temperature but that would require multiple trajectories to be computed.

In figure 10, we plotted the absorption spectrum of the QD obtained using both the independent boson model and HOPS. As previously discussed, the HOPS simulation was performed by propagating a single trajectory at a hierarchy depth of $\mathcal{K} = 7$. We see that the spectra exhibit a strong agreement. Figure 11 displays absorption spectra of the QD calculated using various hierarchy depths. Clearly we see that the spectra converge rapidly toward the one obtained with NMQSD. Already at $\mathcal{K} = 4$, we observe nearly perfect convergence, despite the relatively strong phonon coupling strength. In figure 12, the QD absorption spectra are simulated at various temperatures while maintaining a fixed hierarchy depth of $\mathcal{K} = 7$. As expected, we observe a decrease in the peak height and broadening of the spectra as the temperature rises.

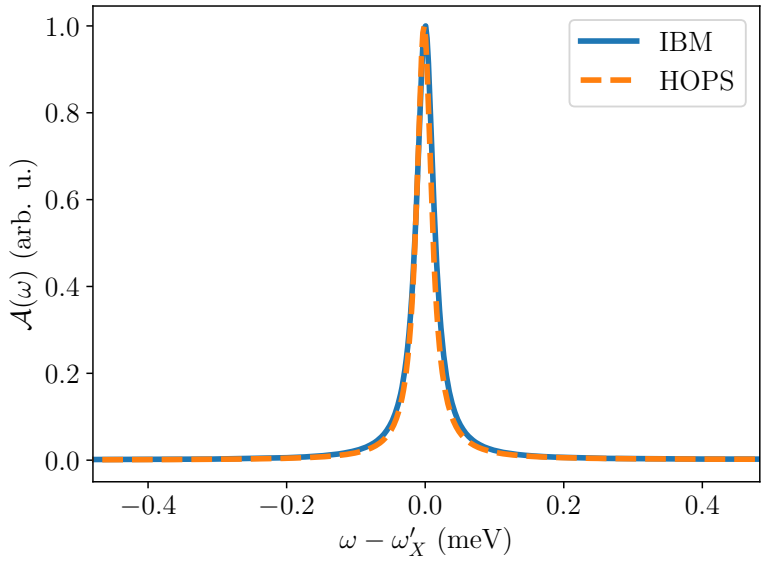

Figure 10. QD absorption spectra calculated exactly for the independent boson model, and with HOPS. Parameters used: $\alpha = 0.027$ ps^2, $\xi = 1.447$ meV, $T = 0$ K and $\mathcal{K} = 7$.

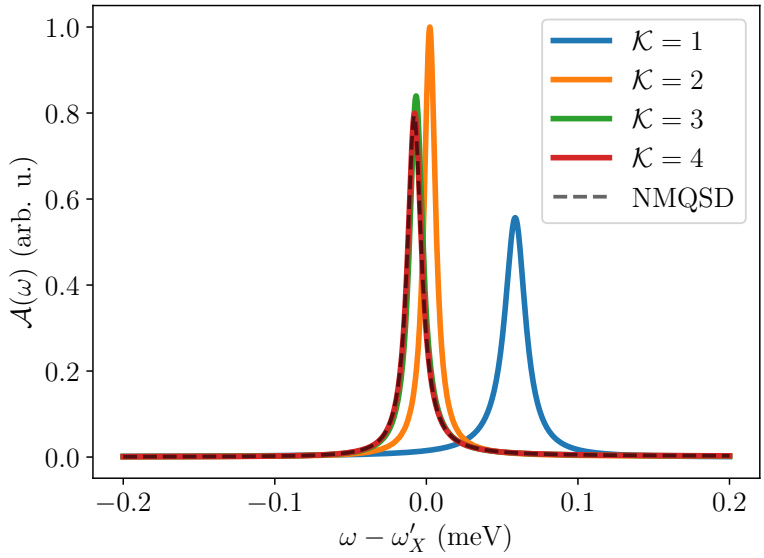

Figure 11. QD absorption spectra calculated with HOPS for different hierarchy depths and compared with NMQSD. Parameters used: $\alpha = 0.1$ ps^2, $\xi = 1.447$ meV and $T = 4$ K.

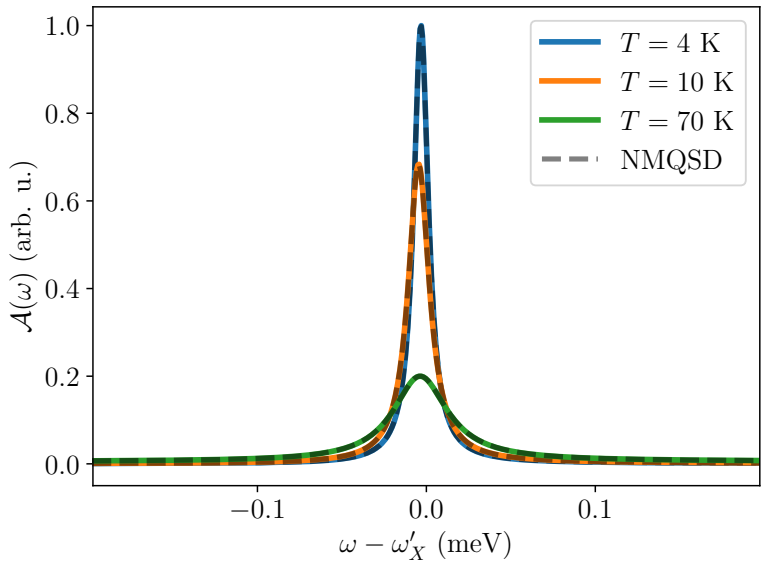

Figure 12. QD absorption spectra with different temperatures. Solid lines are obtained using HOPS and dashed lines are the corresponding NMQSD solutions. Parameters used: $\alpha = 0.027$ ps^2, $\xi = 1.447$ meV and $\mathcal{K} = 7$.

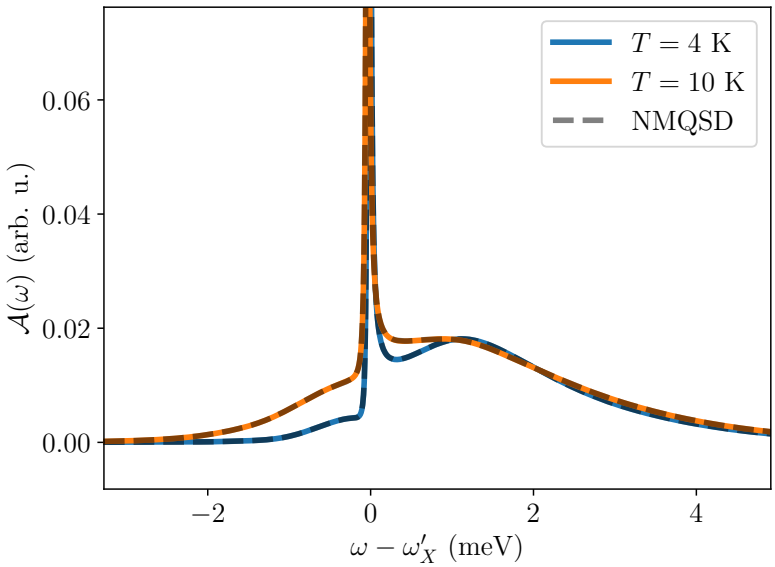

Figure 13. QD absorption spectra with different temperatures with a strong coupling to the environment. Solid lines are obtained using HOPS and dashed lines are the corresponding NMQSD solutions. Parameters used: $\alpha = 0.376$ ps^2, $\xi = 1.447$ meV and $\mathcal{K} = 8$.

In figure 13, we have calculated the absorption spectra at two different temperatures with strong phonon coupling. We observe qualitative agreement with the spectra calculated in reference [76] (FIG. 2). Here, we notice that although the spectrum is dominated by the independent boson model lorenzian peak, slight sidebands are also present. The asymmetry of the sidebands, particularly noticeable in the $T = 4$ K case, arise from varying probabilities of phonon absorption and emission. Specifically, at the lower temperature, phonon emission tends to be more probable than phonon absorption [76].

4.3 Response Functions

The response function $\phi_{BA}(t)$ of an observable B under the influence of the operator A is given by Kubo's theorem (1.29)

$$\phi_{BA}(\tau) = i\mathrm{tr}\{B(\tau)[A, \varrho_{\mathrm{eq}}]\}.$$

This can be rewritten to a more useful form

$$\phi_{BA}(\tau) = i\mathrm{tr}\{B\mathcal{U}_\tau[A, \varrho_{\mathrm{eq}}]\mathcal{U}_\tau^\dagger\},$$

where $\mathcal{U}_\tau = \exp(-iH_0\tau)$ is the propagator for the unperturbed evolution [69]. To utilize HOPS, we assume that the equilibrium state factorizes $\varrho_{\mathrm{eq}} \approx \rho_{\mathrm{S}}^{\mathrm{eq}} \otimes \rho_{\mathrm{E}}^{\mathrm{eq}}$. With this assumption, and defining $\kappa(\tau) = \mathcal{U}_\tau[A, \varrho_{\mathrm{eq}}]\mathcal{U}_\tau^\dagger$, we can write

$$\begin{aligned}
\phi_{BA}(\tau) &= i\mathrm{tr}_{\mathrm{S}}\{B\kappa(\tau)\}, \\
\kappa(\tau) &= \mathrm{tr}_{\mathrm{E}}\{\mathcal{U}_\tau[A, \rho_{\mathrm{S}}^{\mathrm{eq}}] \otimes \rho_{\mathrm{E}}^{\mathrm{eq}}\mathcal{U}_\tau^\dagger\} \\
&= \mathrm{tr}_{\mathrm{E}}\{\mathcal{U}_\tau\kappa_{\mathrm{S}} \otimes \rho_{\mathrm{E}}^{\mathrm{eq}}\mathcal{U}\tau^\dagger\},
\end{aligned}$$

where $\kappa_{\mathrm{S}} = [A, \rho_{\mathrm{S}}^{\mathrm{eq}}]$. To compute the response function, all that needs to be done is to compute $\kappa(\tau)$. To be able to do this with HOPS, κ_{S} needs to be expressed as a composition of pure states [69]. If we assume that A is Hermitian, then κ_{S} is a

normal operator and it can be expressed using the spectral decomposition [77]

$$\kappa_{\mathrm{S}} = \sum_{\lambda} a_{\lambda} \left|\varphi_{\lambda}\right\rangle \left\langle\varphi_{\lambda}\right|,$$

where a_λ are the eigenvalues of κ_{S} and $|\varphi_\lambda\rangle$ the corresponding eigenvectors. Assuming that the equilibrium state for the environment is the thermal state, we can write

$$\kappa(\tau) = \sum_{\lambda} a_{\lambda} \mathrm{tr}_{\mathrm{E}}\{\mathcal{U}_{\tau} \left|\varphi_{\lambda}\right\rangle \left\langle\varphi_{\lambda}\right| \otimes \rho_{\mathrm{E}}^{\mathrm{eq}} \mathcal{U}_{\tau}^{\dagger}\} = \sum_{\lambda} a_{\lambda} \mathcal{M}[|\varphi_{\lambda,t}(z^*)\rangle \left\langle\varphi_{\lambda,t}(z)\right|].$$

Thus $\kappa(\tau)$ can be computed by propagating each eigenvector $|\varphi_\lambda\rangle$ using HOPS. Note that the propagation of the eigenvectors $|\varphi_\lambda\rangle$ is done by using same noise processes. The reduced equilibrium state $\rho_{\mathrm{S}}^{\mathrm{eq}}$ can be obtained by either calculating the exact expression $\rho_{\mathrm{S}}^{\mathrm{eq}} = \exp(-\beta H_{\mathrm{S}})/\mathrm{tr}[\exp(-\beta H_{\mathrm{S}})]$ or by approximately computing $\rho_{\mathrm{S}}^{\mathrm{eq}} \approx \rho_{\mathrm{S}}(\infty)$, where $\rho_{\mathrm{S}}(\infty)$ denotes the asymptotic reduced density matrix, which can be computed using HOPS.

We again neglect the cavity coupling. The Hamiltonian used for the subsequent calculations is of the form

$$H_{\mathrm{S}} = \Delta \left|X\right\rangle \left\langle X\right| + \frac{\Omega}{2}(\left|g\right\rangle \left\langle X\right| + \left|X\right\rangle \left\langle g\right|)$$

with $\Delta = 0.2$ meV and $\Omega = 0.3$ ps^{-1}. We compute the response function $\phi_{BA}(t)$ for $A = B = \sigma_x$ across various temperatures and phonon coupling strengths. In figures 14 and 15, we have computed the response functions at a temperature of $T = 4$ K for both cases, with coupling strengths $\alpha = 0.027$ ps^2 and $\alpha = 0.15$ ps^2, respectively. The propagation was performed with non-linear HOPS with a hierarchy depth of $\mathcal{K} = 6$. We notice that only a few trajectories need to be calculated. With 16 trajectories, we observe the response function taking its overall shape and already with 256 trajectories we achieve significant convergence. In figure 16 we have calculated the response function at $T = 70$ K. In this case we see that more trajectories are needed to obtain a smooth result. At 512 trajectories significant

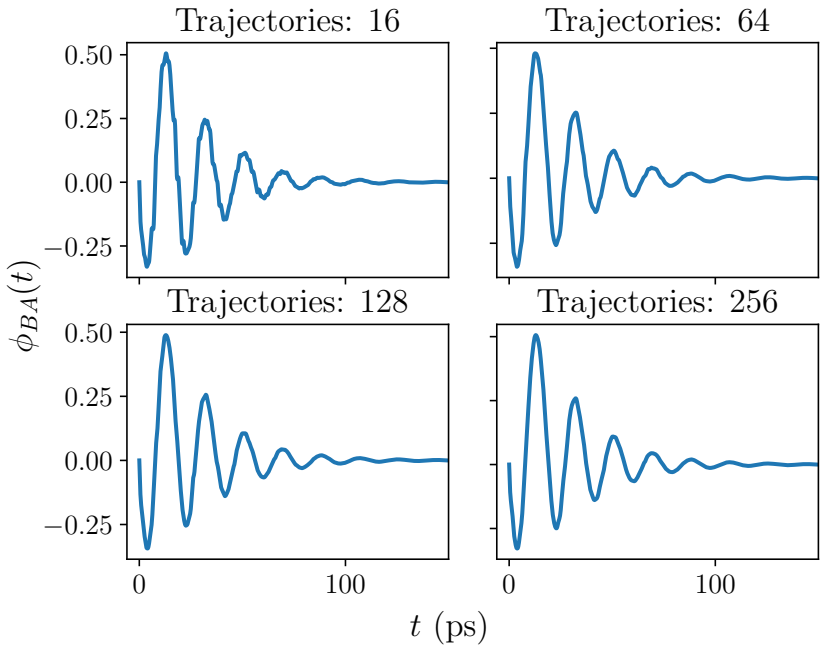

Figure 14. Response function $\phi_{BA}(t)$, $A = B = \sigma_x$, calculated with different amounts of trajectories. QD parameters used: $\alpha = 0.027$ ps^2, $\xi = 1.447$ meV and $T = 4$ K.

artifacts are present and with 5120 trajectories some faint noise can still be seen. The increase in needed trajectories is expected since the variance of the coefficients in the generated noise (3.13) increases as the temperature increases. This increase is due to the fact that the variance of the coefficients depend on the Bose-Einstein distribution, which increases as temperature increases. With a greater variance, the thermal noise process fluctuates significantly more and consequently this requires more trajectories to be computed to smooth out the contribution of the thermal processes.

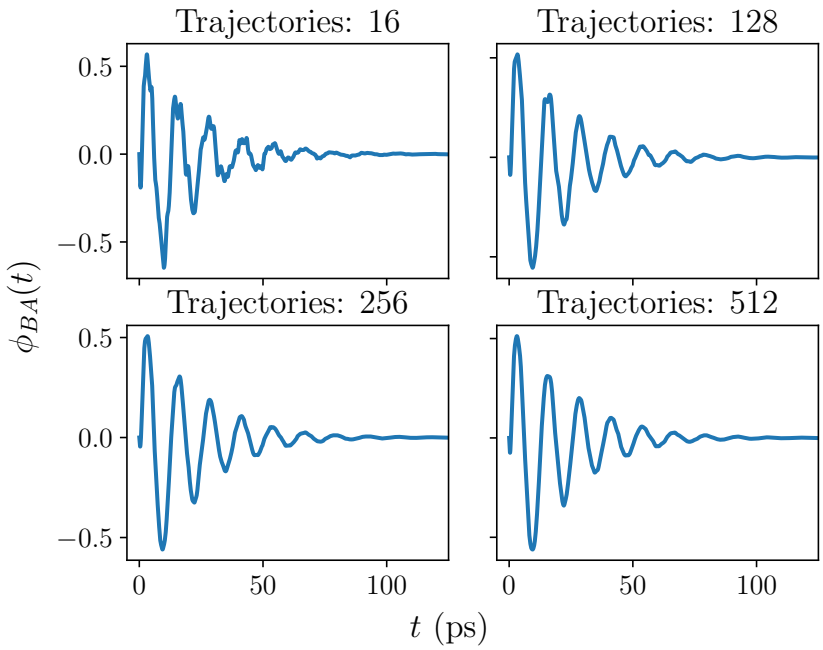

Figure 15. Response function $\phi_{BA}(t)$, $A = B = \sigma_x$, calculated with different amounts of trajectories. QD parameters used: $\alpha = 0.15$ ps^2, $\xi = 1.447$ meV and $T = 4$ K.

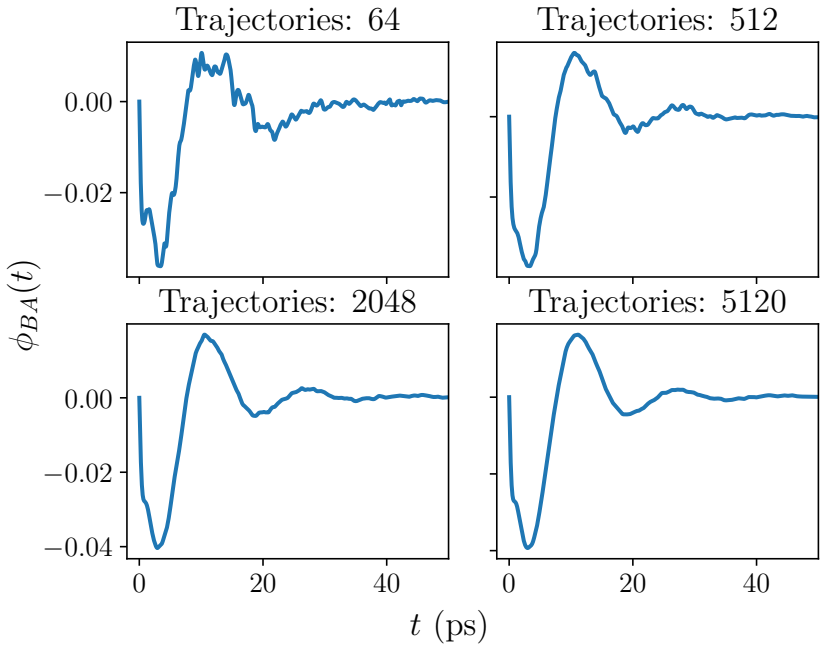

Figure 16. Response function $\phi_{BA}(t)$, $A = B = \sigma_x$, calculated with different amounts of trajectories. QD parameters used: $\alpha = 0.027$ ps^2, $\xi = 1.447$ meV and $T = 70$ K.

4.4 Emission Spectra

4.4.1 Directly Driven QD

Let us first consider the QD being directly driven by an external monochromatic drive without coupling to the cavity, with the Hamiltonian given in (1.23) in the rotating wave approximation. The spectrum of resonance fluorescence for incoherent scattering is given by (1.40). By assuming the factorization of the system and environment states, the steady state expectation value $\langle\tilde{\sigma}_+\tilde{\sigma}_-(\tau)\rangle_{\rm ss}$ can be calculated by

$$\begin{aligned}\langle\tilde{\sigma}_+\tilde{\sigma}_-(\tau)\rangle_{\rm ss} &= {\rm tr}\{\tilde{\sigma}_+\tilde{\sigma}_-\varrho(\infty)\}\\ &= {\rm tr}_{\rm S}\{\tilde{\sigma}_-{\rm tr}_{\rm E}\{\mathcal{U}_\tau\varrho(\infty)\tilde{\sigma}_+\mathcal{U}_\tau^\dagger\}\}\\ &= {\rm tr}_{\rm S}\{\tilde{\sigma}_-{\rm tr}_{\rm E}\{\mathcal{U}_\tau\kappa_{\rm S}\otimes\rho_{\rm E}^{\rm eq}\mathcal{U}_\tau^\dagger\}\},\end{aligned}$$

where we have defined $\kappa_{\rm S} = \rho_{\rm S}(\infty)\tilde{\sigma}_+$. As discussed previously, the steady state $\rho_{\rm S}(\infty)$ can be computed by using HOPS. In general $\kappa_{\rm S}$ is neither Hermitian nor normal so we cannot express it by using the spectral decomposition. However, since we are considering a two-level system, we can utilize the fact that any complex matrix $A \in \mathcal{M}_{2\times2}(\mathbb{C})$ can be expressed uniquely by using the Pauli spin matrices

$$A = \lambda_0\mathbb{1} + \lambda_x\sigma_x + \lambda_y\sigma_y + \lambda_z\sigma_z,$$

where the coefficients λ_i are obtained from the entries of the matrix

$$\begin{aligned}\lambda_0 &= \frac{1}{2}(A_{00}+A_{11}),\ \lambda_x = \frac{1}{2}(A_{01}+A_{10}),\\ \lambda_y &= \frac{i}{2}(A_{01}-A_{10}),\ \lambda_z = \frac{1}{2}(A_{00}-A_{11}).\end{aligned}$$

Since Pauli matrices are Hermitian, they can be decomposed into a sum of orthogonal pure states and therefore any matrix can be decomposed as well. In particular for

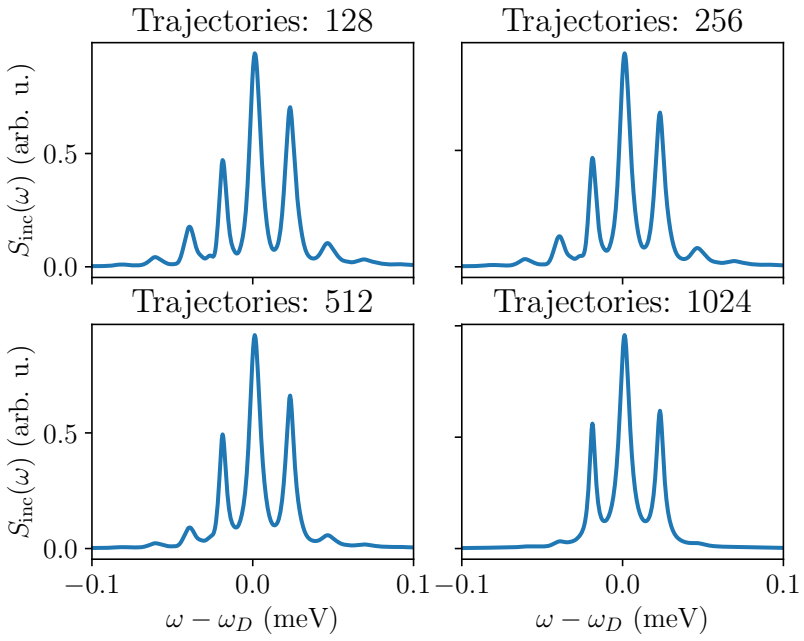

Figure 17. Spectrum of resonance fluorescence for the QD being directly driven. Parameters used: $\Omega = 0.06$ ps^{-1}, $\alpha = 0.027$ ps^2, $\xi = 1.447$ meV and $T = 4$ K.

κ_{S} we have

$$\begin{aligned}\kappa_{\mathrm{S}} = (\lambda_0 + \lambda_z)\,|g\rangle\langle g| + (\lambda_0 - \lambda_z)\,|X\rangle\langle X| \\ + \lambda_x(|+\rangle_{x\,x}\langle +| - |-\rangle_{x\,x}\langle -|) + \lambda_y(|+\rangle_{y\,y}\langle +| - |-\rangle_{y\,y}\langle -|),\end{aligned} \tag{4.2}$$

where $|\pm\rangle_x = \frac{1}{\sqrt{2}}(|g\rangle \pm |X\rangle)$ and $|\pm\rangle_y = \frac{1}{\sqrt{2}}(|g\rangle \pm i\,|X\rangle)$. Thus $\kappa(\tau)$ can be computed by propagating each of the pure states present in the decomposition.

Figure 17 displays the incoherent emission spectrum of the QD across various numbers of trajectories. The QD was driven with the phonon-shifted transition frequency (1.16), i.e., $\omega_D = \omega'_X$, and we propagated each of the pure states obtained from the pure state decomposition (4.2) using non-linear HOPS with a hierarchy depth of $\mathcal{K} = 5$. With 128 trajectories, the distinct triple peaks of the Mollow triplet are visible, albeit with significant noise. Increasing to 1024 trajectories reduces the noise significantly, resulting in a smoother spectrum. Additionally we observe, more prominently with 512 trajectories and fewer, the asymmetry of the sideband peaks,

which is caused by the phonon coupling [76, 78].

4.4.2 Adiabatic Elimination

Thus far we have not taken into account the cavity. The QD has just been driven directly by an external drive. We can approach this from a different viewpoint and suppose that the QD is coupled with both the cavity and the phonon bath, but instead now the cavity is being driven by an external drive. This however makes the dynamics more complicated due to the additional Hilbert space that needs to be considered for the cavity modes. To simplify the analysis, we eliminate the cavity operators by using adiabatic elimination. Adiabatic elimination is a general technique to reduce the number of equations that need to be considered to solve the dynamics of the system. It is based on the fact that the system evolves in two time scales, fast and slow. Initially the system evolves over the fast times scales and the evolution is determined by the fast variables. At this stage the slowly evolving variables are assumed to be constant. The fast variables eventually settle to values that are determined by the slow variables and this results in a relation between the fast and slow variables [79, 80].

To simplify the situation even further, we consider only a single cavity mode being present. Omitting the phonon environment terms, the Hamiltonian is given by

$$H = \omega_X \left|X\right\rangle \left\langle X\right| + \omega_c b^\dagger b + u(\sigma_- b^\dagger + \sigma_+ b) + f(t)b^\dagger + f^*(t)b,$$

where $f(t)$ is some arbitrary driving term. The corresponding NMQSD equation is

$$\begin{aligned}\partial_t \left|\psi_t(z^*)\right\rangle = &- iH \left|\psi_t(z^*)\right\rangle + z_t^* L \left|\psi_t(z^*)\right\rangle - L^\dagger \int_0^t \mathrm{d}s \alpha(t-s) \frac{\delta}{\delta z_s^*} \left|\psi_t(z^*)\right\rangle \\ &+ \xi_t b^\dagger \left|\psi_t(z^*)\right\rangle - \frac{1}{2}\kappa b^\dagger b \left|\psi_t(z^*)\right\rangle,\end{aligned}$$

where we have added the term $\xi_t b^\dagger - \frac{1}{2}\kappa b^\dagger b$ which describes the cavity damping [79]. Here ξ_t is a white noise process with $\mathcal{M}[\xi_t] = 0$ and $\mathcal{M}[\xi_t \xi_s^*] = \kappa\delta(t-s)$. This

damping term corresponds to the Lindblad term $\kappa(b^\dagger \rho_S b - \frac{1}{2}\{b^\dagger b, \rho_S\})$.

Now we eliminate the creation and annihilation operators $b^\dagger$ and b by employing adiabatic elimination with a mean-field approximation. We start by considering the time-evolution of the annihilation operator expectation value $\langle b \rangle_{z^*,\xi} = \langle \psi_t(z)|b|\psi_t(z^*)\rangle$ for a single trajectory

$$\begin{aligned}\frac{\partial \langle b \rangle_{z^*,\xi}}{\partial t} = & i \langle [H, b] \rangle_{z^*,\xi} + (z_t + z_t^*) \langle Lb \rangle_{z^*,\xi} - \langle (\bar{\mathcal{O}}^\dagger L + L\bar{\mathcal{O}}) b \rangle_{z^*,\xi} \\ & + \xi_t^* \langle b^\dagger b \rangle_{z^*,\xi} + \xi_t \langle bb \rangle_{z^*,\xi} - \frac{1}{2}\kappa \langle b^\dagger bb + bb^\dagger b \rangle_{z^*,\xi} .\end{aligned}$$

Here we have used $L = L^\dagger$ and denoted $\bar{\mathcal{O}} = \int_0^t \mathrm{d}s \alpha(t-s) \frac{\delta}{\delta z_s^*}$. We now approximate that $\langle AB \rangle \approx \langle A \rangle \langle B \rangle$, where A is a system operator and B is an operator for the cavity. With this approximation and by the properties of the creation and annihilation operators we have

$$\begin{aligned}\frac{\partial \langle b \rangle_{z^*,\xi}}{\partial t} = & - i\omega_c \langle b \rangle_{z^*,\xi} - iu \langle \sigma_- \rangle_{z^*,\xi} - if(t) + (z_t + z_t^*) \langle L \rangle \langle b \rangle_{z^*,\xi} \\ & - \langle (\bar{\mathcal{O}}^\dagger L + L\bar{\mathcal{O}}) \rangle_{z^*,\xi} \langle b \rangle_{z^*,\xi} + \xi_t^* \langle b^\dagger b \rangle_{z^*,\xi} + \xi_t \langle bb \rangle_{z^*,\xi} - \kappa \langle b^\dagger bb \rangle_{z^*,\xi} \\ & - \frac{1}{2}\kappa \langle b \rangle_{z^*,\xi} . \end{aligned} \tag{4.3}$$

The expectation value is given by the ensemble average $\langle b \rangle = \mathcal{M}[\langle \psi_t(z^*)|b|\psi_t(z)\rangle]$. By averaging (4.3) over both z_t^* and ξ_t and utilizing the Furutsu-Novikov theorem we obtain

$$\frac{\partial \langle b \rangle}{\partial t} = -i\omega_c \langle b \rangle - iu \langle \sigma_- \rangle - if(t) - \frac{1}{2}\kappa \langle b \rangle .$$

Now we can solve the steady state by setting $\frac{\partial \langle b \rangle}{\partial t} = 0$ to obtain

$$\langle b \rangle_{\mathrm{ss}} = -i \frac{u \langle \sigma_- \rangle + f(t)}{i\omega_c + \frac{\kappa}{2}}.$$

We can simplify this further by assuming weak coupling between the QD and the cavity, high photon leakage from the cavity $u << \kappa$, and a strong driving field. We then obtain

$$\langle b \rangle_{\mathrm{ss}} \approx \frac{f(t)}{-\omega_c + i\frac{\kappa}{2}}.$$

Now we replace the annihilation and creation operators with the steady state expectation values to obtain

$$\begin{aligned}\tilde{H} =&\omega_X \left|X\right\rangle \left\langle X\right| + u\left(\frac{f^*(t)}{-\omega_c - i\frac{\kappa}{2}}\sigma_- + \frac{f(t)}{-\omega_c + i\frac{\kappa}{2}}\sigma_+\right),\\ \partial_t \left|\psi_t(z^*)\right\rangle =&-i\tilde{H}\left|\psi_t(z^*)\right\rangle + z_t^* L - L^\dagger \int_0^t \mathrm{d}s\alpha(t-s)\frac{\delta}{\delta z_s^*},\end{aligned}$$

where we have discarded the terms that are proportional to the identity operator since they have no effect in the corresponding master equation. For the following we consider the drive to be of the form $f(t) = \Omega\cos(\omega_D t)$, where ω_D is the driving frequency. Moving to the rotating frame of the drive and performing the rotating wave approximation we obtain the Hamiltonian

$$\tilde{H}_{\mathrm{RWA}} = \Delta\left|X\right\rangle\left\langle X\right| - \tilde{\Omega}\left(\omega_c\sigma_x + \frac{\kappa}{2}\sigma_y\right),$$

where $\Delta = \omega_X - \omega_D$ and $\tilde{\Omega} = \frac{u\Omega}{2\omega_c^2 + \frac{\kappa^2}{2}}$, with the assumptions that $\Delta << \omega_D$ and $\tilde{\Omega} << \omega_D$.

Figure 18 shows the spectrum of resonance fluorescence of the QD with cavity coupling. As for the directly driven case, we again drive with the phonon-shifted transition frequency and the hierarchy depth of the non-linear HOPS was $\mathcal{K} = 5$. The spectra has great similarity to the directly driven case. One notable difference is the more pronounced asymmetry of the sidepeaks of the Mollow triplet. In this case the right peak is noticeably higher compared to the left peak.

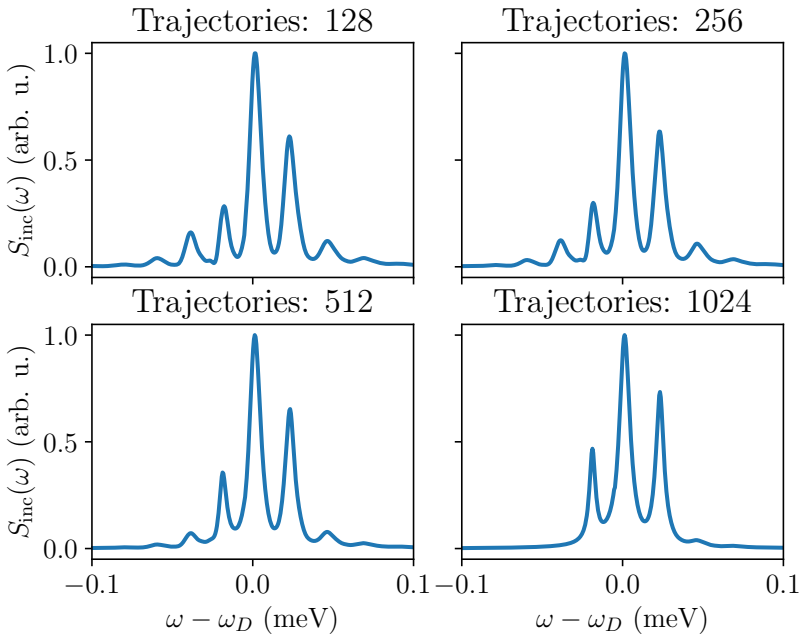

Figure 18. Spectrum of resonance fluorescence for the QD being driven through the cavity coupling. Parameters used: $\tilde{\Omega} = 1.46 \cdot 10^{-5}$ meV, $\kappa = 0.02$ ps^{-1}, $\omega_c = \omega_X$, $\alpha = 0.027$ ps^2, $\xi = 1.447$ meV and $T = 4$ K.

4.5 Weak Coupling

When the coupling between the QD and the phonon environment is weak, one can approach the situation by using perturbation theory. In the context of a quantum system coupled weakly to an environment, this approach is sometimes called Redfield theory named after Alfred Redfield who first applied it to nuclear magnetic resonance [81, 82]. In particular, Redfield theory is a second order perturbation theory. In the case of the QD system, we consider the phonon coupling strength up to second order g_λ^2. This can be done explicitly by truncating the HOPS at the first level. To see this, we consider the zeroth level

$$\partial_t \left|\psi_t(z^*)\right\rangle = (-iH_{\mathrm{S}} + z_t^* L)\left|\psi_t(z^*)\right\rangle - L^\dagger \sum_\mu \left|\psi_t^{\mathbf{e}_\mu}(z^*)\right\rangle . \tag{4.4}$$

Since the BCF is already second order in g_λ, any higher level terms are neglected and by (3.9) we obtain for the first level auxiliary state $|\psi_t^{\mathbf{e}_\mu}(z^*)\rangle$

$$\begin{aligned}\partial_t |\psi_t^{\mathbf{e}_\mu}(z^*)\rangle &= (-iH_{\mathrm{S}} - W_\mu + z_t^* L)|\psi_t^{\mathbf{e}_\mu}(z^*)\rangle + L\mathcal{G}_\mu |\psi_t(z^*)\rangle - L^\dagger \sum_\nu |\psi_t^{\mathbf{e}_\mu+\mathbf{e}_\nu}(z^*)\rangle \\ &\approx (-iH_{\mathrm{S}} - W_\mu)|\psi_t^{\mathbf{e}_\mu}(z^*)\rangle + L\mathcal{G}_\mu |\psi_t(z^*)\rangle .\end{aligned}$$

This has the formal solution

$$|\psi_t^{\mathbf{e}_\mu}(z^*)\rangle = \int_0^t \mathrm{d}s \mathcal{G}_\mu e^{-W_\mu(t-s)} e^{-iH_{\mathrm{S}}(t-s)} L |\psi_s(z^*)\rangle . \tag{4.5}$$

This can be simplified further. By definition of $|\psi_s(z^*)\rangle$ we have

$$|\psi_s(z^*)\rangle = \langle \mathbf{z}||\mathcal{U}_s|\Psi_0\rangle = \langle \mathbf{z}||\mathcal{U}_{t-s}^\dagger|\Psi_t\rangle \approx e^{iH_{\mathrm{S}}(t-s)}|\psi_t(z^*)\rangle ,$$

where we have kept the contribution of the propagator that is zeroth order in g_λ, i.e., $\mathcal{U}_{t-s}^\dagger \approx e^{iH_{\mathrm{S}}(t-s)}$. Inserting this into (4.5), we obtain

$$|\psi_t^{\mathbf{e}_\mu}(z^*)\rangle \approx \int_0^t \mathrm{d}s \mathcal{G}_\mu e^{-W_\mu(t-s)} e^{-iH_{\mathrm{S}}(t-s)} L e^{iH_{\mathrm{S}}(t-s)} |\psi_t(z^*)\rangle .$$

Now inserting this back to the zeroth level (4.4) we have the corresponding NMQSD equation

$$\partial_t |\psi_t(z^*)\rangle \approx (-iH_{\mathrm{S}} + z_t^* L)|\psi_t(z^*)\rangle - L^\dagger \int_0^t \mathrm{d}s \alpha(t-s) e^{-iH_{\mathrm{S}}(t-s)} L e^{iH_{\mathrm{S}}(t-s)} |\psi_t(z^*)\rangle .$$

In light of the derivation, solving this NMQSD equation corresponds to solving HOPS where only the first level is included. For the triangular truncation condition this means $\mathcal{K} = 1$.

Figure 19 shows the expectation values $\langle\sigma_x\rangle$, $\langle\sigma_y\rangle$ and $\langle\sigma_z\rangle$ for the exact and Redfield solutions. The Hamiltonian used was

$$H_{\mathrm{S}} = \Delta |X\rangle\langle X| + \frac{\Omega}{2}(|g\rangle\langle X| + |X\rangle\langle g|),$$

where $\Delta = 0.012$ meV and $\Omega = 0.12$ ps^{-1}. For the exact case, we solved HOPS with $\mathcal{K} = 9$. For the weakest coupling, we effectively see identical dynamics for both cases.

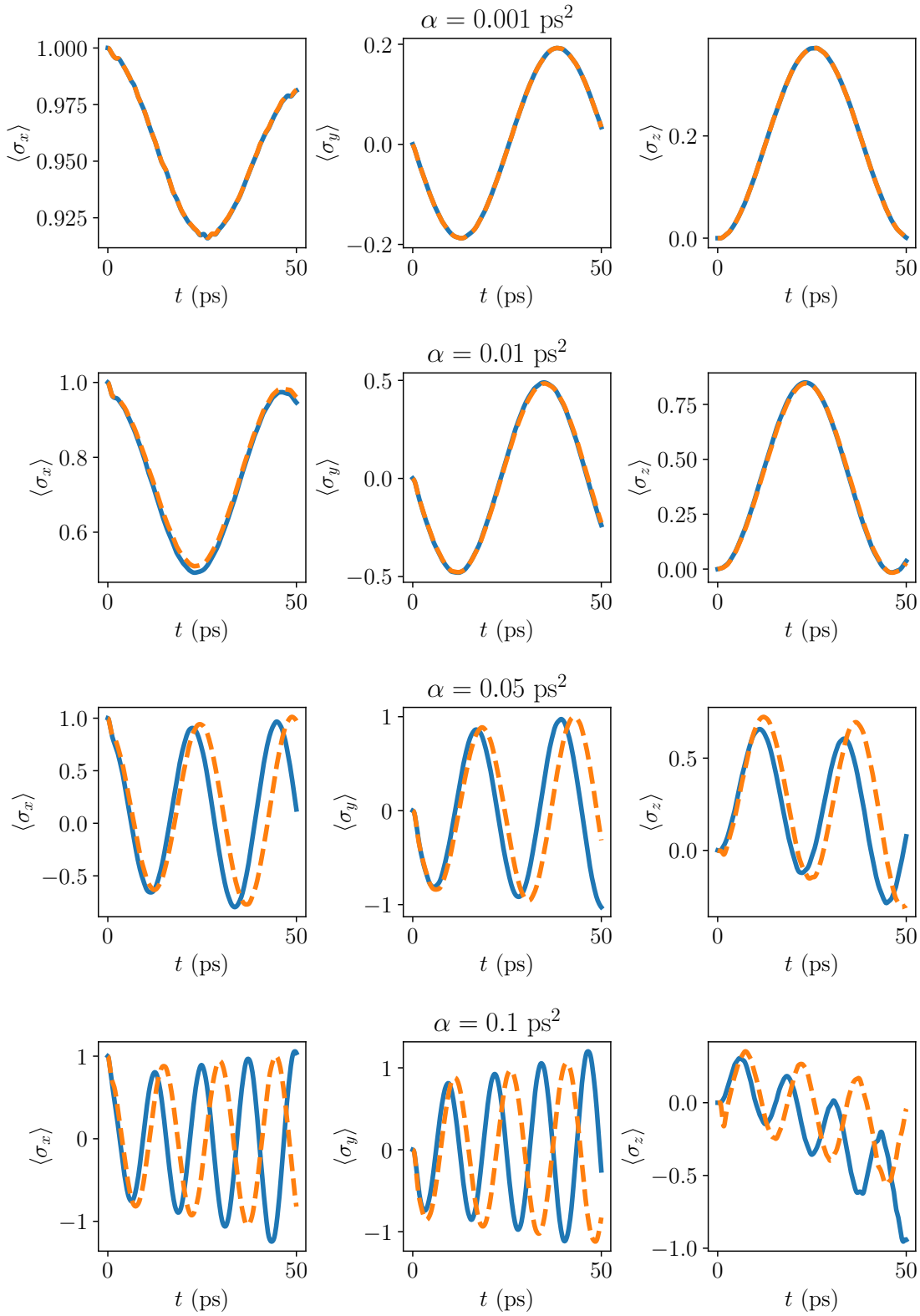

Figure 19. Exact (solid lines) and Redfield (dashed lines) expectation values $\langle\sigma_x\rangle$, $\langle\sigma_y\rangle$ and $\langle\sigma_z\rangle$ for increasing phonon coupling strengths. The simulations were performed with 10000 trajectories at zero temperature and cut-off frequency $\xi = 1.447$ meV

Increasing the coupling to $\alpha = 0.01$ ps^2 resulted again in almost identical dynamics, expect the slight deviation in the expectation value $\langle \sigma_x \rangle$. Further increase in the coupling strength lead to the Redfield solutions to deviate noticeably from the exact solutions. This deviation is expected since Redfield theory assumes weak coupling to the environment, which in this case means values below $\alpha = 0.01$ ps^2.

5 Conclusions

We derived and studied the NMQSD formalism to solve the dynamics of open quantum systems and in particular our quantum dot system. This is achieved by solving the corresponding NMQSD equation for an ensemble of trajectories and then taking the average over them. While the derivation was done in zero-temperature, we presented two ways of incorporating temperature into the model, either by the thermo field method or by adding a separate stochastic process to model the temperature fluctuations.

For some special cases, such as the independent boson model, we can directly use NMQSD to solve the dynamics of the QDs. In the general case this isn't possible and some kind of approximations need to be made to compute the functional derivative appearing in the NMQSD equation. For this general case we derived the HOPS method where the functional derivative is turned into a hierarchy of pure states and, in principle, allows any NMQSD equation to be solved numerically exactly. We briefly described qualitatively how the HOPS method in its linear and nonlinear forms can be implemented with efficiency in mind. We also presented how the various stochastic processes can be generated for practical implementations and how the exponential sum expansion of the BCF can be approximated with the t-PFD method.

The HOPS method was then applied to study the dynamics of the QD. Firstly, we compared it to the independent boson model as a benchmark. Subsequently, we simulated the absorption spectra of the QD under various coupling strengths and temperatures. This application also demonstrated the usefulness of incorporating temperature using the thermo field method, reducing the necessity to consider multiple trajectories to only a single trajectory. Additionally, we presented a procedure illustrating how HOPS can be used to compute response functions in general.

The emission spectrum of the QD was considered from two perspectives. First

the QD was driven directly with a monochromatic drive and decoupled from the cavity. In the second case we coupled the QD to the cavity, but instead of driving the QD, we drove the cavity with the monochromatic drive. We demonstrated how to eliminate the cavity operators by using adiabatic elimination and computed the spectrum of resonance fluorescence for both cases with HOPS and observed the expected Mollow triplets. We also illustrated how, particularly in the case of two-level systems, HOPS enables the propagation of arbitrary operators. Finally we compared the dynamics given by Redfield theory and HOPS and observed the weak coupling assumption being necessary for the Redfield case.

The linear version of HOPS proved to be especially useful for the calculation of absorption spectra where only one trajectory needed to be considered. To be able to use the non-linear version for this, we would have needed to consider multiple trajectories. However, for the cases where multiple trajectories were needed, e.g. the independent boson model, and temperature was high or the phonon coupling was strong, the non-linear HOPS has significantly better convergence properties compared to the linear version. Conducting a quantitative analysis of the error associated with the HOPS method would provide valuable and instructive insights, given that the error analysis in this thesis was primarily qualitative.

These results not only highlight the applicability of HOPS in studying the optical properties of QDs but also suggest that it potentially provides a reliable framework for accurately simulating QD dynamics in strong coupling regimes. Throughout most of this thesis, we neglected the cavity coupling. For further study, it would be interesting to explore if HOPS yields good results when the cavity coupling is included. This is particularly relevant in the strong cavity coupling regime where adiabatic elimination isn't applicable. In the light of the obtained results, the HOPS methods shows promise as an effective tool for further exploration in understanding the dynamics of quantum dots.

A P-representation for the Thermal State

The thermal state of the phonon environment is given by

$$\rho_E = \frac{e^{-\beta H_{\rm Ph}}}{\mathrm{tr}\{e^{-\beta H_{\rm Ph}}\}}.$$

This can be represented in terms of coherent states by using the Glauber-Sudarshan P representation

$$\rho_E = \int d^2\boldsymbol{\xi} P(\boldsymbol{\xi}) \left|\boldsymbol{\xi}\right\rangle \left\langle\boldsymbol{\xi}\right|,$$

where $d^2\boldsymbol{\xi} \equiv \prod_\lambda d\mathrm{Re}(\xi_\lambda) d\mathrm{Im}(\xi_\lambda)$. Since we consider the case where each phonon in the bath is independent, we can express $\exp(-\beta H_{\rm Ph}) = \prod_\lambda \exp(-\beta\omega_\lambda a_\lambda^\dagger a_\lambda)$. Thus we consider only a single factor in the following. Using the over-completeness of coherent states and the fact that for coherent states

$$e^{-\frac{\beta\omega}{2}a^\dagger a}\left|\alpha\right\rangle = e^{-\frac{|\alpha|^2}{2}(1-e^{-\beta\omega})}\left|\alpha e^{-\frac{\beta\omega}{2}}\right\rangle,$$

we have

$$\begin{aligned}
\frac{e^{-\beta\omega a^\dagger a}}{\mathrm{tr}[e^{-\beta\omega a^\dagger a}]} &= (1-e^{-\beta\omega}) e^{-\frac{\beta\omega}{2}a^\dagger a}\mathbb{1} e^{-\frac{\beta\omega}{2}a^\dagger a} \\
&= \frac{1-e^{-\beta\omega}}{\pi}\int d^2\alpha e^{-\frac{\beta\omega}{2}a^\dagger a}\left|\alpha\right\rangle\left\langle\alpha\right| e^{-\frac{\beta\omega}{2}a^\dagger a} \\
&= \frac{1-e^{-\beta\omega}}{\pi}\int d^2\alpha e^{-|\alpha|^2(1-e^{-\beta\omega})}\left|\alpha e^{-\frac{\beta\omega}{2}}\right\rangle\left\langle\alpha e^{-\frac{\beta\omega}{2}}\right|.
\end{aligned}$$

Performing the change of variables $\xi = \alpha e^{-\frac{\beta\omega}{2}}$ we get the final form

$$\begin{aligned}
\frac{e^{-\beta\omega a^\dagger a}}{\mathrm{tr}[e^{-\beta\omega a^\dagger a}]} &= \frac{e^{\beta\omega}(1-e^{-\beta\omega})}{\pi}\int d^2\xi e^{-|\xi|^2(e^{\beta\omega}-1)}\left|\xi\right\rangle\left\langle\xi\right| \\
&= \int d^2\xi \frac{e^{-\frac{|\xi|^2}{\bar{n}}}}{\pi\bar{n}}\left|\xi\right\rangle\left\langle\xi\right|,
\end{aligned}$$

where $\bar{n} = (e^{\beta\omega}-1)^{-1}$ is the Bose-Einstein distribution. Comparing with (1.13) we can read out the Glauber-Sudarshan P function of the thermal state

$$P(\xi) = \frac{e^{-\frac{|\xi|^2}{\bar{n}}}}{\pi\bar{n}}.$$

For the phonon bath we have immediately

$$\rho_E = \int d^2\mathbf{z} P(\mathbf{z}) \left|\mathbf{z}\right\rangle \left\langle\mathbf{z}\right|, \tag{A.1}$$

with $d^2\mathbf{z} = \prod_\lambda d^2 z_\lambda$ and $P(\mathbf{z}) = \prod_\lambda P_\lambda(z_\lambda)$.

B BCF Fit Data

Table I. BCF fitting data for parameters $\alpha = 0.001$ ps^2, $\xi = 1.447$ meV, $K_r = 4$, $K_i = 4$ and $T = 0$ K.

μ	$\mathcal{G}_\mu$	W_μ
1	4.3463279e-4+9.6657029e-4i	$0.62374785 + 0.29260882i$
2	4.3463279e-4−9.6657029e-4i	$0.62374785 - 0.29260882i$
3	2.0897779e-3−1.1158370e-3i	$0.50699151 + 0.14516732i$
4	2.0897779e-3+1.1158370e-3i	$0.50699151 - 0.14516732i$
5	2.8179460e-5+7.8984774e-4i	$0.68810647 + 0.31255675i$
6	−2.8179460e-5+7.8984774e-4i	$0.68810647 - 0.31255675i$
7	−2.9452570e-3−7.8505231e-4i	$0.66378872 - 0.16225912i$
8	2.9452570e-3−7.8505231e-4i	$0.66378872 + 0.16225912i$

Table II. BCF fitting data for parameters $\alpha = 0.01$ ps^2, $\xi = 1.447$ meV, $K_r = 4$, $K_i = 4$ and $T = 0$ K.

μ	$\mathcal{G}_\mu$	W_μ
1	−8.0902226e-3−2.7225979e-2i	$1.2386066 - 2.7269830i$
2	−8.0902226e-3+2.7225979e-2i	$1.2386066 + 2.7269830i$
3	3.3768959e-2−4.1970595e-2i	$1.0306663 + 0.13366070i$
4	3.3768959e-2+4.1970595e-2i	$1.0306663 - 1.3366070i$
5	7.3323847e-3+2.7962142e-2i	$1.0732976 + 2.5648023i$
6	−7.3323847e-3+2.7962142e-2i	$1.0732976 - 2.5648023i$
7	1.0747893e-2−2.8668058e-2i	$0.79269244 + 1.1798854i$
8	−1.0747893e-2−2.8668058e-2i	$0.79269244 - 1.1798854i$

Table III. BCF fitting data for parameters $\alpha = 0.027$ ps^2, $\xi = 1.45$ meV, $K_r = 2$, $K_i = 2$ and $T = 0$ K.

μ	$\mathcal{G}_\mu$	W_μ
1	9.1008110e-2$-$2.6598924e-2i	$0.72610079 + 1.6328803i$
2	9.1008110e-2$+$2.6598924e-2i	$0.72610079 - 1.6328803i$
3	$-0.10464960 +$ 3.0355629e-3i	$0.75841966 - 1.7819431i$
4	$0.10464960 +$ 3.0355629e-3i	$0.75841966 + 1.7819431i$

Table IV. BCF fitting data for parameters $\alpha = 0.027$ ps^2, $\xi = 1.45$ meV, $K_r = 3$, $K_i = 3$ and $T = 0$ K.

μ	$\mathcal{G}_\mu$	W_μ
1	$-0.24861094 -$ 2.7974794e-12i	$1.9357470 +$ 3.0427833e-13i
2	$0.18235040 -$ 5.3330420e-2i	$1.1265958 - 1.8847615i$
3	$0.18235040 +$ 5.3330420e-2i	$1.1265958 + 1.8847615i$
4	$-0.12583471 +$ 1.2775555e-2i	$0.91550670 - 1.8788396i$
5	$0.12583471 +$ 1.2775555e-2i	$0.91550670 + 1.8788396i$
6	2.0084342e-14$+$4.7255434e-3i	$0.14804665 +$ 2.4447566e-12i

Table V. BCF fitting data for parameters $\alpha = 0.027$ ps^2, $\xi = 1.45$ meV, $K_r = 4$, $K_i = 4$ and $T = 0$ K.

μ	$\mathcal{G}_\mu$	W_μ
1	$-$1.1630818e-2+7.6279499e-2i	$1.2030471 + 2.6752567i$
2	$-$1.1630818e-2$-$7.6279499e-2i	$1.2030471 - 2.6752567i$
3	8.0807990e-2$-$0.11048017i	$1.0102923 + 1.3089856i$
4	8.0807990e-2+0.11048017i	$1.0102923 - 1.3089856i$
5	2.9365640e-2+0.10655663i	$1.1883583 + 2.4460374i$
6	$-$2.9365640e-2+0.10655663i	$1.1883583 - 2.4460374i$
7	$-$5.4086552e-3$-$0.10950872i	$0.93848951 + 1.0235189i$
8	5.4086552e-3$-$0.10950872i	$0.93848951 - 1.0235189i$

Table VI. BCF fitting data for parameters $\alpha = 0.027$ ps^2, $\xi = 1.447$ meV, $K_r = 4$, $K_i = 4$ and $T = 0$ K.

μ	$\mathcal{G}_\mu$	W_μ
1	$-$1.0445559e-2$-$7.6017052e-2i	$1.1979284 - 2.6626106i$
2	$-$1.0445559e-2+7.6017052e-2i	$1.1979284 + 2.6626106i$
3	7.8941658e-2+0.10922132i	$1.0059459 - 1.3031258i$
4	7.8941658e-2$-$0.10922132i	$1.0059459 + 1.3031258i$
5	$-$2.9452464e-2+0.10649790i	$1.1886753 - 2.4375437i$
6	2.9452464e-2+0.10649790i	$1.1886753 + 2.4375437i$
7	6.3953461e-3$-$0.10942159i	$0.94015781 - 1.0180596i$
8	$-$6.3953461e-3$-$0.10942159i	$0.94015781 + 1.0180596i$

Table VII. BCF fitting data for parameters $\alpha = 0.027$ ps^2, $\xi = 1.447$ meV, $K_r = 4$, $K_i = 4$ and $T = 4$ K.

μ	$\mathcal{G}_\mu$	W_μ
1	$-$2.5852605e-2+9.5061909e-2i	$1.2934167 + 2.6341258i$
2	$-$2.5852605e-2$-$9.5061909e-2i	$1.2934167 - 2.6341258i$
3	9.8261018e-2$-$0.15245563i	$1.1833395 + 1.2489527i$
4	9.8261018e-2+0.15245563i	$1.1833395 - 1.2489527i$
5	1.9568450e-2+7.1948428e-2i	$1.0543061 + 2.5760800i$
6	$-$1.9568450e-2+7.1948428e-2i	$1.0543061 - 2.5760800i$
7	3.1813505e-2$-$7.3689153e-2i	$0.77649304 + 1.1980856i$
8	$-$3.1813505e-2$-$7.3689153e-2i	$0.77649304 - 1.1980856i$

Table VIII. BCF fitting data for parameters $\alpha = 0.027$ ps^2, $\xi = 1.447$ meV, $K_r = 4$, $K_i = 4$ and $T = 10$ K.

μ	$\mathcal{G}_\mu$	W_μ
1	$-$1.8545215e-2+0.10636416i	$1.2376754 + 2.5659422i$
2	$-$1.8545215e-2$-$0.10636416i	$1.2376754 - 2.5659422i$
3	$0.11497826 - 0.19377765i$	$1.1040011 + 0.98964777i$
4	$0.11497826 + .019377765i$	$1.1040011 - 0.98964777i$
5	$-$1.3819159e-2+5.2283541e-2i	$0.95559479 - 2.6949511i$
6	1.3819159e-2+5.2283541e-2i	$0.95559479 + 2.6949511i$
7	5.0452919e-2$-$5.3298032e-2i	$0.70110901 + 1.3444128i$
8	$-$5.0452919e-2$-$5.3298032e-2i	$0.70110901 - 1.3444128i$

Table IX. BCF fitting data for parameters $\alpha = 0.027$ ps^2, $\xi = 1.447$ meV, $K_r = 4$, $K_i = 4$ and $T = 25$ K.

μ	$\mathcal{G}_\mu$	W_μ
1	$-3.8939725\text{e-}2+0.19698108i$	$1.2085893 + 2.4642518i$
2	$-3.8939725\text{e-}2-0.19698108i$	$1.2085893 - 2.4642518i$
3	$0.23149718 + 0.36149994i$	$1.0079069 - 0.93012682i$
4	$0.23149718 - 0.36149994i$	$1.0079069 + 0.93012682i$
5	$-1.3819159\text{e-}2+5.2283541\text{e-}2i$	$0.95559479 - 2.6949511i$
6	$1.3819159\text{e-}2+5.2283541\text{e-}2i$	$0.95559479 + 2.6949511i$
7	$5.0452919\text{e-}2-5.3298032\text{e-}2i$	$0.70110901 + 1.3444128i$
8	$-5.0452919\text{e-}2-5.3298032\text{e-}2i$	$0.70110901 - 1.3444128i$

Table X. BCF fitting data for parameters $\alpha = 0.027$ ps^2, $\xi = 1.447$ meV, $K_r = 4$, $K_i = 4$ and $T = 70$ K.

μ	$\mathcal{G}_\mu$	W_μ
1	$-0.13486909 - 0.57807569i$	$1.2356936 - 2.4013976i$
2	$-0.13486909 + 0.57807569i$	$1.2356936 + 2.4013976i$
3	$0.65007290 + 1.1050674i$	$1.0483730 - 0.89116928i$
4	$0.65007290 - 1.1050674i$	$1.0483730 + 0.89116928i$
5	$1.6776230\text{e-}2+6.2383255\text{e-}2i$	$1.0093977 + 2.6291021i$
6	$-1.6776230\text{e-}2+6.2383255\text{e-}2i$	$1.0093977 - 2.6291021i$
7	$4.1148269\text{e-}2-6.3778140\text{e-}2i$	$0.73651329 + 1.2656890i$
8	$-4.1148269\text{e-}2-6.3778140\text{e-}2i$	$0.73651329 - 1.2656890i$

Table XI. BCF fitting data for parameters $\alpha = 0.027$ ps^2, $\xi = 1.447$ meV, $K_r = 4$, $K_i = 4$ and $T = 75$ K.

μ	$\mathcal{G}_\mu$	W_μ
1	$-0.14577563 + 0.6.2114742i$	$1.2369851 + 2.3996228i$
2	$-0.14577563 - 0.6.2114742i$	$1.2369851 - 2.3996228i$
3	$0.69731557 - 1.1893839i$	$1.0503321 + 0.88993013i$
4	$0.69731557 + 1.1893839i$	$1.0503321 - 0.88993013i$
5	$-1.6888717\text{e-}2+6.2750665\text{e-}2i$	$1.0111855 - 2.6268666i$
6	$1.6888717\text{e-}2+6.2750665\text{e-}2i$	$1.0111855 + 2.6268666i$
7	$-4.0794171\text{e-}2-6.4158924\text{e-}2i$	$0.73794037 - 1.2629214i$
8	$4.0794171\text{e-}2-6.4158924\text{e-}2i$	$0.73794037 + 1.2629214i$

Table XII. BCF fitting data for parameters $\alpha = 0.05$ ps^2, $\xi = 1.447$ meV, $K_r = 4$, $K_i = 4$ and $T = 0$ K.

μ	$\mathcal{G}_\mu$	W_μ
1	$1.2118168\text{e-}2+0.14826670i$	$1.1582410 + 2.5595171i$
2	$1.2118168\text{e-}2-0.14826670i$	$1.1582410 - 2.5595171i$
3	$0.11238764 - 0.19120777i$	$0.97197806 + 1.2493642i$
4	$0.11238764 + 0.19120777i$	$0.97197806 - 1.2493642i$
5	$-6.4599805\text{e-}2+0.22339575i$	$1.2310522 - 2.3896601i$
6	$6.4599805\text{e-}2+0.22339575i$	$1.2310522 + 2.3896601i$
7	$-4.7641241\text{e-}2-0.22956713i$	$1.0071974 + 0.96242667i$
8	$4.7641241\text{e-}2-0.22956713i$	$1.0071974 - 0.96242667i$

Table XIII. BCF fitting data for parameters $\alpha = 0.1$ ps^2, $\xi = 1.447$ meV, $K_r = 4$, $K_i = 4$ and $T = 0$ K.

μ	$\mathcal{G}_\mu$	W_μ
1	9.6256494e-2$-0.31047592i$	$1.1307878 - 2.4480531i$
2	9.6256494e-2$+0.31047592i$	$1.1307878 + 2.4480531i$
3	$0.14806583 + 0.35442458i$	$0.93592755 - 1.1807664i$
4	$0.14806583 - 0.35442458i$	$0.93592755 + 1.1807664i$
5	$0.14499922 + 0.47104872i$	$1.2451339 + 2.3623288i$
6	$-0.14499922 + 0.47104872i$	$1.2451339 - 2.3623288i$
7	$-0.13875902 - 0.48376063i$	$1.0404338 + 0.93261628i$
8	$0.13875902 - 0.48376063i$	$1.0404338 - 0.93261628i$

Table XIV. BCF fitting data for parameters $\alpha = 0.1$ ps^2, $\xi = 1.447$ meV, $K_r = 4$, $K_i = 4$ and $T = 4$ K.

μ	$\mathcal{G}_\mu$	W_μ
1	$-0.12417207 - 0.37870149i$	$1.3393008 - 2.6201118i$
2	$-0.12417207 + 0.37870149i$	$1.3393008 + 2.6201118i$
3	$0.39315064 + 0.61599424i$	$1.2255907 - 1.2583633i$
4	$0.39315064 - 0.61599424i$	$1.2255907 + 1.2583633i$
5	9.4315302e-2$+0.34655229i$	$1.1432982 + 2.4838809i$
6	-9.4315302e-2$+0.34655229i$	$1.1432982 - 2.4838809i$
7	3.3474864e-2$-0.35590542i$	$0.87837636 + 1.0758240i$
8	-3.3474864e-2$-0.35590542i$	$0.87837636 - 1.0758240i$

Table XV. BCF fitting data for parameters $\alpha = 0.15$ ps^2, $\xi = 1.447$ meV, $K_r = 4$, $K_i = 4$ and $T = 0$ K.

μ	$\mathcal{G}_\mu$	W_μ
1	$0.18521883 + 0.46682905i$	$1.1167548 + 2.4109850i$
2	$0.18521883 - 0.46682905i$	$1.1167548 - 2.4109850i$
3	$0.17941942 - 0.50978092i$	$0.91986393 + 1.1521383i$
4	$0.17941942 + 0.50978092i$	$0.91986393 - 1.1521383i$
5	$-0.22180270 + 0.70847666i$	$1.2442160 - 2.3590786i$
6	$0.22180270 + 0.70847666i$	$1.2442160 + 2.3590786i$
7	$0.21669971 - 0.72754587i$	$1.0436690 - 0.92780958i$
8	$-0.21669971 - 0.72754587i$	$1.0436690 + 0.92780958i$

Table XVI. BCF fitting data for parameters $\alpha = 0.15$ ps^2, $\xi = 1.447$ meV, $K_r = 4$, $K_i = 4$ and $T = 4$ K.

μ	$\mathcal{G}_\mu$	W_μ
1	$-0.18998725 - 0.57172931i$	$1.3432012 - 2.6185949i$
2	$-0.18998725 + 0.57172931i$	$1.3432012 + 2.6185949i$
3	$0.59354399 + 0.93078202i$	$1.2290989 - 1.2592063i$
4	$0.59354399 - 0.93078202i$	$1.2290989 + 1.2592063i$
5	$0.15012128 + 0.54972408i$	$1.1628602 + 2.4644149i$
6	$-0.15012128 + 0.54972408i$	$1.1628602 - 2.4644149i$
7	1.5678644e-2$-0.56477703i$	$0.90430030 + 1.0506685i$
8	-1.5678644e-2$-0.56477703i$	$0.90430030 - 1.0506685i$

Table XVII. BCF fitting data for parameters $\alpha = 0.15$ ps^2, $\xi = 1.447$ meV, $K_r = 4$, $K_i = 4$ and $T = 25$ K.

μ	$\mathcal{G}_\mu$	W_μ
1	$-0.36040209 - 1.3345957i$	$1.2966219 - 2.4093338i$
2	$-0.36040209 + 1.3345957i$	$1.2966219 + 2.4093338i$
3	$1.4345122 - 2.6715878i$	$1.1291186 + 0.87918611i$
4	$1.4345122 + 2.6715878i$	$1.1291186 - 0.87918611i$
5	$-0.10455615 + 0.38333887i$	$1.0401172 - 2.5907333i$
6	$0.10455615 + 0.38333887i$	$1.0401172 + 2.5907333i$
7	$0.19231323 - 0.39250001i$	$0.76372937 + 1.2171690i$
8	$-0.19231323 - 0.39250001i$	$0.76372937 - 1.2171690i$

Table XVIII. BCF fitting data for parameters $\alpha = 0.15$ ps^2, $\xi = 1.447$ meV, $K_r = 4$, $K_i = 4$ and $T = 75$ K.

μ	$\mathcal{G}_\mu$	W_μ
1	$-1.1902524 - 4.0694381i$	$1.3083749 - 2.3549745i$
2	$-1.1902524 + 4.0694381i$	$1.3083749 + 2.3549745i$
3	$4.2665533 - 8.3663831i$	$1.1500307 + 0.85025323i$
4	$4.2665533 + 8.3663831i$	$1.1500307 - 0.85025323i$
5	$0.11758970 + 0.43222364i$	$1.0798305 + 2.5482906i$
6	$-0.11758970 + 0.43222364i$	$1.0798305 - 2.5482906i$
7	$0.14398553 - 0.44319447i$	$0.80333735 + 1.1609627i$
8	$-0.14398553 - 0.44319447i$	$0.80333735 - 1.1609627i$

Table XIX. BCF fitting data for parameters $\alpha = 0.376$ ps^2, $\xi = 1.447$ meV, $K_r = 4$, $K_i = 4$ and $T = 4$ K.

μ	$\mathcal{G}_\mu$	W_μ
1	$-0.47941730 - 1.4370274i$	$1.3445088 - 2.6178105i$
2	$-0.47941730 + 1.4370274i$	$1.3445088 + 2.6178105i$
3	$1.4911597 - 2.3401589i$	$1.2305360 + 1.2594535i$
4	$1.4911597 + 2.3401589i$	$1.2305360 - 1.2594535i$
5	$-0.42615767 + 1.5324728i$	$1.2000151 - 2.4261460i$
6	$0.42615767 + 1.5324728i$	$1.2000151 + 2.4261460i$
7	$0.15217999 - 1.5750671i$	$0.95723069 - 1.0036216i$
8	$-0.15217999 - 1.5750671i$	$0.95723069 + 1.0036216i$

Table XX. BCF fitting data for parameters $\alpha = 0.376$ ps^2, $\xi = 1.447$ meV, $K_r = 4$, $K_i = 4$ and $T = 10$ K.

μ	$\mathcal{G}_\mu$	W_μ
1	$-0.49885639 + 1.9404215i$	$1.3568296 + 2.4941702i$
2	$-0.49885639 - 1.9404215i$	$1.3568296 - 2.4941702i$
3	$1.8505523 - 3.9099381i$	$1.2790571 + 0.92994070i$
4	$1.8505523 + 3.9099381i$	$1.2790571 - 0.92994070i$
5	$-0.29349356 + 1.0784415i$	$1.0783015 - 2.5498444i$
6	$0.29349356 + 1.0784415i$	$1.0783015 + 2.5498444i$
7	$-0.36594430 - 1.1057278i$	$0.80166356 - 1.1631235i$
8	$0.36594430 - 1.1057278i$	$0.80166356 + 1.1631235i$

References

[1] A. Tartakovskii, *Quantum Dots* (Cambridge University Press, 2012).

[2] U. Banin, Y. Cao, D. Katz and O. Millo, Nature **400**, 542 (1999).

[3] M. Bayer, O. Stern, P. Hawrylak, S. Fafard and A. Forchel, Nature **405**, 923 (2000).

[4] S.-V. B. H. G. Physics, in book *Semiconductor Quantum Dots*, edited Y. Masumoto and T. Takagahara (Springer, 2002).

[5] T. Fujisawa, D. G. Austing, Y. Tokura, Y. Hirayama and S. Tarucha, Nature **419**, 278 (2002).

[6] P. Lodahl, S. Mahmoodian and S. Stobbe, Reviews of Modern Physics **87**, 347 (2013).

[7] L. Jacak, A. Wójs and P. Hawrylak, *Quantum Dots* (Springer Berlin Heidelberg, 1998).

[8] H. Kamada, H. Gotoh, J. Temmyo, T. Takagahara and H. Ando, Physical Review Letters **87**, 246401 (2001).

[9] T. H. Stievater, X. Li, D. G. Steel, D. Gammon, D. S. Katzer, D. Park, C. Piermarocchi and L. J. Sham, Physical Review Letters **87**, 133603 (2001).

[10] A. Zrenner, E. Beham, S. Stufler, F. Findeis, M. Bichler and G. Abstreiter, Nature **418**, 612 (2002).

[11] A. J. Ramsay, T. M. Godden, S. J. Boyle, E. M. Gauger, A. Nazir, B. W. Lovett, A. M. Fox and M. S. Skolnick, Physical Review Letters **105**, 177402 (2010).

[12] Y.-J. Wei, Y. He, Y.-M. He, C.-Y. Lu, J.-W. Pan, C. Schneider, M. Kamp, S. Höfling, D. P. McCutcheon and A. Nazir, Physical Review Letters **113**, 097401 (2014).

[13] A. Ulhaq, S. Weiler, S. M. Ulrich, R. Roßbach, M. Jetter and P. Michler, Nature Photonics **6**, 238 (2012).

[14] A. N. Vamivakas, Y. Zhao, C.-Y. Lu and M. Atatüre, Nature Physics **5**, 198 (2009).

[15] K. Konthasinghe, J. Walker, M. Peiris, C. K. Shih, Y. Yu, M. F. Li, J. F. He, L. J. Wang, H. Q. Ni, Z. C. Niu and A. Muller, Physical Review B **85**, 235315 (2012).

[16] C. Santori, M. Pelton, G. Solomon, Y. Dale and Y. Yamamoto, Physical Review Letters **86**, 1502 (2001).

[17] Y.-J. Wei, Y.-M. He, M.-C. Chen, Y.-N. Hu, Y. He, D. Wu, C. Schneider, M. Kamp, S. Höfling, C.-Y. Lu and J.-W. Pan, Nano Letters **14**, 6515 (2014).

[18] M. A. M. Versteegh, M. E. Reimer, K. D. Jöns, D. Dalacu, P. J. Poole, A. Gulinatti, A. Giudice and V. Zwiller, Nature Communications **5**, 5298 (2014).

[19] A. Nazir and D. P. S. McCutcheon, Journal of Physics: Condensed Matter **28**, 103002 (2016).

[20] A. Imamoglu, D. D. Awschalom, G. Burkard, D. P. DiVincenzo, D. Loss, M. Sherwin and A. Small, Physical Review Letters **83**, 4204 (1999).

[21] A. J. Ramsay, S. J. Boyle, R. S. Kolodka, J. B. Oliveira, J. Skiba-Szymanska, H. Y. Liu, M. Hopkinson, A. M. Fox and M. S. Skolnick, Physical Review Letters **100**, (2008).

[22] N. W. Hendrickx, W. I. L. Lawrie, L. Petit, A. Sammak, G. Scappucci and M. Veldhorst, Nature Communications **11**, 3478 (2020).

[23] D. Suess, A. Eisfeld and W. T. Strunz, Physical Review Letters **113**, (2014).

[24] L. Diósi, N. Gisin and W. T. Strunz, Physical Review A **58**, 1699 (1998).

[25] J. Ziman, *Electrons and Phonons* (Oxford University Press, 2001).

[26] P. Kok and B. W. Lovett, *Introduction to Optical Quantum Information Processing* (Cambridge University Press, 2010).

[27] G. D. Mahan, *Many-Particle Physics* (Springer US, 2000).

[28] B. Krummheuer, V. M. Axt and T. Kuhn, Physical Review B **65**, 195313 (2002).

[29] U. Hohenester, Journal of Physics B: Atomic, Molecular and Optical Physics **40**, S315 (2007).

[30] W. G. Unruh, Physical Review A **51**, 992 (1995).

[31] G. M. Palma, K.-A. Suominen and A. K. Ekert, Proceedings of the Royal Society of London. Series A: Mathematical, Physical and Engineering Sciences **452**, 567 (1996).

[32] H.-P. Breuer and F. Petruccione, *The Theory of Open Quantum Systems* (Oxford University Press, 2007).

[33] E. C. G. Sudarshan, Physical Review Letters **10**, 277 (1963).

[34] R. J. Glauber, Physical Review **131**, 2766 (1963).

[35] C. C. Gerry and P. L. Night, Introductory Quantum Optics, 2005.

[36] E. Jaynes and F. Cummings, Proceedings of the IEEE **51**, 89 (1963).

[37] R. Kubo, Journal of the Physical Society of Japan **12**, 570 (1957).

[38] H. Bruus and K. Flensberg, Many-body quantum theory in condensed matter physics, 2002.

[39] V. May and O. Kühn, *Charge and Energy Transfer Dynamics in Molecular Systems* (Wiley, 2003).

[40] M. Cáceres and S. Grigera, Physica A: Statistical Mechanics and its Applications **291**, 317 (2001).

[41] B. Schumacher and M. Westmoreland, *Quantum Processes Systems, and Information* (Cambridge University Press, 2010).

[42] S. Mukamel, *Principles of Nonlinear Optical Spectroscopy* (Oxford University Press, 1995).

[43] J. D. Jackson, *Classical Electrodynamics*, 3 ed. (Wiley, 1998).

[44] M. D. Allan, *Statistical Mechanics*, 1st ed. (Harper & Row, 1976).

[45] B. R. Mollow, Physical Review **188**, 1969 (1969).

[46] H. Carmichael, *An Open Systems Approach to Quantum Optics* (Springer Berlin Heidelberg, 1993), Vol. 18.

[47] H. J. Carmichael, *Statistical Methods in Quantum Optics 1* (Springer Berlin Heidelberg, 1999).

[48] Daniel A. Steck, *Quantum and Atom Optics*, available online at `http://steck.us/teaching` (revision 0.13.21, 5 June 2023).

[49] G. Lindblad, Communications in Mathematical Physics **48**, 119 (1976).

[50] V. Gorini, A. Kossakowski and E. C. G. Sudarshan, Journal of Mathematical Physics **17**, 821 (1976).

[51] J. Dalibard, Y. Castin and K. Mølmer, Physical Review Letters **68**, 580 (1992).

[52] M. B. Plenio and P. L. Knight, Reviews of Modern Physics **70**, 101 (1998).

[53] N. Gisin and I. C. Percival, Journal of Physics A: Mathematical and General **25**, 5677 (1992).

[54] L. Diosi and W. T. Strunz, Physics Letters A **235**, 569 (1997).

[55] R. Hartmann and W. T. Strunz, Journal of Chemical Theory and Computation **13**, 5834 (2017).

[56] V. Bargmann, Communications on Pure and Applied Mathematics **14**, (1961).

[57] R. Feynman and F. Vernon, Annals of Physics **24**, 118 (1963).

[58] K. Furutsu, 1963, J. Res. Natl. Inst. Stand. Technol.Vol. 67D, No. 3, 303.

[59] E. A. Novikov, 1965, Sov. Phys. J.E.T.P. 20, 1290.

[60] I. K. Valery, *Dynamics of Stochastic Systems* (Elsevier, 2005).

[61] H. Kahn, Random sampling (Monte Carlo) techniques in neutron attenuation problems–I, *Nucleonics*, 6(5) (1950).

[62] H. Kahn and T. E. Harris, Estimation of particle transmission by random sampling, National Bureau of Standards applied mathematics series, 12:27–30 (1951).

[63] A. A. Novikov, Theory of Probability & Its Applications **17**, 717 (1973).

[64] C. Gardiner, *Stochastic Methods: A Handbook for the Natural and Social Sciences* (Springer Berlin, Heidelberg, 2009).

[65] G. Semenoff and H. Umezawa, Nuclear Physics B **220**, 196 (1983).

[66] J. Roden, W. T. Strunz and A. Eisfeld, Journal of Chemical Physics **134**, (2011).

[67] T. Yu, L. Diósi, N. Gisin and W. T. Strunz, Physical Review A **60**, 91 (1999).

[68] C. Meier and D. J. Tannor, The Journal of Chemical Physics **111**, 3365 (1999).

[69] R. Hartmann and W. T. Strunz, Journal of Physical Chemistry A **125**, 7066 (2021).

[70] J. Dormand and P. Prince, Journal of Computational and Applied Mathematics **6**, 19 (1980).

[71] P. Virtanen, R. Gommers, T. E. Oliphant, M. Haberland, T. Reddy, D. Cournapeau, E. Burovski, P. Peterson, W. Weckesser, J. Bright, S. J. van der Walt, M. Brett, J. Wilson, K. J. Millman, N. Mayorov, A. R. J. Nelson, E. Jones, R. Kern, E. Larson, C. J. Carey, İ. Polat, Y. Feng, E. W. Moore, J. VanderPlas, D. Laxalde, J. Perktold, R. Cimrman, I. Henriksen, E. A. Quintero, C. R. Harris, A. M. Archibald, A. H. Ribeiro, F. Pedregosa, P. van Mulbregt and SciPy 1.0 Contributors, Nature Methods **17**, 261 (2020).

[72] J. Hu, M. Luo, F. Jiang, R.-X. Xu and Y. Yan, The Journal of Chemical Physics **134**, (2011).

[73] Z.-H. Chen, Y. Wang, X. Zheng, R.-X. Xu and Y. Yan, The Journal of Chemical Physics **156**, (2022).

[74] K. D. Ikramov, Computational Mathematics and Mathematical Physics **52**, 1 (2012).

[75] G. Beylkin and L. Monzón, Applied and Computational Harmonic Analysis **19**, 17 (2005).

[76] C. Roy and S. Hughes, Physical Review B **85**, 115309 (2012).

[77] P. Busch, P. Lahti, J.-P. Pellonpää and K. Ylinen, *Quantum Measurement* (Springer International Publishing, 2016).

[78] K. Roy-Choudhury, N. Mann, R. Manson and S. Hughes, Physical Review B **93**, 245421 (2016).

[79] H. J. Carmichael, *Statistical Methods in Quantum Optics 2* (Springer Berlin Heidelberg, 2008).

[80] L. Lugiato, F. Prati and M. Brambilla, *Nonlinear Optical Systems* (Cambridge University Press, 2015).

[81] A. Redfield, in book *The Theory of Relaxation Processes* (Elsevier, 1965), pp. 1–32.

[82] C. P. Poole and H. A. Farach, in book *The Redfield Theories* (Elsevier, 1971), pp. 106–123.